A study on

MORPHOLOGICAL AND DYNAMICAL PROPERTIES OF NEURONAL GROWTH CONES

Thesis submitted for the degree of

"*Doctor Philosophiæ*"

S.I.S.S.A. - I.S.A.S.

Neurobiology Sector

CANDIDATE:

Jummi Laishram

SUPERVISOR:

Prof. Vincent Torre

SISSA, Via Beirut 2-4, 34014 TRIESTE, ITALY

To my family and Carlo,
for everything.

DECLARATION

The work described in this thesis was carried out at the International School for Advanced Studies, Trieste, between November 2004 and March 2009, under the supervision of Professor Vincent Torre.

TABLE OF CONTENTS

ABSTRACT vi
OVERVIEW OF THE THESIS vii
ACRONYMS AND ABBREVIATIONS viii
LIST OF FIGURES AND TABLES ix

1. INTRODUCTION 1
2. GROWTH CONES 3
   2.1. Cytoskeleton: Structure and Organization 5
   2.2. Polymerization and Motility 7
   2.3. Exploration by growth cones 13
   2.4. Mechanical Computation in Neuronal Growth Cones 14
   2.5. Approaches to Study Exploratory Behavior of Neurons 15
3. MORPHOLOGY OF GROWTH CONES 16
   3.1. Registration of Images: Concept 17
   3.2. 0 pN Force Image 17
   3.3. Characterization of Morphology 18
4. AIMS OF THE THESIS 19
5. METHODS AND PROCEDURES FOR DATA EXTRACTION AND ANALYSIS 20
   - Recovery of filopodium backbone 20
   - Degree of bending 21
   - Correlation of growth and retraction 22
   - Global Correlation or Orchestration 23
   - Exploration of local environment 24
   - Mechanical Computation 25
   - Image Registration 29
   - 0 pN Force Image 30
   - Invaginations and Holes 31
   - Comparison with immunofluorescent images 34
6. TECHNIQUES 35
   6.1. Preparation of Cell Culture 35
   6.2. Fixation Protocols 35
   6.3. Immunofluorescence and Transfection 36
   6.4. Confocal Microscopy 36
   6.5. Atomic Force Microscopy 37
   6.6. Optical Tweezers 37
7. RESULTS 38
   7.1. Mechanical computation in neurons (under revision. Full Manuscript: Appendix 1.) 38
   7.2. A morphological analysis of growth cones of DRG neurons combining Atomic Force and Confocal Microscopy (under revision. Full Manuscript: Appendix 2.) . . . 39

8. Discussion and Conclusions 40
8.1. Mechanical Computation in Neurons 40
8.2. Morphological Analysis of Growth Cones 43
9. Additional Material - Live Cell Imaging 45
9.1. Material and Method 45
- Cell culture 45
- Transfection Protocols: 45
  - Fugene 6 45
  - Microinjection 45
  - Electroporation 46
- Immunofluorescence 46
- Microscopy 46
- Reagents and Constructs 47
9.2. Results 47
- Live Imaging of fluorescent neurons in 3-D 47
- Comparison with Immunofluorescent Analysis 47
9.3. Conclusion 49
10. Appendices 50
10.1. Manuscript 1 under revision: *Mechanical Computation in Neurons* 50
10.2. Manuscript 2 under revision: *A morphological analysis of growth cones of DRG neurons combining Atomic Force and Confocal Microscopy* 77
11. Bibliography 98
12. Acknowledgment 103

ABSTRACT

In the developing nervous system and in the adult brain, neurons constantly need to solve mechanical problems. Neuronal growth cones are the main motile structures located at the tip of neurites and are composed of a lamellipodium from which thin filopodia emerge. They are responsible for extension of neurite processes and for transducing signals from extracellular cues to alter directionality, branching, and motility. They must decide how to explore the environment and in which direction to grow; they also need to establish appropriate contacts, to avoid obstacles and to determine how much force to exert. The complete understanding of the nervous system and its basic unit, the neuron, demands a quantification of the behavioral pattern and the morphological characteristics.

The first part of my thesis presents the analysis of the kinetics and dynamics of growth cones with the aim to understand two major issues: firstly, the strategy used by filopodia and lamellipodia during their exploration and navigation; secondly, what kind of mechanical problems neurons need to solve during their operation. We show that in sparse cultures, filopodia grow and retract following statistical patterns, nearly optimal for an efficient exploration of the environment. In a dense tissue, filopodia exploration is still present although significantly reduced. Analysis on pairs of filopodia, not necessarily neighbors, of DRG, PC12 and Hippocampal neurons respectively showed that the correlation coefficient of the growth (or retraction) of more than 50% of these pairs was larger than 0.15. These observations allow us to understand the fine orchestration of filopodial motion. From a computational point of view, filopodia and lamellipodia motion can be described by a random process in which errors are corrected by efficient feedback loops. We argue that neurons not only process sensory signals, but also solve mechanical problems throughout their entire lifespan, from the early stages of embryogenesis to adulthood.

The second part of the thesis presents the results from morphological analyses performed on neuronal growth cones using conventional Laser Scanning Confocal Microscopy (LSCM) and Atomic Force Microscopy (AFM). In order to reduce changes of the image surface caused by the pressure of the AFM tip, we have developed a procedure to obtain 0 pN AFM images. Further analysis of these images revealed topographical structures with nanoscale dimensions, referred to as “invaginations” or “holes”. Images of immunofluorescent DRG growth cones colabeled for actin and tubulin were superimposed to images obtained with AFM at different scanning forces. Comparative analysis with LSCM images showed that these holes correspond to regions where staining of both actin and tubulin was negligible. These results show that the combination of LSCM and AFM reveal structural details with a nanoscale dimension of DRG growth cones, difficult to resolve with conventional microscopy. Such studies can be applied to achieve a better understanding of neurodegenerative diseases where the mechanical and morphological properties of neurons and of growth cones in particular can be of great importance.

OVERVIEW OF THE THESIS

CHAPTER 1: INTRODUCTION- This chapter gives a brief and general introduction on neuronal growth cones.

CHAPTER 2: GROWTH CONES- This chapter provides a review of neuronal growth cones.

CHAPTER 3: MORPHOLOGY OF GROWTH CONES- This chapter discusses in more detail the morphology of growth cone.

CHAPTER 4: AIMS OF THE THESIS- This chapter describes the goals of this thesis.

CHAPTER 5: METHODS AND PROCEDURES FOR DATA EXTRACTION, ANALYSIS AND COMPARISON- This chapter provides definitions and explanations on how data have been extracted and analyzed.

CHAPTER 6: TECHNIQUES EMPLOYED- This section provides a detailed description of the different techniques used to study the different topics outlined in this thesis.

CHAPTER 7: RESULTS- This chapter illustrates the results obtained during the thesis.

CHAPTER 8: DISCUSSION AND PERSPECTIVES- This chapter provides a discussion and perspectives of the presented work.

CHAPTER 9: ADDITIONAL MATERIAL- LIVE CELL IMAGING- This chapter describes the procedures used to transfect neurons for live cell imaging.

APPENDICES- Two manuscripts submitted in the course of this thesis are enclosed here.

ACRONYMS AND ABBREVIATIONS

AFM	Atomic Force Microscopy
Arp	Actin-Related Protein
ATP	Adenosine TriPhosphate
CCD	Charged-Coupled Device
DAPI	4',6-diamidino-2-phenylindole
DIC	Differential Interference Contrast
DRG	Dorsal Root Ganglion
EB1-GFP	End-binding-Green Fluorescent Protein
LSCM	Laser Scanning Confocal Microscopy
MAP	Microtubule-Associated Protein
MARK	Microtubule-Affinity-Regulating-Kinase
NGF	Nerve Growth Factor
PC12	Pheochromocytoma
SEM	Scanning Electron Microscopy

LIST OF FIGURES

2.1 Growth Cone structure and organization 3
2.2 Double-helical structure of actin filaments 6
2.3 Representation of a microtubule 7
5.1 Reconstruction of the filopodial backbone 20
5.2 Classification of filopodia on degree of bending 21
5.3 Selected frames of a growth cone with two filopodia 22
5.4 Correlation in growth/retraction between two filopodia 22
5.5 Global orchestration or correlation 23
5.6 Determination of the explorable and explored space around a growth cone 25
5.7 Obstacle avoidance: filopodium tip avoiding obstacles and reaching the final destination 27
5.8 Formation of physical contacts 28
5.9 Obstacle avoidance and removal 28
5.10 Registration of LSCM Image with respect to AFM image 30
5.11 Data fitting 31
5.12 Defining holes 32
5.13 3D view of the information from the two images superimposed 34
9.1 PC12 cells transfected with EB1-GFP and DsRed-Actin by Fugene 6 48
9.2 PC12 cells transfected with EB1-GFP and DsRed-Actin by Electroporation 48
9.3 Immunofluorescence image of a DRG neuron electroporated with EB1-GFP 48

LIST OF TABLES

2.1 Proteins of the Cytoskeleton 5
5.1 Percentage of correlated filopodial growth in different neuronal growth cones 23
5.2 Hole statistics 33
5.3 Comparison of parameters from growth cones fixed using the two different Protocols 33
5.4 Comparison of Actin Tubulin Ratio in growth cones 34

1. INTRODUCTION

Contemporary neuroscience investigates the nervous system of biological systems and deals with a wide range of problems. It aims to understand the structure, function, physiology, pathology, pharmacology, genetics, biochemistry, computational behavior, informatics, development and evolutionary history of the nervous system. Critical information has come to light with advances in imaging techniques, electrophysiological treatment, genetic analysis, etc. and has given significant insight to many important physiological behaviors. Recent theoretical advances in neuroscience have been aided by the use of computational modeling. Comparative studies using experimental and computational methods have made it possible to understand how neurons process sensory inputs and transform them into appropriate motor outputs.

It is tempting to compare cells - and neurons, in particular - to the most sophisticated contemporary computing electronic devices due to the nature of the electrical and chemical signals for the transmission, processing and exchange of information. This comparison is understandable if one considers the fact that neurons have the processing power better than a high-speed calculator. But their superiority lies in the fact that neurons are not only able to handle complicated information/ mathematical operations but also motile. Indeed, neurons can explore the environment and are able to traverse distances several microns, even millimeters, away from their original location *(Solecki et al., 2006; Ghashghaei et al., 2007*).

The beginning of the research aiming at understand how nerve fibers elongate from the cell body and navigate to their correct destinations dates to the early 1900s, when Santiago Ramón y Cajal (1852-1934) first proposed the existence of individual neurons as distinct entities in a neuronal network. In the same period, Camillo Golgi (1843-1926) proposed the “reticular” neural networks and argued that neurons in the nervous tissue were a continuous open network of interconnected cells. With the invention of the Electron microscope, it became apparent that a plasma membrane completely enclosed each neuron, supporting Cajal's theory, and weakening Golgi's reticular theory. However, with the discovery of electrical synapses that provides some continuity to the network, Golgi was at least partially correct. For this work, Ramón y Cajal and Golgi shared the Nobel Prize in Physiology or Medicine in 1906.

Ramón y Cajal’s studies on the fine structure of the central nervous system led to the conclusion that the fibers of the nervous system grew from neuronal soma and formed connections with neighboring cells, thus forming the observed network. His observation on the tissue sections introduced the concept of the growth cone. He proposed that the way axons grow is via a growth cone at their ends. This highly motile structure at the leading edge is responsible for neuronal motility and its major components are now referred to as lamellipodia and filopodia and are constantly expanding and retracting as they explore and sample the local environment in search of their final destination and lead the growth cone into new territory. There is also an extensive collection of proteins that regulate the structure and dynamics of the different

components of the cytoskeleton (*Stossel, 1993*). Much work is under progress to elucidate the pathways that guidance receptors use to communicate with proteins to produce local polymerization and changes in motility in the guidance process. How the growth cone interprets multiple cues in time and space to regulate directional motility has only been partially elucidated and careful quantification of growth cone dynamics is a requirement for the development of a statistically relevant understanding of the finer aspects of neuronal motility.

Studies on the neuron cannot be considered complete unless the morphology is accurately described. The structure of the neuron, in simple words, consists of the cellular membrane, the nucleus and various organelles. The cell membrane separates and isolates the nucleus and internal organelles from the external environment but allows specific ions to permeate though it (*Kandel et al., 2000*). The mechanical properties of this membrane are essential for maintaining the structural configuration of the neuron. It has been observed that when neurons move and migrate, and when they retract or undergo pruning or other endocytotic processes, changes occur in its mechanical properties, such as the Young's modulus (*Kuznetsova et al., 2007*).

Since the development of techniques such as Atomic Force Microscopy (AFM) and their increasing use on biological samples to study previously unfeasible topics, the sub-microscopic world of cells and neurons is now accessible and can be investigated to a great extent. The use of Laser Scanning Confocal Microscopy (LSCM) has also provided information about the structure and functioning of the neuron in detail. Previous investigations on the morphology of neurons with AFM (*Parpura et al., 1993; Bonfiglio et al., 1995*) have allowed a precise measurement of characteristics such as filopodia height. However, they have also shown that such invasive techniques can be destructive since the tip of the probe or the cantilever used touches the sample and can alter and misrepresent the topology of imaged neurons. Even though this side-effect is utilized in the form of nano-surgery, the morphology of neurons can not be accurately described unless this problem is resolved to study the morphology, and its consequences, without modifying the sample.

Thus, while neuronal motility is critical for attaining reliable development of the nervous system, morphological studies are also vital to understand its effect on the neuron. Such studies lead to a knowledge that is required to fully understand and appreciate the complexity and beauty of nature, and life itself. This thesis, in the first half, will discuss the behavior of a neuronal cell when it explores its local three-dimensional environment and quantify the exploration through experimental and computational methods; the second half will present a solution to eliminate the changes in the morphology of the neuron caused by the probe and results from comparative studies using AFM and LSCM.

2. GROWTH CONES

A typical neuron has four morphologically defined areas: the cell body, dendrites, the axon and presynaptic terminals. The growth cone is a highly motile structure at the tip of a neuronal axon (Figure 2.1) and is the fundamental structure that drives the growing axon forward. It is a region of specialized cell machinery used for extension of the neurite processes and for transducing signals from extracellular cues that alter directionality, branching, and motility.

It consists of three operationally defined cytoplasmic domains: the central or proximal region, the peripheral or distal region and the transition region. The central region is relatively non-motile and well attached to the substrate but can be displaced during elongation. It is spread over several microns in diameter and contains intracellular organelles. In contrast, the peripheral region of the cone is more motile, much thinner, and organelle-poor. The third domain, the transition region, occupies the area between these two. Typically, the boundaries between these three regions are less well-defined in vertebrate growth cones as compared to those from the commonly studied mollusk *Aplysia.*

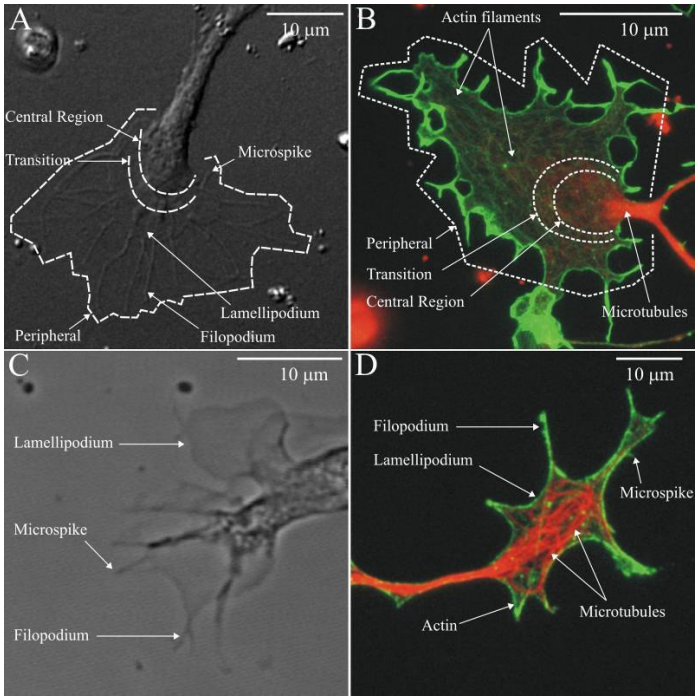

Figure 2.1: Growth Cone structure and organization. **A** and **C:** DIC images of DRG neuronal growth cones. **B** and **D**: Immunofluorescent images. Panels show the operational regions of the growth cone- the central, transition and peripheral regions, and the different structural components of the growth cone- the filopodia, lamellipodium, ruffles and microspikes.

In the peripheral region, the actin filaments are arranged in different types of structures (Figure 2.1). Parallel bundles of actin filaments are called ribs and if they protrude from the body of the growth cone, they are called FILOPODIA. Between these ribs, there is an expansive network of filaments associated with areas of the growth cone that are extending forward. If they are closely coupled to the substrate, they are called LAMELLIPODIA. If they appear on the apical surface of the growth cone, they are called MEMBRANE RUFFLES. Their formation is usually the result of lamellipodia that do not adhere to the substrate and collapse back to the growth cone. Highly motile lamellipodia, filopodia, microspikes and ruffles are the major features of the peripheral region. Both the central and peripheral regions of the growth cone can display microspikes and the longer, highly motile filopodia. Actin filaments are found predominantly in the peripheral domain, whereas microtubules are localized mainly in the central domain. The transition region contains contractile actin bundles (actin arcs) orientated perpendicular to filopodia and is characterized by actin-based ruffling. Many distal tips of the microtubules reside in this zone.

The lamellipodium is a flat extension and generally extrude in the direction of a strong stimulus such as chemoattractant that induces cell migration. The extracellular signal induces a cascade of events resulting in the activation of a series of proteins that trigger actin branching and polymerization leading to a directed and regulated protrusive force. Filopodia are actin-rich finger-like structures; they are the sensors of the local environment essential for navigation and probe the space ahead of the lamellipodium. They also act as mechanical devices that penetrate the environment and serve as a robust scaffold for the lamellipodial protrusion.

The growth cone can assume a variety of shapes through constant remodeling. Such changes can occur within a timescale of tens of minutes. For example, cones displaying a predominantly lamellipodial form can evolve into cones with many more filopodia and microspikes and vice versa. Other structures are interchangeable. Ruffles can transform into lamellipodia and varicosities can migrate forward and merge with the cone, or the cone may form and leave behind a varicosity as elongation proceeds (*Aletta and Greene, 1998*). The motion of these structures plays a major role in morphogenesis and neuronal differentiation, and their significance in axonal elongation is demonstrated by the finding that elimination of filopodia and lamellipodia reduces the rate of axon elongation by a great margin (*Marsh and Letourneau, 1984; Letourneau et al., 1987*). Even though axons with growth cones devoid of filopodia are able to advance, they are unable to detect and respond to guidance cues (*Bentley and Toroian-Raymond, 1986; Chien et al., 1993; Challacombe et al., 1996*).

2.1. CYTOSKELETON: STRUCTURE AND ORGANIZATION

Over the recent years, it has become evident that neuronal growth cone structure, motility and guidance are dependent on the underlying CYTOSKELETON (*Suter and Forscher, 1998*). The cytoskeleton is an elaborate array of protein fibers that besides providing architectural support and mechanical strength also participate in motile events within and of the cell (such as aiding chromosome separation during mitosis and facilitating the intracellular transport of organelles). In the nervous system, the cytoskeleton plays an important part in axon and dendrite formation, which allows neurons to establish their exquisite and complex morphology. The cytoskeleton also helps in the wiring of neural circuitry by driving both the guidance of neuronal processes and the formation of synapses, which are the sites of interneuronal communication.

There are three major types of protein filaments that make up the cytoskeleton: cable-like ACTIN FILAMENTS (or microfilaments), rope-like INTERMEDIATE FILAMENTS, and pipe-like MICROTUBULES. The remodeling of these protein filaments by multiple intrinsic and extrinsic cues, which act through conserved signaling pathways, enables the cytoskeleton to control the cell shapes, and moreover, to modify dynamic cellular behaviors. Actin filaments and microtubules are composed of actin and tubulin monomers respectively. Microtubules dominate the central region of the growth cone whereas actin filaments form a network of microfilaments concentrated in the peripheral region of the cone forming the cytoskeletons of filopodia and lamellipodia. The lamellipodia contain a dense network of actin filaments and microtubules, while the filopodia are composed of mainly actin filaments and occasionally microtubules. There are also a large number of accessory proteins that bind to the filaments. They serve to crosslink the filaments together or to crosslink the filaments to other cellular structures, for example, the plasma membrane, membrane-bound organelles and chromosomes. Table 1 shows the exhaustive list of the proteins in the cytoskeleton of all species. The main families involved in neuronal motility and environment exploration are actin and tubulin.

TABLE 2.1: PROTEINS OF THE CYTOSKELETON

MICROFILAMENTS	Actins, Actin-binding proteins, Actinin, Arp2/3 complex, Cofilin, Destrin, Gelsolin, Myosins, Profilin, Tropomodulin, Troponin (T, C, I), Tropomyosin, Wiskott-Aldrich syndrome protein
INTERMEDIATE FILAMENTS	type 1 and 2 (Cytokeratin, type I, type II), type 3 (Desmin, GFAP, Peripherin, Vimentin), type 4 (Internexin, Nestin, Neurofilament, Synemin, Syncoilin), type 5 (Lamin A, B)
MICROTUBULES	Dyneins, Kinesins, MAPs (Tau protein, Dynamin), Stathmin, Tektin, Tubulins
CATENINS	α catenin, β catenin, Plakoglobin (γ catenin), δ catenin
NONHUMAN	Major sperm proteins - Prokaryotic cytoskeleton (Crescentin, FtsZ, MreB)
OTHER	APC, Dystrophin (Dystroglycan), Plakin (Desmoplakin, Plectin), Spectrin, Talin, Utrophin, Vinculin

ACTIN FILAMENTS are polymers of actin. The network of actin filament is responsible for resisting tension and maintaining the shape of the cell, and actin dynamics plays a key role in a variety of cellular processes such as cell motility, division and morphogenesis. In developing neurons, actin cytoskeleton is essential in neurite formation, extension and branching and synaptogenesis. In mature neurons, actin is the major protein at synapses, both at the pre- and postsynaptic terminals. Actin is also prominent in dendritic spines, which are special postsynaptic protrusion mediating a large amount of excitatory synaptic transmission in the brain. Actin filaments are organized into two populations at the leading edge: long bundled filaments in filopodia, and a branching network extending throughout lamellipodia. Since actin filaments are the main components of filopodia, a neuronal growth cone without its actin structure do not respond to guidance cues or molecules. They also act as both barrier and guide for microtubules.

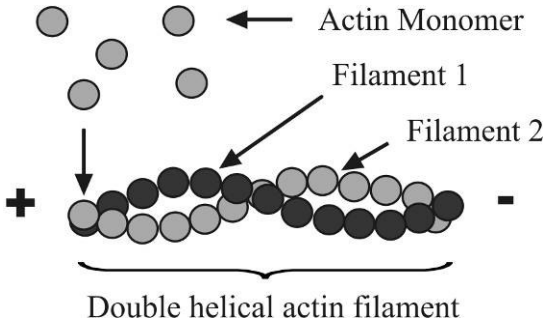

Figure 2.2: Double-helical structure of actin filaments.

INTERMEDIATE FILAMENTS are polymers of various proteins called the intermediate filament proteins such as keratins, vimentin, etc, and in neurons, neurofilament proteins. The common structural unit is a ~340 amino acid region. The structural organization is currently not known but it is predicted that intermediate filaments have an average diameter of 10 nanometers, which is between that of actin (microfilaments) and microtubules. Most types of intermediate filaments are cytoplasmic, but one type, the lamins, is nuclear. Unlike actin or tubulin, intermediate filaments do not contain a binding site for a nucleoside triphosphate and lack polarity. They are the most rigid of the filaments and are responsible for the maintenance of the overall cell shape.

MICROTUBULES are the major cytoskeletal components of axons, and resist both internal and external forces to maintain cell shape and changes of shape by virtue of their rigidity and resistance to compression. They also allow organelle and protein movement throughout the cell, serving as tracks for the axonal transport, and are involved in functions such as mitosis, motility. They also contribute to the polarity of cells. The organization of microtubules in growth cones suggests that they are also instrumental in axonal formation behind the advancing growth cone. Disrupting the microtubule network causes the growth cone to collapse. Microtubules are capable of growing and shrinking, a process called dynamic instability, in order to generate force and

provide support to motor proteins to generate forces required for cell movement. There are also motor proteins that allow organelles to move along the microtubule.

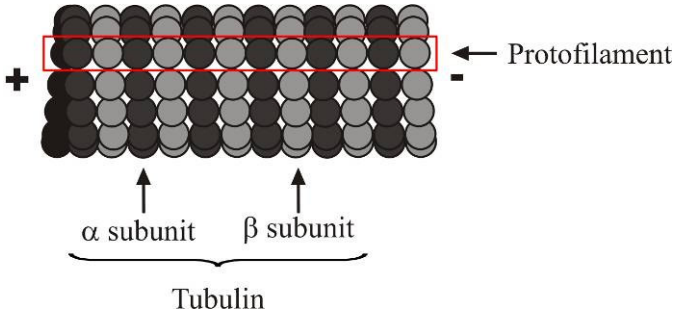

Figure 2.3: Representation of a microtubule.

2.2. POLYMERIZATION AND MOTILITY

ACTIN POLYMERIZATION: Actin filaments are polymers of ACTIN. Actin is a globular, 43 kDa protein that is very highly conserved between species. The Actin family contains over a dozen classes of proteins. The three main actin isotypes (α, β and γ) show more than 90% amino-acid homology between them and more than 98% homology within members of a particular isotypic group. Under physiological conditions, GLOBULAR-ACTIN (G-actin) readily polymerizes to form FILAMENTOUS-ACTIN (F-actin). F-actin is a double-helical filament (Figure 2.2). Each monomer is ~ 5.4 nm in size. The full period of a filament is 72 nm, and one period contains 26 subunits. As the actin monomer is asymmetrical, the actin filament is polar and its ends are structurally different. Hence, polymerization is faster at one end than the other. The fast-growing end is called the barbed or plus (+) end, whereas the slow-growing end is called the pointed or minus (-) end END (Figure 2.2). Actin nucleators stimulate the formation of actin filament assembly and facilitate the formation of an actin nucleus which is the rate limiting step for actin-filament growth. In neurons, there are four classes of Actin nucleators: Arp2/3 complex, formin proteins, Spir proteins and cofilin.

The propensity of actin to polymerize is dependent upon the affinity of actin monomers for filament ends. Thus, there is an actin monomer concentration, termed the Critical Concentration (CC), below which actin will not polymerize. At monomer concentrations above the CC, the actin will polymerize until the free monomer concentration is equal to the CC. The actin molecule has a nucleotide-binding pocket and can associate with ATP or ADP. The affinity of ATP-bound G-actin for F-actin filament is much higher than that of ADP-bound G-actin. Although, actin can polymerize from both ends *in vitro*, the rate of polymerization is not equal. ATP-hydrolysis together with the polar structure of actin filaments can lead to "treadmilling", a state in which filaments assemble at one end and disassemble at the other end. This model protrusion is important as it is based on the processes that control actin dynamics and the

underlying proteins involved in these processes. This mechanism is often compared to the clutch of an automobile where the actin network engages or hooks up with receptors that grasp the extracellular environment (*Mitchison and Kirschner, 1988*) and occurs at the leading edge. Depolymerization on the other hand occurs at the back of the network resulting in a treadmilling of actin filaments. ATP which has been incorporated into F-actin as a form of ATP-bound G-actin is hydrolyzed to ADP inside the filament. ATP-bound actins thus concentrate on the barbed-end side while ADP-bound actins concentrate on the pointed-end side when treadmilling occurs. It should be noted that even when actin polymerization has reached equilibrium, the chemical energy of ATP is consumed and used for actin dynamics in treadmilling (*Ishikawa and Kohama, 2007*).

Actin polymerization produces the major propulsive force that drives cell motility by slowing the rate of retrograde flow of the actin network and translating the actin polymerization at the leading edge into forward motion (*Lin and Forscher, 1995; Mallavarapu and Mitchison, 1999*). The orchestration of F-actin polymerization, depolymerization, and retrograde transport is responsible for the behavior of lamellipodia and filopodia. Following actin polymerization at the leading edge of lamellipodia and filopodia, F-actin is retrogradely transported to the central domain of the growth cone where it is depolymerized. Proteins that regulate the nucleation and addition of actin monomers to filaments control the polymerization of F-actin (*Letourneau, 1996*). The depolymerization of F-actin is also under the control of regulatory proteins e.g., actin depolymerizing factor (*Kuhn et al., 2000*). Notably, molecular motors can transduce the chemical energy released during this process into mechanical work. In this way, molecular motors can generate stresses in the actin network and directionally transport cargos along filaments. In this way, molecular motors can generate stresses in the actin network and directionally transport cargos along filaments.

The growth of actin filaments is an essential factor for the mobility of almost all cells. A number of actin-binding proteins regulate how actin networks are assembled, organized and remodeled. The formation of an actin nucleus is the rate limiting step for actin-filament growth and is facilitated by actin nucleators which stimulate the formation of actin filament assembly. This assembly is initiated and occurs preferentially at the leading edge spontaneously (*Chi, Flynn and Bamburg, 2008*). The growth of such networks is believed to provide the force necessary for extending cell protrusions such as lamellipodia, and for propelling intracellular pathogens such as Listeria through the cytoplasm. Recent experiments (*Loisel et al., 1999*) have shown that motile forces can be generated by the actin polymerization energetics alone, without the help of motor proteins such as myosin.

Retrograde transport of F-actin involves the myosin family of motor proteins (*Lin et al., 1996; Jay, 2000; Suter and Forscher, 2000*). The net protrusion of lamellae and filopodia is largely determined by the rates of F-actin polymerization and retrograde flow (*Lin et al., 1994*). If actin polymerization is blocked, leading edge protrusion does not occur, and F-actin is removed

from the P-domain by retrograde transport. On the other hand, if F-actin retrograde flow is inhibited, then the rate of protrusion of the leading edge will be determined primarily by the polymerization of F-actin. The rate of retrograde transport of F-actin can be modulated by the degree of linkage between F-actin and receptor-mediated adhesive contacts (*Suter et al., 1998*). The importance of the regulation of F-actin retrograde flow by extrinsic signals is exemplified by the observation that during growth cone turning toward a contact with a positive guidance cue retrograde flow is attenuated along the axis of filopodial contact and results in preferential protrusion of lamellipodia toward the contact, thereby initiating a turn (*Lin and Forscher, 1993; Suter et al., 1998*). F-actin polymerization and retrograde flow are also under complex intrinsic control and regulated both spatially and temporally (*Mallavarapu and Mitchison, 1999; Gallo and Pollack, 1995, 1997*).

MICROTUBULE POLYMERIZATION: Microtubules are polymers of TUBULIN. Tubulin is a globular protein composed of a heterodimer of two closely related 55 kDa members: α and β tubulin. The Tubulin family contains five classes of proteins. The tubulin dimers polymerize end to end into PROTOFILAMENTS initially with the α subunit of one tubulin dimer contacting the β subunit of the next. Therefore, in a protofilament, one end will have the α subunit exposed while the other end will have the β subunit exposed. The protofilaments then bundle or arrange themselves in an imperfect helix with one turn of the helix containing 13 tubulin dimers each from a different protofilament into long, hollow, unbranched cylindrical filaments to form Microtubules (Figure 2.3). These bundles are parallel to one another, so in a microtubule, there is one end with only β subunits exposed while the other end only has α subunits exposed. These, and the fact that the dimers are asymmetrical, give rise to the intrinsic polarity of microtubules. Similar to actin filaments, the fast-growing end, the β subunit end, is called the plus (+) end, whereas the slow-growing end, the α subunit end, is called minus (-) end. Tubulin can polymerize from both ends *in vitro*, however, the rate of polymerization is not equal. Most cellular microtubules are composed of 13 protofilaments and are 25 nm in diameter; each μm of microtubule length is composed of 1650 heterodimers. Typically, the protofilaments arrange themselves in an imperfect helix with one turn of the helix containing 13 tubulin dimers each from a different protofilament. They could have lengths varying from 200 nanometers to 25 micrometers. Figure 2.3 illustrates a small section of microtubule, a few αβ dimers in length. All the microtubules in the axonal and dendritic growth cones are oriented with their plus ends pointing towards the actin filament network in the peripheral domain. The minus ends are either attached to a microtubule nucleating center or capped. Polymerization of microtubules is nucleated in a microtubule organizing center (MTOC). The MTOC contains another type of tubulin, γ-tubulin, which is distinct from the α and β subunits. The γ-tubulin combines with several other associated proteins to form a circular structure known as the γ - TUBULIN RING COMPLEX. This complex acts as a scaffold for α/β tubulin dimers to begin polymerization; it acts as a cap of the minus end and microtubule growth continues in the plus end away from the MTOC.

During polymerization, both the α- and β-subunits of the tubulin dimer are bound to a molecule of GTP. The GTP bound to α-tubulin is stable, but the GTP bound to β-tubulin may be hydrolized to GDP shortly after assembly. The kinetics of GDP-tubulin is different from those of GTP-tubulin; GDP-tubulin is prone to depolymerization. A GDP-bound tubulin subunit at the tip of a microtubule will fall off, though a GDP-bound tubulin in the middle of a microtubule cannot spontaneously pop out. Since tubulin adds onto the end of the microtubule only in the GTP-bound state, there is generally a cap of GTP-bound tubulin at the tip of the microtubule, protecting it from disassembly. When hydrolysis catches up to the tip of the microtubule, it begins a rapid depolymerization and shrinkage. This switch from growth to shrinking is called a catastrophe. GTP-bound tubulin can begin adding to the tip of the microtubule again, providing a new cap and protecting the microtubule from shrinking. This is referred to as rescue. Numerous ligands also bind to tubulin affecting their assembly properties during the creation of microtubules.

MICROTUBULE-ASSOCIATED PROTEINS (MAPS) are proteins that interact with the microtubules of the cytoskeleton. MAPs bind in a nucleotide-insensitive manner to the MT lattice. They stabilize and promote the assembly of MTs. Their functions include both stabilizing and destabilizing microtubules, guiding microtubules towards specific cellular locations, cross-linking microtubules and mediating the interactions of microtubules with other proteins in the cell. MAPs weakly increase the polymerization rate of pure tubulin, strongly suppress catastrophes, and promote rescues. MAPS bind to the tubulin and this binding can occur with either polymerized or depolymerized tubulin, and in most case leads to the stabilization of microtubule structure, further encouraging polymerization. Neuronal MAPs weakly increase the polymerization rate of pure tubulin, strongly suppress catastrophes, and promote rescues (*Desai and Mitchison, 1997*). The net effect of these changes is to reduce the turnover rate and increase the fraction of tubulin in polymer at steady state. Usually, the C-terminal domain of the MAP interacts with tubulin, while the N-terminal domain binds with cellular vesicles, intermediate filaments or other microtubules. The tubulin-binding sites in neuronal MAPs often consist of repeated motifs (*Lewis et al., 1988*), and these cross links have the effect of suppressing subunit dissociation and, perhaps, also inhibiting protofilament peeling, thus inhibiting catastrophe and promoting rescue. MAP-microtubule binding is regulated through MAP phosphorylation. This is accomplished through the function of the microtubule-affinity-regulating-kinase (MARK) protein. Phosphorylation of the MAP by the MARK causes the MAP to detach from any bound microtubules. This detachment is usually associated with a destabilization of the microtubule causing it to fall apart. In this way the stabilization of microtubules by MAPS is regulated within the cell through phosphorylation.

RECEPTORS PROTEINS: It is now accepted that neural cells sense chemical signals that indicate a direction for growth, a process called CHEMOTAXIS. A myriad of guidance cues which are secreted or present on the surface of the growth cone serves as lighthouses for the wandering

filopodia thereby allowing neurons to find the right target and establish the appropriate synaptic connections. They could also be repulsive factors that initiate signals to remodel the growth cone cytoskeleton (*Huber et al., 2003; Luo, 2002*). For example, the contact of a single filopodium with a guidance cue (which could also be another neuron or filopodia) is sufficient to redirect axonal elongation either toward or away from the point of contact. Netrins, Semaphorins, Slits and Ephrins are the most well-known factors controlling axon growth and guidance. They bind to specific receptors on the growth cone surface and initiate signals to remodel the growth cone cytoskeleton (*Huber et al., 2003; Luo, 2002*). Netrins are diffusible guidance molecules mediating long or short range chemoattraction or chemorepulsion. Semaphorins are membrane bound or secreted guidance molecules. Slits are secreted guidance molecules. Ephrins are membrane (e.g. the extracellular matrix) bound guidance molecules. Thus, the formation, extension and retraction of these structures represent important dynamic processes that regulate cell motility in a wide variety of contexts.

Rho-family GTPases (i.e., Rho, Rac, and Cdc42) are involved in axonal guidance (*Luo et al., 1997, and Gallo and Letourneau, 1998*) and growth cone responses to collapsing guidance cues (*Jin and Strittmatter, 1997; Kuhn et al., 1999*). They also mediate the formation of lamellipodia and filopodia, even though it is still not clear whether they act as switches activating the mechanisms underlying cell surface protrusion or whether they also regulate the dynamics of extension and retraction of filopodia and lamellipodia.

Additional actin-associated proteins (e.g. gelsolin) may be involved in more specific aspects of leading edge protrusion and retraction (*Letourneau, 1996; Stossel, 1993*) such as retraction of growth cone filopodia without altering filopodial protrusion (*Lu et al., 1997*). The identification of specific actin or microtubule regulatory elements and their involvement in the responses to extracellular signals will be of particular importance in elucidating the regulation of neuronal growth cone motility.

MOTOR PROTEINS: Motor proteins are molecular machines that convert chemical energy into mechanical work. This is achieved by hydrolyzing ATP and the energy thus released is used to generate forces and power cellular motility (*Howard, 2001*). They utilize the cytoskeleton for movement and fall into two categories based on their substrates along which they move or "walk".

- ACTIN MOTORS: Actin motors move along microfilaments through interaction with actin.

  MYOSINS are actin motors and form myosin complexes consisting of two heavy chains with motor heads and two light chains. By non-processively walking along actin filaments, many molecules of myosin generate enough force to contract muscle tissue. Myosins are also vital in the process of cell division. They are also involved in cytoplasmic streaming, wherein movement along microfilament networks in the cell

allows organelles and cytoplasm to stream in a particular direction. Eighteen different classes of myosins are known.

- MICROTUBULE MOTORS: Microtubule motors move along microtubules through interaction with tubulin. There are two basic types of microtubule motors: plus-end motors and minus-end motors, depending on the direction in which they walk along the microtubule cables within the cell.

  KINESINS are a group of related motor proteins that use a microtubule track along which to walk. They generally move towards the plus end of the microtubule. They are vital to movement of chromosomes during mitosis and are also responsible for shuttling mitochondria, Golgi bodies, and vesicles within eukaryotic cells. Kinesins typically contain two heavy chains with motor heads which move along microtubules which can be towards the plus-end or the minus-end, depending on the type of kinesin. Fourteen distinct kinesin families are known, with some additional kinesin-like proteins that cannot be classified into these families.

  DYNEINS are microtubule motors capable of a sliding movement. They generally move towards the minus end of the microtubule. Dynein complexes are much larger and more complex than kinesin and myosin motors. Dynein facilitates the movement of cilia and flagella. Compared to 15 types of dynein for this function, only two cytoplasmic forms are known.

Pharmacological agents that disrupt the actin cytoskeleton cause defects in the growth and guidance of the axon (*Marsh and Letourneau, 1984; Letourneau et al., 1987; Chien et al., 1993; Kaufmann et al., 1998*), whereas contact with preferred substrates causes focal bursts of actin accumulation at the site of interaction that leads to a redirection of the growth cone (*Lin and Forscher, 1993; O'Connor and Bentley, 1993*). There are many other proteins which affect microtubule behavior, such as catastrophin, which destabilizes microtubules, katanin, which severs them, and a number of motor proteins that transport vesicles along them.

MICROTUBULE-ACTIN INTERACTION: In the neuronal growth cone, a sharp, highly dynamic interface exists between growing microtubules in the axon shaft, and peripheral actin networks. Directed axon guidance depends on coordinated interactions between microtubules and actin filaments in growth cones. During axon guidance, actin based motility is harnessed to promote microtubule growth and steering. Individual unbundled microtubules invade the actin-rich peripheral domain and appear to display properties of dynamic instability. Microtubule growth and shortening may activate Rac1 and RhoA signaling, respectively, to control actin dynamics. Microtubule dynamics are necessary for converting actin-based motility into directed, persistent growth. Dampening dynamics of microtubules also inhibits growth cone turning in

response to guidance cues. Immunofluorescence studies have also noted striking coalignment of filopodial actin filament bundles with microtubules in growth cones. Thus, an actin-dependent gradient in microtubule dynamic-instability parameters in cells may feed back through the activation of specific signaling pathways to perpetuate the polarized actin assembly dynamics required for cell motility.

2.3. EXPLORATION BY GROWTH CONES

During neuronal differentiation, neurites are guided towards their final target by molecular cues that are sensed by filopodia and lamellopodia. Filopodia explore the environment by rapidly moving in all directions, searching for the correct pathway and lamellipodia follow, opening the way to the growing neurite. It is also well known that in both developing and mature brain, spines are being continuously formed and pruned (*Engert and Bonhoeffer 1999; Maletic-Savatic, Malinow and Svoboda 1999; Ahmari and Smith 2002; Fonseca, Nagerl and Bonhoffer, 2006*) and it is not surprising that filopodia growth and retraction also occur in a dense medium, but this exploration is restricted and filopodia move primarily along specific paths where the local density of biological material is less pronounced. The formation of new spines, synaptic terminals and dendritic arboritazion in a dense tissue requires the generation of significant forces, which must be well planned and computed. During long term potentiation, a sophisticated biochemical and genetic program is activated but the insertion of new biological structures in synapses and dendrites requires a careful mechanical computation performed by the actin network and controlling proteins (*Cingolani and Goda, 2008*).

A quantitative characterization of forces exerted by neurons during neuronal differentiation is necessary for understanding this motility and the precise role of molecular motors. The use of optical tweezers has facilitated the study of the way filopodia and lamellipodia interact with its surrounding. To mimic/duplicate the natural environment of a growth cone, a bead (diameter of 1 μm) is usually used to simulate an obstacle in our experiments.

In vitro experiments (*Janson, de Dood and Dogterom, 2003; Kerssemakers et al., 2006; Footer et al., 2007*) have established that polymerization-driven force generation can take place without additional proteins (even though in the living cell, other proteins are required). In such experiments, monomeric subunits of actin or tubulin are loaded into a membrane vesicle and polymerization is initiated by various means (such as warming the solution in the case of tubulin or increasing the ionic strength in the case of actin). The growing polymers do work against the membrane's elasticity thereby deforming the vesicle. Forces in the range 1 to 4 pN have been inferred from these polymerizing and depolymerizing experiments performed by various groups over the years.

In vivo experiments performed in our laboratory has demonstrated that filopodia cannot exert forces larger than 2-3 pN (*Cojoc et al., 2007*) while lamellipodia are able to exert forces one order higher (upto 20 pN). Therefore, filopodia act as "feelers" that gently probe the environment while the lamellipodia are able to generate higher force to remove obstacles in the path of the growing neurite.

2.4. MECHANICAL COMPUTATION IN NEURONAL GROWTH CONES

Due to the nature of the electrical and chemical signals for the transmission, processing and exchange of information and the complexity of its branched form, a single neuron has the processing power of a high-speed calculator. Neural networks can rival computer processors in the extraction and manipulation of information due to the exceptional levels of interconnectivity and the parallel processing abilities. Even the most powerful computers available today have not reached the processing power of a single human brain, not to mention the plasticity that allows brain circuits to adapt rapidly to a changing environment.

To achieve the connectivity that gives the neural networks incomparable processing powers, the neuron must navigate its way through the maze of organic matter and it is this navigation that exemplifies the intelligent behavior of a single cell. Neurons have the constant necessity to solve computational as well as mechanical problems. Growth cones need to explore the environment, establish the appropriate contacts, avoid obstacles, decide in which direction to grow and how much force to exert.

The random exploration of the environment by filopodia and their reaction when an obstacle is encountered is coupled to a variety of feed-back loops. These feedback loops are constituted by guidance molecules and their receptors which are present on the growth cone membrane. These receptors are tightly coupled to the cytoskeleton and to the internal cytoskeletal machinery. For example, when a signal is detected by the appropriate receptor, the filopodia, acting like mechanical devices, gently penetrate the environment and lead the way for the more robust lamellipodia, thereby undergoing phenomenon like the growth cone turning. The combination of a random exploration with efficient feed-back loops provides the basis of what is proposed in first part of this thesis as MECHANICAL COMPUTATION, a strategy based on random trials, but with an efficient feedback able to correct errors. Using this optical procedure, neurons establish appropriate physical and chemical contacts, migrate to their final destination, enlargement or reduction of spines and synapses, etc.

The two major issues that will be addressed are:

i. the strategy used by filopodia and lamellipodia during their exploration and navigation, and
ii. the kind of mechanical problems neurons need to solve during their operation.

2.5. APPROACHES TO STUDY EXPLORATORY BEHAVIOR OF NEURONS

Many approaches have been adopted in order to study the exploratory behavior of growth cones and their correlation to navigation and establishment of neural contacts. The method of computer-assisted tracing of neurons has a long history and the tools to quantify neuronal motility from time-lapse images of dynamic growth cones are in constant development. Systematic studies of lamellipodial behavior have been achieved by using kymograph analysis (*Mongiu et al., 2007*) and in studies examining growth cones guided by laser light (*Betz et al., 2007*). Most available procedures need human interaction, but significant progress in levels of accuracy and automation has been achieved (*Al-Kofahi et al., 2002; He et al., 2003; Meijering et al., 2004; Zhang et al., 2007*). Comparatively, examination of filopodial dynamics has relied on manual tracking of individual filopodia; a prohibitively time-consuming approach for large-scale analysis. Neurite-tracing algorithms varying in complexity and accessibility have also been developed over many years (*Capowski, 1989*) that automatically recognize and trace long extensions such as axons, dendrites and neurites from consecutive images sequences from a stack of images acquired with techniques such as the Confocal Microscope. Some recent studies include quantitative analysis of motility and neurite extension rates (*Endo et al., 2003, 2007*) but these studies consider the movement of the growth cone as a whole and changes in filopodial extension are considered over long-time scales by manual analysis.

Live imaging of growth cones in culture has emerged as a powerful tool to study growth cone responses to guidance cues but the dynamic nature of the growth cone requires careful quantitative analysis. Space time kymographs have been developed as a tool to quantify lamellipodia dynamics in a semi-automated fashion but no such tools exist to analyze filopodial dynamics. But most approaches utilize fast acquisition and sacrifice the real volumetric exploration. Thus, a method to precisely assess the 3-D filopodial dynamics in time is still lacking.

An optimal exploration requires a sampling of the surrounding environment evenly in space and time, and is achieved by an orchestrated growth and retraction of neighboring filopodia complemented by their ability to lift up their tips. In this thesis, we will present an approach to describe the exploratory behavior of growth cones. By analyzing the dynamics the 3-D kinetics and dynamics of filopodia observed in their natural state and without any pharmacological treatment we will extract information regarding the exploratory behavior and correlate this behavior to the navigation and establishment of contacts. We will also provide solutions from a computational point of view in order to strengthen our findings.

3. MORPHOLOGY OF GROWTH CONES

The growth cone is often compared to a human hand because of their similarities. The peripheral region of a growth cone consists of a palm-like lamellipodium from which finger-like filopodia extrude. It is now established that the filopodia is almost entirely made up of actin filaments, and the lamellipodium consists of a network of actin filaments. But a study on the growth cone is not complete without a description of its morphology.

In recent years, there has been an increase in the application of different techniques on biological samples, the most common example being microscopy. Atomic Force Microscopy (AFM) is a powerful tool for imaging, manipulating, and force mapping that provides a high resolution (up to nanometer precision) measurement of the shape - size, height and surface irregularity - of a biological sample, and in our case of growth cones and its main features, the lamellipodia and filopodia. The process by which AFM obtains the topographical information of the sample under investigation is via the interaction i.e., the repulsion or attraction between the probe and the sample. The probe is typically a tip at the free end of a silicon cantilever and scans the region of interest. A small laser, focused on the cantilever, detects small deflection of its tip, providing therefore a precise measurement of the distance between the tip and the sample. The result is an image of interaction values providing a three-dimensional (3D) map of the sample height. This information provides a precise characterization of the surface topography of the sample under investigation. Similarly, the Laser Scanning Confocal Microsope (LSCM) is a very handy tool for biologists as it offers a variety of information from fluorescently labeled matter, and many research studies have been augmented by exploiting the LSCM. For studying live events, the CCD cameras offer one of the best time resolution, and studies that require fast acquisition such as synaptic events like calcium signaling or calcium signaling events often use these devices.

However, each system requires different software for handling the set-up which also means that the results, most commonly images, are in different formats so that comparison of details is often not trivial. Thus, the use of different techniques for the acquisition of images often causes complications and it is not obvious how to superimpose them so that relevant parameters can be compared directly. Moreover, the use of such invasive techniques can also often be unhelpful since the tip of the probe or the cantilever used touches the sample and can alter and misrepresent the topology of imaged neurons. Even though such side-effects are finding utilization as in the case of nano-surgery, the morphology of neurons can not be accurately described unless this problem is resolved and one comes up with a way to study the morphology, and its consequences, without coming in contact with the sample.

There have been many attempts to provide a simple, elegant and efficient solution to this problem. Methods have been developed over the years to compare small details such as filopodia by following images of a moving biological structure in time. This is convenient only if small

details are imaged, such as filopodia (*McNally et al., 2005*) or if high temporal resolution is not required (*Yunxu et al., 2006*). Hence, there is a requirement for a tool that can reduce the images acquired with different techniques into comparable formats and hence make it easier to extract and correlate information after eliminating any possible distortions to avoid representing data as misleading results. For this purpose, we investigated and developed a technique to overcome these restrictions.

3.1. REGISTRATION OF IMAGES: CONCEPT

The problem of comparing two images intelligently has been extensively addressed in the field of Computer Vision particularly in Medical Imaging and is referred to as REGISTRATION. Registration is the process of geometrically aligning two or more images of the same event taken at different time points, and/or by different imaging systems. The differences between the images could be due to the difference of imaging conditions. Image registration is a crucial step in all image analysis tasks in which the final information is gained from the combination of various data sources like in image fusion (*Zitova and Flusser, 2003*). Images taken from different systems may undergo an affine deformation (linear deformation in scale, translation, rotation and sometimes shearing). The use of confocal microscopes for imaging different fluorescent structures also makes automatic registration difficult as the images would not necessary correlate.

The word REGISTRATION is used with two different meanings (*Hill et al., 2001*). The first meaning is to determine a transformation of one image so that features in the sensed image can be put in a one-to-one correspondence to features in the reference image; the second meaning enables also the comparison of the intensity at corresponding positions which incorporates the concepts of re-sampling and interpolation. In our approach and analysis, the first meaning of registration is used and the procedure is described in the following sections.

3.2. 0 pN FORCE IMAGE

The use of techniques such as AFM has facilitated studies on biological samples mainly due to the high resolution it offers. Thus information of the shape, size, height and surface irregularities can be obtained precisely with nanometer resolution. But as pointed out earlier, the fact that the AFM cantilever tip touches the sample to collect this information is a source of misinformation. The minimal force required to acquire a stable height map of a sample is of the order of 100 pN and higher scanning forces tend to press the more flexible structures. In order to eliminate this problem, a procedure to obtain the 0 pN force image was developed. This uses *spline* interpolation of the pixel intensities obtained at different forces. The procedure is discussed in detail in the later sections. This image provides an accurate description of the

sample. This procedure can also be used to obtain the height map at any desired scanning force. In that case, one should interpolate between the available scanning force and the desired one.

3.3. CHARACTERIZATION OF MORPHOLOGY

Using the procedures outlined above, we combined different techniques (*Kondra et al., 2009*) for a qualitative study on the morphology of the neuronal growth cone. When imaged with AFM, the outer membrane of DRG growth cones often exhibits significant morphological structures which are termed "invaginations" or "holes". They could not be seen with conventional optical microscopes. These invaginations or holes are structures similar to craters and are reminiscent of those described by Godement et al. (*1994*) and Mason and Erskine (*2000*) in *in vivo* retinal ganglion axons, presumably originating from the fusion or contact of lamellar extensions of the growth cone with glial processes. We have not been able to determine why they form, but ongoing work suggests a correlation of the formation of these topographical structures with the exploratory state of the growth cone. This section of the thesis aims to:

- provide a characterization of these holes, and
- correlate these structures with cytoskeletal components.

4. AIMS OF THE THESIS

The present thesis provides a description of the studies that were carried out on neuronal growth cones with the aim to:

- understand the strategy used by filopodia and lamellipodia during their exploration and navigation,
- correlate the motion for an efficient exploration of the environment,
- determine the kind of mechanical problems neurons need to solve during their operation,
- provide a characterization of these holes, and
- correlate these structures with cytoskeletal components.

5. METHODS AND PROCEDURES FOR DATA EXTRACTION AND ANALYSIS

In this section, how data is extracted from the raw images and analyzed is described. It is divided into two sub-sections: the first one provides an explanation of the how the mechanical computation in neurons is studied; the second section gives a description of how the morphology of the growth cone is studied after eliminating deformations caused by the techniques used.

In order to study and analyze the motion of filopodia, different type of cultures were used (all procedures are described in detail in the previous section):

- DRG neurons were grown in culture and DIC images were obtained with a confocal microscope,
- PC12 cell are treated with NGF to induce differentiating and DIC images of filopodia coming in contact with each other were obtained with a confocal microscope,
- Hippocampal neuronal cultures were grown for two weeks and then transfected. Images were obtained with a confocal microscope.

For the analysis, the backbone of every visible filopodium is recovered. Using this information various quantities such as degree of bend of the filopodia, correlation in growth and retraction, and percentage of volume explored are calculated.

RECOVERY OF FILOPODIUM BACKBONE: Once the time lapse movies of images are acquired, they are processed using an operator assisted program in MATLAB to recover the 3D backbone of the filopodia. To do this, each portion of filopodia in focus at a particular focal plane is marked respectively by the user and is repeated for all the frames (each frame is a z-stack of usually four images taken at 0, 1, 2 and 3 μm above the coverslip). Spline interpolation is then performed on the series of discontinuous lines. In this way, one gets the 3D backbone of the filopodium (red dots in Figure 5.1).

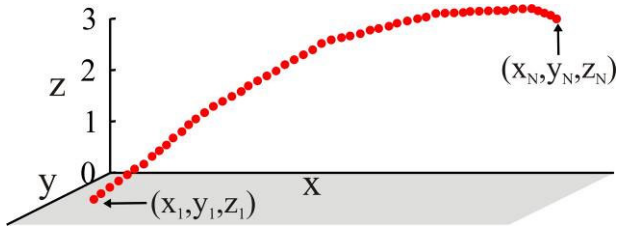

Figure 5.1: Reconstruction of the filopodial backbone

If each filopodium is considered to be made up of N points, that is (x_1,y_1,z_1) … (x_n,y_n,z_n)… (x_N,y_N,z_N), then the distance and the (total) length between the endpoints (x_1,y_1,z_1) and (x_N,y_N,z_N) are given by:

$$D = \sqrt{(x_N - x_1)^2 + (y_N - y_1)^2 + (z_N - z_1)^2}$$

$$L = \sum_{n=1}^{N-1} \sqrt{(x_{n+1} - x_1)^2 + (y_{n+1} - y_1)^2 + (z_{n+1} - z_1)^2}$$

The length thus calculated gives an idea about the length of the filopodia. It has been established that the persistence length of actin filaments in vivo is in the order of 9 µm (*Isambert et al., 1995*), and thus the length of filopodia, on an average, cannot be more than this value. Indeed, our calculations give results very close to this value.

DEGREE OF BENDING: After the backbones of the filopodia are recovered, the ratio between the values of D and L is calculated. This gives information about the rigidity of the motion of filopodia and can be classified into three classes: Rigid (with $D/L \approx 1$), lateral motion (with $0.8 > D/L > 1$) and bending (with $D/L < 0.8$). Rigidly moving filopodia are those that grow or retract typically in only one direction. They may or may not change their orientation with respect to the lamellipodium. Those filopodia that are sweeping across freely without much bend in their backbones are understood as filopodia in lateral motion. Finally, the class of filopodia with a bend of more than 165º is classified as bending filopodia. Of all the filopodia that were examined, 29% were rigidly moving, 18% were in lateral motion and 32% were bending. The remaining 21% could not be classified into any of these categories (Figure 5.2).

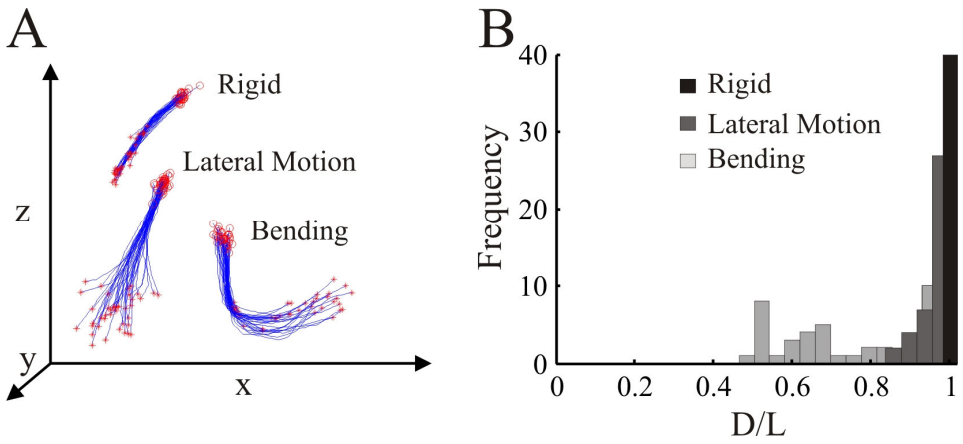

Figure 5.2: Classification of filopodia on degree of bending. A: Representative filopodium of the different classes. B: Frequency distribution of the ratio D/L for three classes of filopodia

CORRELATION OF GROWTH AND RETRACTION: In order to establish if there is any correlation in the growth and retraction of neighboring filopodia and among filopodia of the same growth cone, the correlation coefficient ρ_{ij} of the change in the length of two filopodia, not necessarily neighbors (such as those shown in Figure 5.3), are calculated (Figure 5.4) using the following formula:

$$\rho_{ij} = \frac{E[(x-\mu_i)(y-\mu_j)]}{\sqrt{E[(x-\mu_i)^2]E[(y-\mu_j)^2]}}$$

where, E[**.**] is the average value of **.** computed over all frames 1,…,N; and μ_i and μ_j are the mean values of the lengths x_i and y_j over all frames 1…N. ρ_{ij} could be positive or negative indicating correlated and anticorrelated growth respectively. In order to establish the existence of correlated or anticorrelated growth, two thresholds corresponding to ±0.15 and ±0.5 were considered (see Table 5.1). If the absolute value of ρ_{ij} was less than 0.15, the motion of filopodia was considered uncorrelated.

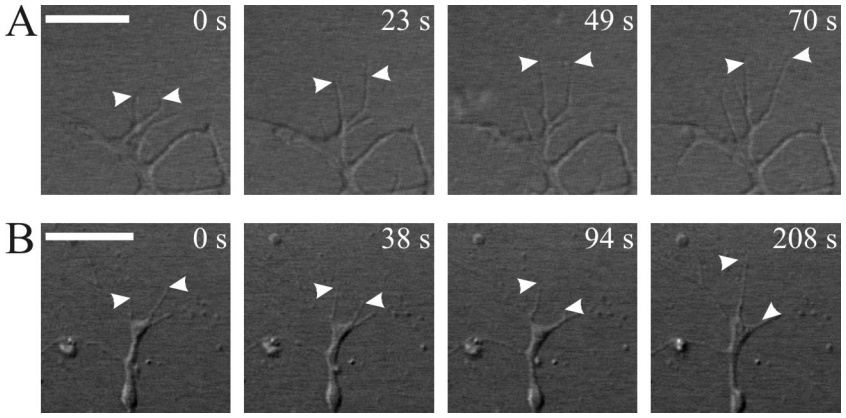

Figure 5.3: Selected frames of a growth cone with two filopodia (indicated by white arrows) growing in a correlated way (**A**) and growing in an anti-correlated way (**B**) Scale bar: 10 µm.

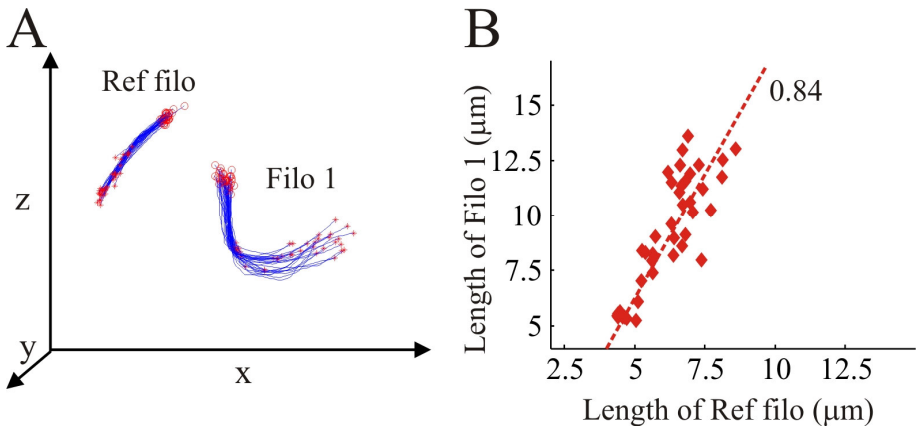

Figure 5.4: Correlation in growth/retraction between two filopodia. **A:** Example of two filopodia. **B:** Changes in length of the filopodia *Filo 1* was positively correlated to the changes in length of the filopodium *Ref filo*.

Table 5.1: Percentage of correlated filopodial growth in different neuronal growth cones

Type of neuron	Percentage of filopodia with (ρ is correlation coefficient) (A = Anticorrelated; C = Correlated)		
	Uncorrelated $\|\rho\|<0.15$	Moderately correlated $0.15\leq\|\rho\|\leq0.5$	Correlated $\|\rho\|<0.50$
DRG (n=19; 1271 pairs)	18.3	42.9 20.9 (A) + 22 (C)	38.8 14.1 (A) + 24.7 (C)
PC12 (n=6; 6432 pairs)	43.3	43.3 25.7 (A) + 17.6 (C)	13.4 1.4 (A) + 12 (C)
Hippocampal (n=7; 185 pairs)	38.4	39.8 28.2 (A) + 11.6 (C)	21.8 1.5 (A) + 20.3 (C)

GLOBAL CORRELATION OR ORCHESTRATION: If filopodia grow and retract in a random independent way, there will be pairs of filopodia whose growth is correlated and other pairs will be anticorrelated, as shown in Figures 5.3. In order to verify the existence of an orchestrated behavior of filopodia emerging from the same growth cone, the following statistical test was performed:

Consider that at frame *n* there are *N(n)* filopodia emerging from the same growth cone and that their average length is $\langle l \rangle_n$. If growth and retraction of these filopodia are completely independent - and therefore there is no correlation or orchestrated pattern - and if σ_l is the standard deviation of their length, the standard deviation of $\langle l \rangle_n$ - computed over all frames n - $\sigma_{\langle l \rangle n}$ is expected to be equal to $\sigma_l / \sqrt{N(n)}$. This is a simple consequence of statistical properties of independent random variables. If $\sigma_{\langle l \rangle n}$ is consistently less than $\sigma_l / \sqrt{N(n)}$, then the growth and retraction of filopodia is not independent but has global orchestration or correlation.

The results of this analysis are shown in Fig 5.5.

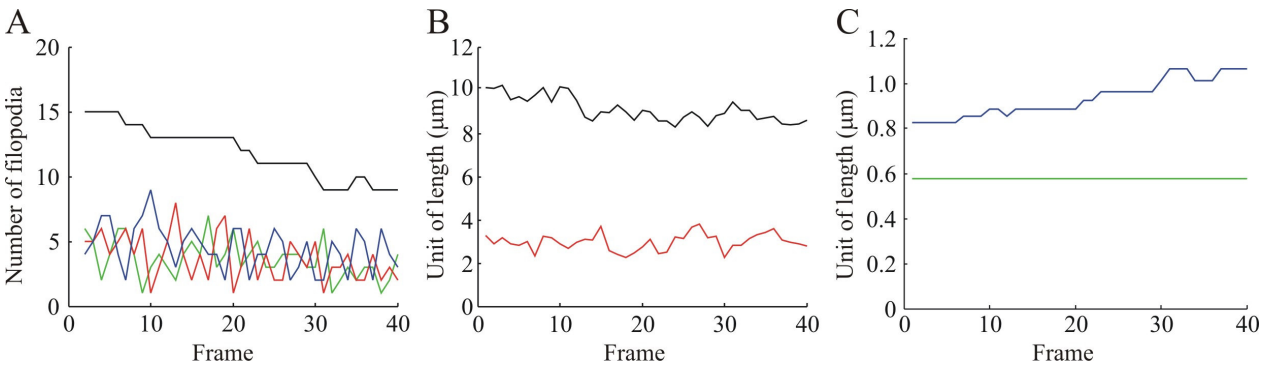

Fig. 5.5: Global orchestration or correlation. **A**: Number of filopodia (black) emerging from a growth cone at each frame. Green, red and blue lines indicate the number of growing, retracting and stationary filopodia. **B**: Mean $\langle l \rangle_n$ (black) and standard deviation σ_l (red) of filopodia length at each frame. **C**: Comparison between $\sigma_l / \sqrt{N(n)}$ (blue trace) and $\sigma_{\langle l \rangle n}$ (green)

The black trace in Fig. 5.5A shows the total number of filopodia emerging from the growth cone at each frame. A significant portion of these filopodia grow (green), retract (red) and some are stationary (blue). As shown in Figure 4E, the value of $<l>_n$ (black) was stable around a mean value of 9.1 μm and its standard deviation $\sigma_{<l>n}$ was equal 0.6 μm. The value of σ_l computed over all filopodia present at each frame varied around 3.2 μm, as shown by the red line in Fig. 5.5B. This value is in agreement with the standard deviation computed over all filopodia emerging from all 19 considered growth cones and reported in the text. As shown in Figure 5.5C, the value of $\sigma_{<l>n}$ (green) was significantly less than the value of $\sigma_l/\sqrt{N(n)}$ (blue) which varied between 0.8 and 1.1 μm. The same statistical analysis performed on all growth cones (n=19) indicated that the value of $\sigma_{<l>n}$ was less than the value of $\sigma_l/\sqrt{N(n)}$ in 18/19 growth cones. These results show that growth and retraction of filopodia follow an orchestrated pattern, by which the average filopodia length is maintained stable, more than what expected from simple independent fluctuations.

EXPLORATION OF LOCAL ENVIRONMENT: The neuronal growth cone must carefully scan the local environment in search of target. In order to study this behavior, the volume explored by neurons is calculated. Two types of neuronal cultures are used: sparse DRG neuronal cultures and dense cultures of hippocampal neurons. In DRG neuronal cultures, the growth cones are in a free environment, i.e., there are no restrictions to the movement of the filopodia or lamellipodia. In the case of hippocampal neuronal cultures, the movements of these growth cone components are restricted as they are spread over an uneven surface of glial cells and neurons and thus the filopodia are exploring in a confined environment. In this case, we used the following calculation to estimate the volume that surrounding cells exclude (all numbers come from unpublished data and their analysis):

The mean diameter of the hippocampal neuronal cell body is 8 ± 2 μm and the volume of the dendritic tree is 3-7 times the volume of the soma (average value is 5.4±1.3 μm^3). Thus, the total volume occupied by 25±15 cells (from DAPI staining, DAPI stains all nuclei indiscriminately) is:

$$\left(\frac{4}{3}\pi(8\pm 2)^3\right)\cdot(1+(5.4\pm 1.3))\cdot(25\pm 15)\,\mu m^3$$

Considering the thickness of the culture to be 50±15 μm, the volume of an area of 100 x 100 μm^2 is:

$$100\cdot 100\cdot 50\pm 15\,\mu m^3$$

Hence, the volume excluded by all cell types is between 37 and 79% of the total volume, indicating that the filopodia of dense hippocampal neuronal growth cone can explore just 21 to 63% of the total volume available.

- **EXPLORATION OF FREE SPACE:** The starting and end points of all filopodia of DRG usually lie on the perimeter of a circular sector with inner radius *R* and an outer radius *R+A*, where *R* corresponds approximately to the radius of the growth cone and *A* is the maximal length of filopodia. If *C* is the centre of this circular sector (see Figure 5.6), filopodia starting and end points cover approximately an angle θ. Therefore, the explored 3D space at frame n is defined as

$$Free(n) = h \cdot \pi((R+A)^2 - R^2) \cdot \frac{\theta(n)}{2\pi}$$

where, *h* is the maximal height to which the filopodium tip can arise, estimated to be 3 µm. $\theta(n)$ depends on the frame *n* whereas *R* and *A* are assumed to be constant. The explorable 3D space *ExplFree* is the maximum value of *Free(n)* over the entire image sequence *n*=1,…, *N* and the fraction of explored free space at frame *n* is

$$Free(n)/ExplFree.$$

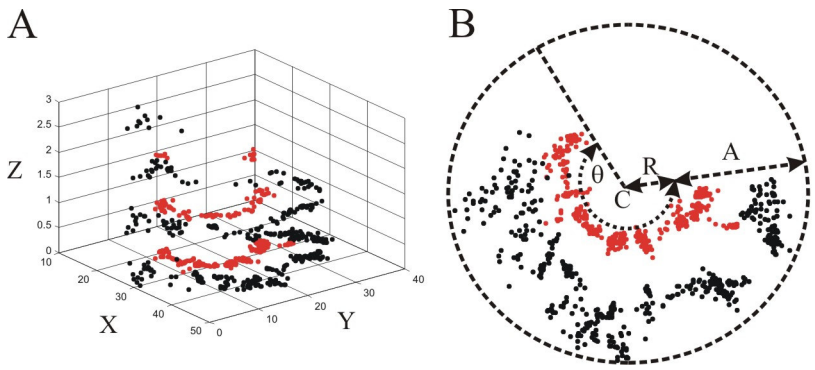

Figure 5.6: Determination of the explorable and explored space around a growth cone. **A**: Red and black points are the starting and end points respectively of DRG filopodia identified during 10 minutes of observation. **B**: Determination of the explored free space by filopodia of a growth cone in a free environment.

- **EXPLORATION OF DENSE ENVIRONMENT:** For Hippocampal neurons, the explorable free space around a growth cone is assumed to be

$$ExplDense = \frac{4}{3}\pi((R+A)^3 - R^3)$$

i.e. the volume of a sphere of radius R+A minus the volume of the sphere of radius R.
In these cultures, the explored space $Dense_{cyl}(n)$ at frame *n* is defined in the following way: for each filopodia *i*, we consider the segment S_{in} joining the starting $s_i(x,y,z,n)$ and ending point $e_i(x,y,z,n)$ and draw the cylinder Cyl_{in} with axis S_{in} and radius R_{cyl}. The radius R_{cyl} is assumed to be the standard deviation of lateral filopodia fluctuations corresponding to approximately 1 µm as measured by video microscopy. The volume of the cylinder that each filopodium explores is

$$Cyl_i = \pi.R_{cyl}^2.L_i$$

and the explored space at frame n, $Dense_{cyl}(n)$, is defined as

$$U_i \, Cyl_{in},$$

where U is the union operator.

The fraction of explored free space at frame n is given by

$$Dense_{cyl}(n)/ExplDense.$$

MECHANICAL COMPUTATION: A computational framework is required to understand the kinetics and dynamics of filopodia and lamellipodia. Following the classical view that a computation is the solution to a problem, pseudo-codes able to solve mechanical problems are introduced. To accomplish this, we propose that the apparent random exploration by the filopodia of a neuronal growth cone is coupled to feed-back loops, which are constituted by-

- the factors controlling axon growth and guidance, such as neutrophins, morphogens and molecules of extracellular matrix,
- the receptors present on the growth cone membrane which detect these factors, and
- the consequent activation of a signaling cascade within the growth cone.

These feedback loops are responsible for the rapid formation of physical contacts when two filopodia tips with appropriate receptors meet, or for the rapid retraction of a filopodium when a stiff obstacle is encountered. The combination of a random exploration with efficient feed-back loops which continuously correct errors provides the basis of what we propose to be MECHANICAL COMPUTATION: the process by which neurons establish appropriate physical and chemical contacts, migrate to their final destinations, enlarge and/or prune spines and synapses, etc. In order to appreciate how the combination of a random search and feedback loops can lead to the efficient solution of mechanical problems, let us consider three scenarios: obstacle avoidance, formation of physical contacts and obstable removal.

OBSTACLE AVOIDANCE: For simplicity, consider an idealized filopodium tip moving on a square grid, with the origin (0,0) in the upper left corner. The filopodium tip starts at an initial point on line 0 (such as (0,13)) and its goal is to reach any point on line -20 avoiding the obstacles shown in Figure 5.5. The pseudo-code able to perform this mechanical computation is:

1 Move from (m,k) to (m,k+1)
If an obstacle is encountered, retract to (m,k)
and move with p=½ to to (m-1,k) or to (m+1,k)
Go to 1

The program is composed of one simple reaction, i.e., the instruction to move, and one feed-back loop, i.e., the instruction to retract if an obstacle is encountered (indicated by the bold lines) and by random searches (indicated by the underlined line). A filopodium tip following this

program avoids obstacles and is able to reach its final destination (Figure 5.7) following a simple trajectory.

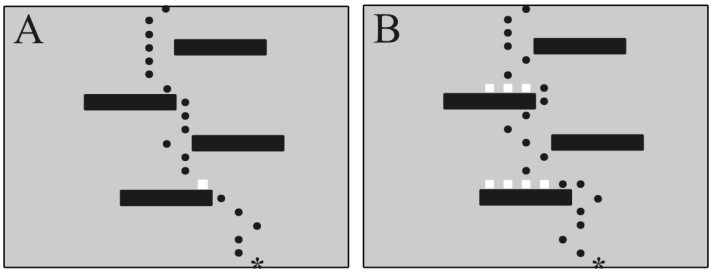

Figure 5.7: Obstacle avoidance: filopodium tip avoiding obstacles (black bars) and reaching the final destination (black star). Moves- black circles; retractions- white squares. **A:** Trajectory with a low number of moves. **B:** Trajectory with several retractions and a high number of moves.

FORMATION OF PHYSICAL CONTACTS: Consider two idealized growth cones each composed of two filopodia (Figure 5.8) so that when one filopodium grows the other one retracts- This correlated behavior can be formalized by assuming that the length of the two filopodia l_1 and l_2 satisfies the relation $l_1 + l_2 = L$ where L is a fixed length. We assume also that one filopodium has at its tip a receptor R_1, able to form a physical contact with the tip of a different filopodium with the same receptor R_1. Another filopodium has at its tip receptor R_2 which can form a physical contact with filopodia bearing at their tips the same receptor R_2. The exploratory motion of all these four filopodia is random but it is constrained by the condition that $l_1 + l_2 = L$. The mechanical computation to be solved is the formation of a physical contact between the filopodia tips with the same receptor R_i. The pseudo-program able to perform this mechanical computation is:

1 *The tip of filopodium 1 of growth cone 1 moves from* (n_1,m_1) *to* (n_1+i,m_1+j) *with probability* $p_{i,j}$
The tip of filopodium 2 of growth cone 1 moves from (k_1,h_1) ***to*** (k_1+i,k_1+j) ***so that*** $l_{1,1}+l_{2,1}=L$
The same for growth cone 2
If filopodia tips with the same receptors meet in the same location go to 2
Go to 1
2 ***Formation of a physical contact***
Stop

where, the parameter "i" is constrained to single grid jumps, i.e. i=[-1,0,1]. The simple reactions/feed-backs and random searches are indicated in the same style as in the previous pseudo-program.

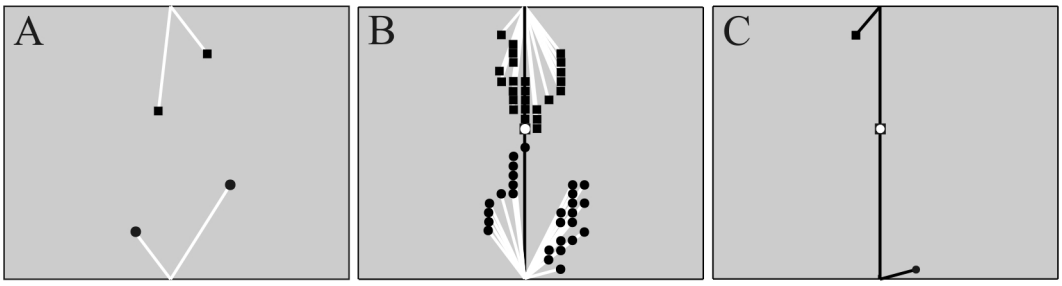

Figure 5.8: Formation of physical contacts. **A:** Initial configuration of two idealized growth cones (black squares and black circles) with two filopodia each. **B**: Representative configurations of the two growth cones before the formation of a physical contact. The total length of filopodia in each growth cone is constant. **C**: Final configuration after the filopodia tips meet (white circle coinciding with black square).

OBSTACLE REMOVAL: Consider a slightly more complicated mechanical computation: a lamellipodium besides retracting or avoiding obstacles also displaces them. At each cycle, the lamellipodium can exert a force $F_1<F_2<...F_i<\ldots<F_n$. Obstacles have varying stiffness $S_1<S_2<,\ldots S_j<...<S_n$ (indicated by the numbers on the black/grey bars in Figure 5.9) and can be displaced when the lamellipodium exerts a force $F_i>S_j$. For this task, when an obstacle is encountered, the lamellipodium has to choose between two options: to retract towards one of the possible directions or to try to exert a force F_i and see whether it will displace the obstacle. If the maximum force exerted by the lamellipodium is not strong enough to displace the obstacle, the lamellipodium will retract.

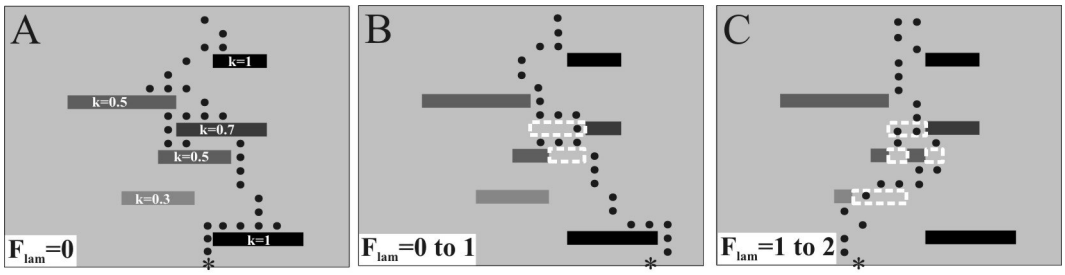

Figure 5.9: Obstacle avoidance and removal. F_{lam} denotes force exerted by the lamellipodium. Each obstacle (black bar) has a stiffness ranging from 0 to 1, as indicated. Force and stiffness are in the same arbitrary units. **A**: Trajectory of a lamellipodium avoiding obstacles and reaching the final destination (black star), corresponding to line 20. **B&C**: Trajectories of a lamellipodium able to displace obstacles. The lamellipodium can exert forces varying from 0 to 1 (**B**), and from 1 to 2 (**C**). The lamellipodium can displace an obstacle and then it could retract, see some cases in **B** and **C**. Removed obstacles are shown as dotted white boxes.

IMAGE REGISTRATION: In order to study and analyze the morphology of neuronal growth cones, comparisons are made between images taken with an AFM and a LSCM to correlate structural details with cytoskeletal components. Before imaging with AFM or LSCM, DRG neurons were fixed. In order to verify that the observed structural details were not caused by the specific fixation method, two fixation procedures were used and compared: with Paraformaldehyde and Glutaraldehyde. After fixing, LSCM images are acquired first, and then the growth cone is scanned with AFM using increasing scanning forces (from 100 pN to 2000 pN) and then again with the lowest scanning force to verify that the structure is still intact and not destroyed by the multiple scanning. To compare different images, REGISTRATION is first performed by determining a transformation of one image so that features in the sensed image can be put in a one-to-one correspondence to features in the reference image.

The procedure of IMAGE REGISTRATION is as follows: If (x,y) is the system of reference of image A and (x',y') the system of reference of image B, the transformation T from A to B is defined as:

$$\begin{bmatrix} a1 & a2 & t_x \\ a3 & a4 & t_y \\ c1 & c2 & 1 \end{bmatrix}$$

where,

$\begin{bmatrix} a1 & a2 \\ a3 & a4 \end{bmatrix}$ is a rotation matrix which defines the kind of the transformation that will be performed, which in our case consists of scaling, rotation, and translation,

$\begin{bmatrix} t_x \\ t_y \end{bmatrix}$ is the translation vector (which simply moves the points), and

$[c1 \quad c2]$ is the projection vector, used for projective transformations. For affine transformations, as those used here, c1 and c2 are zero.

If x and y are the coordinates of a point, the transformation can be done by the simple multiplication:

$$\begin{bmatrix} a1 & a2 & t_x \\ a3 & a4 & t_y \\ c1 & c2 & 1 \end{bmatrix} \times \begin{bmatrix} x \\ y \\ 1 \end{bmatrix} = \begin{bmatrix} x' \\ y' \\ 1 \end{bmatrix}$$

Here, x' and y' are the coordinates of the transformed point.

The unknown parameters in the transformation matrix can be estimated either by matching a selected number of points or landmarks in the two images or by matching entire contours in the two images. POINTS SELECTION METHOD (Figure 5.10) is used when it is possible

to identify enough points in the two images corresponding to the same physical structure, such as the tip of a dendrite, or a small vesicle. PROCRUSTES ANALYSIS is used when rounded biological structures are present, with no obvious marks and it is more convenient to put in correspondence two contours and not isolated points.

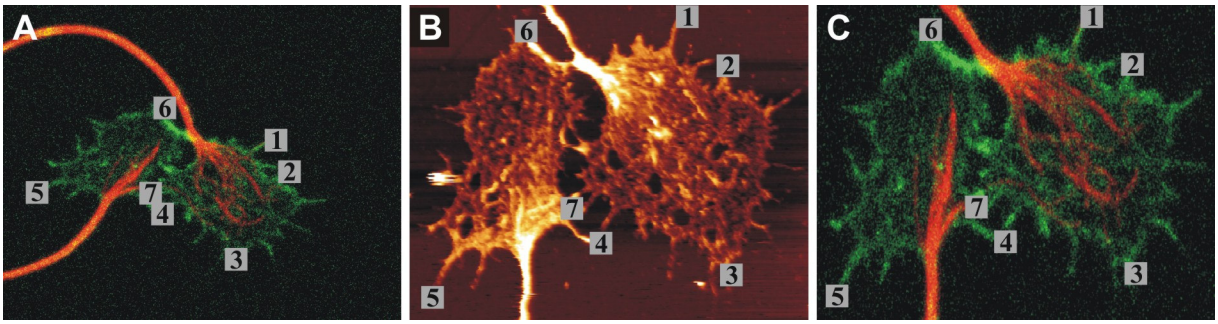

Figure 5.10: Registration of LSCM Image with respect to AFM image. **A**: Original Confocal Image of a growth cone with Alexa488 Phalloidin for Actin and anti-β tubulin III, followed by Alexa594 anti-mouse IgG. **B**: AFM scanning of the same growth cone. **C**: Confocal image after registration with AFM scan.

0 pN FORCE IMAGE: To eliminate any distortion caused by the scanning tip, the 0 pN force image of the AFM series is obtained. To do this all the images in the series are registered and a stack is assembled. Using this stack, extrapolation (using *spline* interpolation function in MATLAB) is performed to obtain the corresponding 0 pN image. This is repeated for different series and for growth cones fixed using different protocols and this serves as a database for extrapolating other images. If comparisons are to be made between two images of different growth cones taken at a different scanning forces, first the corresponding 0 pN force image and the image at the second scanning force (i.e., the scanning force of the second image) are obtained from the series (or otherwise using the database). A function (a 4^{th} degree polynomial) relating these two images and the 0 pN force image of the first growth cone is found. Using this function, the 0 pN scanning force image for the second image of the other growth cone is obtained. Comparisons can then made between the 0 pN force images of the two growth cones. In this way, any deformation due to the scanning probe is eliminated.

The procedure is as follows:

1. Acquire AFM image series from the minimum scanning force to the maximum scanning force.
2. Register all the images with respect to the image acquired with minimum scanning force. Assemble a stack of the register images.
3. Use *spline* interpolation of the pixel intensities at different forces to obtain the 0 pN force image.

If comparisons are to be made between two images of different growth cones taken at a different scanning forces:

1. Obtain the corresponding 0 pN force image of one series first. Also obtain the image at the second scanning force (i.e., the scanning force of the second image). If there is no series, use the database.
2. Find 4^{th} degree polynomial function which relates these two images (Figure 5.11).
3. Use this function to obtain the 0 pN scanning force image for the second image of the other growth cone.

Comparisons can then made between the 0 pN force images of the two growth cones. In this way, any deformation due to the scanning probe is eliminated.

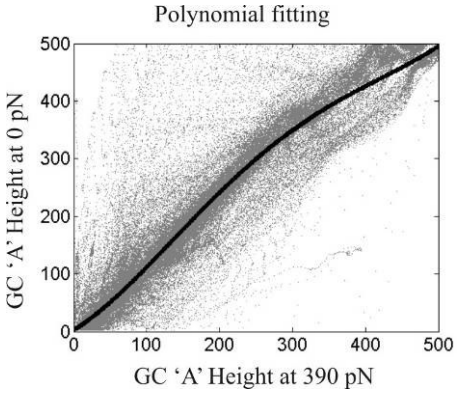

Figure 5.11: Data fitting to obtain a relation between values of AFM height of growth cone 'A' taken at 0 pN and at 390 pN of the image series.

INVAGINATIONS AND HOLES: When imaged with AFM, the DRG neuronal growth cone often exhibit significant invaginations and holes. To characterize these holes, first an algorithm inspired by Computer Vision, known as SNAKE ALGORITHM (Figure 5.12), was applied to the image: an approximating closed region Γ around the growth cone is selected by the user. Application of the snake algorithm drives Γ to the boundary of the growth cone. This separates the growth cone from the background.

The procedure described below was used to detect holes (once again using the SNAKE ALGORITHM) and analyses them (using a graphical interface written in Matlab) (The MathWorks Inc. http://www.mathworks.com):

1. Display AFM image where the intensity corresponds to height.
2. Choose threshold *Th*. *Th* is usually set to 15% of the maximum intensity value of the image.
3. Define a region *R* of the AFM image as a hole if the following conditions are fulfilled:

a. Intensity averaged over *R* (Int(*R*)) is less than *Th*. As AFM images intensity corresponds to height, this procedure is equivalent to set a threshold on its average height,
b. Area of *R* is less than 5% of the total area of the base of the growth cone.
c. *R* is completely surrounded by a non-hole (hilly) region.

False positives are eliminated using these conditions. True holes are shown in Figure 5.10 C.

4. Repeat Step 2 and 3 with increasing values of Th till no holes can be found.
5. Merge all the holes found with all the different values of the threshold.
6. Calculate base area. Scale to real dimension (μm^2 in our case).
7. Calculate height of the 'hill' as the height of a sector of width of 5 pixels surrounding the hole. This gives the depth of the hole. Scale to real dimension (nm in our case).
8. Calculate height of the hole as the difference between the mean height of the 'hill' surrounding the hole and the mean height of the hole i.e., the threshold used to find the holes.
9. Perform triangulation of surface/height given by the AFM image and find area of each triangle. The sum gives total area of the surface. Scale to real dimension (μm^2 in our case).
10. Ratio of total area to base area indicates the texture of the surface: if close to 1, surface is flat and devoid of holes, whereas higher values indicate a surface with many holes.
11. Determine other parameters as required.

If *R* has been classified as a hole, we consider a sector *S* of width of 5 pixels surrounding *R* and the depth or height of the hole *R* is defined as Int(*S*)- Int(*R*). Hole area is calculated as the area of the region *R*, scaled to real dimensions. Holes found this way are shown in Figure 5.10. These holes are then characterized according to their depth and size.

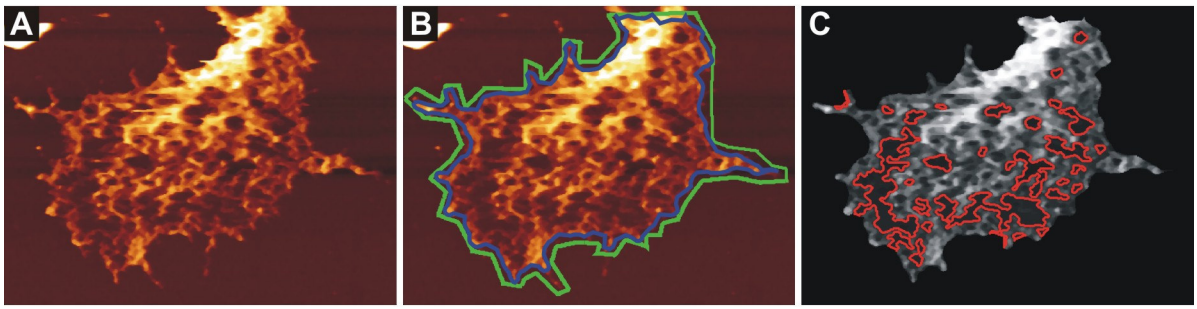

Figure 5.12: Defining holes. A: Original AFM image. B: Selection of growth cone for calculation by Snake Map. C: True holes found after calculation (i.e., below threshold).

Table 5.2: Hole statistics:

Parameters	PFA (n = 6)	GLU (n = 7)	Both fixation protocols (n = 13)
Height Range	2 to 128 nm	2 to 178 nm	2 to 178 nm
Average Height	57 ± 23 nm	45 ± 21 nm	51 ± 23 nm
Base Area of Holes Range	0.04 to 2.3 μm^2	0.01 to 3.5 μm^2	0.01 to 3.5 μm^2
Average Base Area	0.19 ± 0.17 μm^2	0.26 ± 0.24 μm^2	0.22 ± 0.20 μm^2

For each growth cone, we defined and measured the following parameters:

- the *total area* (T), defined as area of the entire growth cone, including the hole walls and various invaginations (i.e., sum of area of the triangles representing the surface approximated by Delaunay triangulation);
- the *base area* (B), defined as the area of the growth cone projected on the XY-plane;
- the *invagination value*, I, a parameter defined as: $I = \frac{T}{B \cdot H_{max}}$, where H_{max} is the maximum height of the growth cone.

A more invaginated growth cone has more folds on the surface and thus this ratio, I, is high (Table 5.3). Two different fixation procedures were also used to eliminate the fixative as a cause of these morphological characteristics (Table 5.3).

Table 5.3: Comparison of parameters from growth cones fixed using the two different Protocols:

Fixation Method	AFM Image	Total Surface Area (μm^2)	Total Hole Area (μm^2)	Base Area (μm^2)	Total Area/ Base Area	Number of Holes	Maximum Height of Holes (nm)	I
PFA	Image-1	599	14	132	4.2	55	200	2.1
	Image-2	136	7	33	4.1	16	140	3
	Image-3	603	51	143	4.2	29	160	2.6
	Image-4	765	108	187	4.1	20	160	2.6
	Image-5	520	46	127	4.1	19	150	2.7
	Image-6	245	10	55	4.5	60	250	1.8
	Average	478±239	39.3±23	112.8±57	4.2±0.16			
GLU	Image-11	1137	30	270	4.2	59	400	1.1
	Image-12	965	144	232	4.2	37	250	1.7
	Image-13	280	17	62	4.5	9	500	0.9
	Image-14	187	9	41	4.6	10	500	0.9
	Image-15	395	62	93	4.3	9	450	1
	Image-16	161	19	37	4.4	70	400	1.1
	Image-17	670	43	159	4.2	16	800	0.5
	Image-18	95	0	19	5	No holes	650	0.8
	Image-19	144	0	32	4.5	No holes	650	0.7
	Average	448.2±285	36.1±23	105±45	4.4±0.3			

COMPARISON WITH IMMUNOFLUORESCENT IMAGES: In order to correlate the measured height with the cytoskeletal components of the analysed growth cones, immunofluorescent techniques were applied where actin is fluorescently label with Alexa488 phalloidin and tubulin with anti-β tubulin III, followed by Alexa594 anti-mouse IgG. In this way, the correspondence of the observed invaginations with the internal cytoskeletal structure, and in particular with the presence or absence of actin filaments and/or tubulin, could be easily visualized. LSCM scanning were performed first on the fluorescently labeled growth cone. 4-7 slices of fluorescence images were acquired with a step size of 500 nm. The stack of these images was then averaged and used for further analysis. AFM was then performed on the same growth cone. Acquired AFM and averaged LSCM images were registered as described earlier. Analyses (Table 5.4) using these two types of images and correlating the information content (Figure 5.13) show that regions of the growth cone with a height more than 100 nm exhibiting a significant co-localization with the staining of actin filaments and tubulin, indicating that these proteins act as pillars inside the growth cones, while holes show poor co-localization with actin filaments and microtubules.

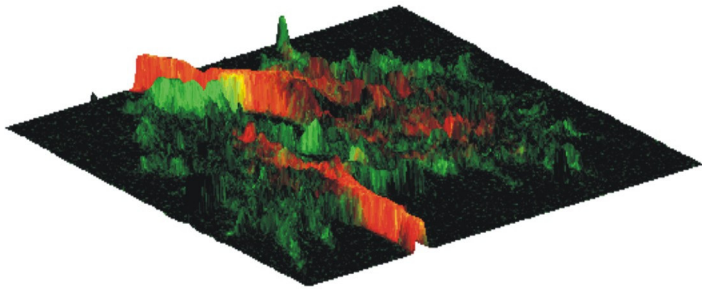

Figure 5.13: 3D view of the information from the two images superimposed.

Table 5.4: Comparison of Actin Tubulin Ratio in growth cones:

Parameters	Image-1	Image-3	Images-4	Image-5	Average ± Standard Deviation
Tubulin inside holes (%)	18	2	6	3	7 ± 7
Actin inside holes (%)	13	18	19	15	16 ± 3
Actin + Tubulin outside holes (%)	55	60	64	62	60 ± 4
Tubulin/Actin ratio of entire growth cone	1.47	0.57	1.05	0.67	
Tubulin Height (nm)	146	162	109	127	136 ± 22
Actin Height (nm)	115	112	79	94	101 ± 16
Tubulin Height /Actin Height	1.27	1.44	1.37	1.35	1.36 ± 0.07

6. TECHNIQUES

This section provides a detailed description of the different techniques used to study the different topics outlined in this thesis.

6.1. PREPARATION OF CELL CULTURE

DORSAL ROOT GANGLION NEURONS (DRG): Wistar rats (P10–P12) were anesthetized with CO_2 and sacrificed by decapitation in accordance with the Italian Animal Welfare Act. DRGs were isolated and incubated with trypsin (0.5 mg/ml), collagenase (1 mg/ml), and DNase (0.1 mg/ml) in 5 ml Neurobasal medium (NBM; Invitrogen) in a shaking bath (37°C, for 35 to 40 minutes). They were mechanically dissociated, centrifuged at 300 rpm and resuspended in culture medium. Dissociated cells were plated on poly-L-lysine-coated (PLL; 0.5 μg/ml) coverslips in NBM supplemented with 10% fetal bovine serum (FBS).

PC12 NEURONS (Pheochromocytoma): PC12 cells were plated on PLL and Matrigel (BD Biosciences, Bedford, MA, USA) coated glass coverslips in RPMI medium supplemented with 5% horse serum and 2.5% FBS. 100 ng/ml NGF (Alomone, Israel) was added to the medium to induce differentiation.

HIPPOCAMPAL NEURONS: Hippocampal neurons were isolated from P0-P2 rats as previously described in Bonifazi et al. (*2005*). Cells were plated on polyornithine (Sigma)/matrigel-coated coverslips and maintained in Minimal Essential Medium with Earle's salts (Invitrogen) supplemented with 5% fetal calf serum, 0.5% D-glucose, 14 mM Hepes, 0.1 mg/ml apo-transferrin, 30 μg/ml insulin, 0.1 μg/ml D-biotin, 1 mM Vit.B12, and 2 μg/ml gentamycin (all supplements were purchased from Sigma). 48 hours after plating, 5 μM cytosine-β-D-arabinofuranoside (Ara-C) was added to the culture medium, in order to block glial cell proliferation. Medium change was performed twice a week.

DRG neurons and PC12 cells were plated at a density of ~10^4 cells/ml. Hippocampal neurons were plated at a density of $8x10^5$ cells/cm^2. All neuronal cultures were kept in an incubator providing a controlled level of CO_2 (5%), temperature (37°C) and moisture (95%).

6.2. FIXATION PROTOCOLS

Before imaging with LSCM or AFM, DRG neurons were fixed. In order to verify that observed structural details were not caused by the specific fixation method, two fixation procedures were used and compared: fixation with Paraformaldehyde and with Glutaraldehyde.

FIXATION USING PARAFORMALDEHYDE: DRG neurons were fixed by incubating in 4% paraformaldehyde in phosphate buffer saline (PBS) for 20 min at room temperature (RT), rinsed

in PBS, and incubated in blocking solution (consisting of 5% fetal bovine serum, 0.3% Triton X-100 in PBS) for 30 min at 37°C.

FIXATION USING GLUTARALDEHYDE: DRG neurons were perfused 3 times with 0.25% glutaraldehyde in buffer solution (consisting of 100 mM Cacodylate (pH 7.4), 5 mM $CaCl_2$ and 10 mM $MgCl_2$) and incubated in buffer solution for 10 minutes at 37°C (*Rochlin et al., 1995*).

6.3. IMMUNOFLUORESCENCE AND TRANSFECTION

IMMUNOFLUORESCENCE: After fixation, DRG neuronal cultures were washed 4X with PBS and then incubated for 30 minutes at RT with the monoclonal antibody TUJ1 (Covance, Berkeley, CA, USA; 1:500 dilution in blocking solution), which recognizes the neuron specific Class III β-tubulin. After washing 2X, cultures were incubated for another 30 minutes RT with Alexa Fluor 594 anti-mouse antibody (Molecular Probes; 1:300 dilution) and Alexa Fluor 488 Phalloidin (Sigma-Aldrich, 1:10 dilution). Nuclei were stained with DAPI (Boehringer Mannheim GmbH, Germany; 1:1000 dilution). After washing, the coverslips were mounted in Vectashield (Vector Labs., Burlingame, CA, USA).

TRANSFECTION: Hippocampal neurons were transfected with pEGFP-N1 (CloneTech, Palo Alto, CA, USA) after 8 to 11 days in vitro (DIV) using the Ca^{2+}-phosphate method (*Köhrmann et. al., 1999*) and live imaging of moving growth cones was performed 2-5 days after transfection. To determine the cell density, parallel hippocampal cultures were immunolabeled (protocol described above) with the anti-β tubulin III antibody TUJ (Covance, USA; 1:750 dilution) and counterstaining with DAPI as previously described (*Bonifazi et al., 2005*). At the time point chosen for live imaging of growth cones, the total cell density was 960±110 cells/mm^2 and the neuron density was 570±75 neurons/mm^2.

6.4. CONFOCAL MICROSCOPY

The SET-UP consists of a Leica DMIR2 confocal microscope, equipped with Diode laser 405nm, Ar/ArKr, He/Ne, He/Ne 633 lasers. The microscope has objectives with magnifications of 10X (dry), 20X (dry), 40X (glycerin-immersion), 40X (1.44 NA oil-immersion) or 63X (1.44 NA oil-immersion). The set-up is also equipped with a temperature control and a brick that infuses the chamber with 70 Ml/hr O_2 and 70 Ml/hr CO_2 maintaining their levels at 19.4% and 7.8%.

PROCEDURE: The plated neurons were transferred to a chamber that fit the imaging apparatus. Prior to the transfer, the chamber was left on for some time (usually 10 minutes) so that the level of gases and the temperature are adequate to maintain the culture in a healthy state. To acquire images of non-transfected growth cones, the microscope was set in DIC configuration. Usually the Ar/ArKr laser was used and the light source set at 11% of its maximal power so to

reduce neuronal damage. Stacks of four images were acquired at different focal planes (0, 1, 2 and 3 μm above the glass where the neurons were plated) with a 63X, 1.4 NA oil immersion objective every 5-10 seconds, for 12 to 35 minutes. To acquire images of transfected growth cones, the appropriate laser is used to excite the fluorochrome and the laser source was set at 25% of its maximal power so to reduce neuronal damage.

6.5. ATOMIC FORCE MICROSCOPY

The SET-UP consists of a commercial AFM (Nanowizard II, JPK Berlin) combined with an inverted optical microscope (Zeiss Axiovert 200), and a fluorescence set-up (Zeiss X-cite). Soft tips from VEECO with low force constant (OBL, 0.03 N/m) were used. AFM scanner position sensors detect the position of the tip with an accuracy of 2-3 nm and AFM images were acquired using the commercial Software (DirectOverlay, JPK, Berlin).

PROCEDURE: Neurons fixed on 24 mm diameter glass coverslips were mounted on the AFM liquid cell, filled with PBS solution and mounted onto the AFM microscope. After laser alignment and tip calibration, the system was left to settle for 30 minutes with laser and microscope condenser on, to minimize thermal and force drift during image acquisition. AFM was operated in contact mode in liquid medium, adjusting the contact force of the cantilever tip during imaging to minimize the force exerted by the tip on the sample during scanning. The cantilever tips were kept between 100 pN and 1 nN during scanning.

6.6. OPTICAL TWEEZERS

The SET-UP consists of an inverted microscope (NIKON TE2000-E) fit with a Peltier device to maintain the temperature of the neuronal culture at 37°C. A 1064 nm fiber laser was used and an oil immersed microscope objective (Nikon; 100X, NA=1.4) was used to visualize the growth cones. Images were acquired with a CCD camera (Epix, VCA1281 sensor) at 10 kHz.

PROCEDURE: A dish containing differentiating neurons was positioned on the stage of the microscope. Before acquisition, the Peltier device was left on for some time (usually 10 minutes) so that the appropriate temperature was reached. The dish was then maintained at 37°C. A laser beam from a laser diode was corrected, expanded and collimated to match the entrance pupil of the microscope objective. A dichroic mirror deflected the laser beam to the objective, allowing upcoming light to image the sample with a CCD camera. Bead position was determined either using video imaging with the CCD camera and/or with a QPD positioned in the back focal plane of the condenser. Another dichroic mirror deflected the laser light towards the QPD.

7. RESULTS

7.1. *Mechanical Computation in Neurons* (article under revision. Full MS: Appendix 1.)

Authors: Jummi Laishram, Daniela Avossa, Rajesh Shahapure, Vincent Torre

ABSTRACT: Growth cones are the main motile structures located at the tip of neurites and are composed of a lamellipodium from which thin filopodia emerge. In this manuscript, we analyze the kinetics and dynamics of growth cones with the aim to understand two major issues: firstly, the strategy used by filopodia and lamellipodia during their exploration and navigation; secondly, what kind of mechanical problems neurons need to solve during their operation. In the developing nervous system and in the adult brain, neurons constantly need to solve mechanical problems. Growth cones must decide how to explore the environment and in which direction to grow; they also need to establish the appropriate contacts, to avoid obstacles and to determine how much force to exert. Here we show that in sparse cultures, filopodia grow and retract following statistical patterns, nearly optimal for an efficient exploration of the environment. In a dense tissue, filopodia exploration is still present although significantly reduced. Analysis on 1271, 6432 and 185 pairs of filopodia of DRG, PC12 and Hippocampal neurons respectively showed that the correlation coefficient $|\rho|$ of the growth of more than 50% of filopodia pairs was larger than 0.15. From a computational point of view, filopodia and lamellipodia motion can be described by a random process in which errors are corrected by efficient feedback loops. The present manuscript argues that neurons not only process sensory signals, but also solve mechanical problems throughout their entire lifespan, from the early stages of embryogenesis to adulthood.

RESULTS:

- Filopodia grow and retract for an efficient exploration of the environment.
- High degree of correlation in growth and retraction.
- Filopodia and lamellipodia behavior when encountering obstacles show statistical patterns.
- Filopodia can exert forces of the order of a 2-3 pN while lamellipodia can generate a much higher force (up to 20 pN).
- Filopodia in a dense environment are also able explore their surrounding, although their exploration is restricted ($4 \pm 4\%$ vs. $66 \pm 24\%$ of the space available).
- Average velocity of the tips of filopida in dense environment is slower than those in a free environment (0.06 ± 0.04 μm/s vs. 0.4 ± 0.3 μm/s).
- Neurons are similar to mechanical devices able to solve computational problems.

7.2. *A morphological analysis of growth cones of DRG neurons combining Atomic Force and Confocal Microscopy* (article under revision. Full MS: Appendix 2.)

Authors: Jummi Laishram, Shripad Kondra, Daniela Avossa, Elisa Migliorini, Marco Lazzarino, Vincent Torre

ABSTRACT: We have analyzed the morphology of growth cones of differentiating neurons from rat dorsal root ganglia (DRG) with conventional Laser Scanning Confocal Microscopy (LSCM) and Atomic Force Microscopy (AFM). Images of immunofluorescent DRG growth cones colabeled for actin and tubulin were superimposed to images obtained with AFM at different scanning forces. In order to reduce changes of the image surface caused by the pressure of the AFM tip, we have developed a procedure to obtain 0 pN AFM images. Further analysis of these images revealed topographical structures with nanoscale dimensions, referred to as "invaginations" or "holes". These holes had an area varying from 0.01 to 3.5 μm^2 with a depth varying from 2 to 178 nm. Comparative analysis with LSCM images showed that these holes correspond to regions where staining of both actin and tubulin was negligible. Filopodia height varied from 40 to 270 nm and their diameter from 113 to 887 nm. These results show that the combination of LSCM and AFM reveal structural details with a nanoscale dimension of DRG growth cones, difficult to resolve with conventional microscopy.

RESULTS:

- *Registration* is used as a method to compare two images taken with different modalities.
- 0 pN force image was developed to reduce deformations of the surface caused by imaging system.
- "Invaginations" or "holes" of nanoscale dimensions are found on the surface of neuronal growth cones.
- We establish that the observed holes are not introduced by the fixation procedure used.
- Characterization of holes show that they have a height ranging from 2 to 178 nm, with a base area ranging from 0.01 to 3.5 μm^2
- Comparison with data from confocal imaging show absence of major cytoskeletal components in these holes.

8. DISCUSSION AND CONCLUSIONS

8.1. MECHANICAL COMPUTATION IN NEURONS

The understanding of the nervous system and its basic unit, the neuron, cannot be considered complete without a quantification of the behavioral pattern. Although, much is known about the intricacies of synapse formation, and the formation and activity of neuronal networks, there is little or no information on the global behavior of the neuronal growth cone as a entity. Studies on the mechanical, chemical and physical properties of the individual actin and microtubule filaments have been complimented by experimental results. But the exploration by filopodia has never been quantified before and there is no statistical information about their behavior. Valuable information about the pattern of behavior and of the volume explored can be obtained by observing how they behave and interact with their environment and how they explore the 3D world in their neighborhood.

In the course of the thesis, we tried to understand if there is any significance in the motion of the filopodia. Observations show that when filopodia and lamellipodia encounter solid, unyielding obstacles while exploring, their reaction appears to follow different patterns.
An isolated filopodium after collision reacts by

- completely retracting,
- retracting partially and branching into a new filopodium, or
- colliding lightly with the obstacle and continue growing.

Similarly, a lamellipodium also reacts by

- colliding with the obstacle and continuing its motion by growing underneath it,
- removing or displacing it in a “shovel like” fashion, or
- retracting.

After data extraction and analyses employing commonly used techniques and statistical analyses, we observed that-

- filopodia in a dense environment explore less than 10 times than those in a free environment (4 ± 4% vs. 66 ± 24% of the space available),
- there is a high correlation in growth and retraction among filopodia of a growth cone of the order of 0.5 or more,
- filopodia in a dense environment move 5-8 times slower than those in a free environment (0.06±0.04 μm/s vs 0.4±0.3 μm/s),
- when encountering obstacles, filopodia and lamellipodia show stereotypical reactions,
- filopodia can exert forces of the order of a 2-3 pN while lamellipodia can generate a much more higher force (up to 20 pN),

- computational models show that the growth cone behaves like a mechanical system able to solve simple calculations.

It is now widely accepted that the filopodia of a growth cone act 'feelers' that explore the environment and this exploratory motion seems random. The fact that filopodia must scan the local environment in search of their destination suggest that they must explore in the most efficient way possible. That they do so is indicated by the high degree of correlation in their growth or retraction.

While filopodia in both free and dense environment explore their environment, the fraction explored is very different: hippocampal filopodia in a dense culture explores about 10 times less than that explored by DRG filopodia in an almost free environment. This difference could be due to the fact that DRG are peripheral sensory neurons while hippocampal neurons are from the central nervous system and have different membrane receptors and motor proteins. In addition, DRG neurons are plated on a glass coated with poly-L-lysine while hippocampal neurons grow on top of other cells, hence their growth cones move on or within the extracellular matrix.

When exploring, filopodia and lamellipodia often encounter obstacles and their reaction appears to follow stereotyped patterns. After collision, an isolated filopodium either completely retracts, or partially retracts and branches new filopodia, or lightly collides with the obstacle exerting forces of the order of 2-3 pN maximum and continues its growth. Similarly, a lamellipodium either collides with the obstacle and continues its motion by growing underneath it, or removes it in a "shovel like" fashion exerting forces up to 20 pN, or retracts. We have not been able to determine when and how a given reaction is chosen or decided and we propose that the choice is the result of a random process leading to a trial and error procedure. These reactions are likely to be mediated by receptors located at the filopodia and lamellipodia tips, such as the integrins, which are coupled to the cytoskeleton acting as signaling transducers and also helping the neuron to attach to the extracellular matrix or to other cells (*Hynes, 2002*). Indeed, a strategy based on random trials, but with an efficient feedback able to correct errors, can be an optimal procedure for the mechanical computation used by neurons.

It is interesting to note the existence of correlation among filopodia, considering the high number of filopodia that an exploring growth cone has at any given time and considering the apparent random behavior. This implies critical planning and pooling of available resources and signals for efficient exploration of the local environment. The computational models in this thesis show existence of an efficient system in which inputs from the environment are continuously being processed and appropriate responses are constantly being sent back to the filopodia. Thus, the ideas proposed and quantified in this thesis give insight to the otherwise untouched subject of volume exploration by a neuronal growth cone.

The notion of mechanical computation which is proposed here is related - to some extent - to information processing and neuronal computation in biological systems. Information processing in neuronal networks has been studied extensively over the past 50 years from the pioneering work of Warren McCulloch and William Pitts (*McCulloch and Pitts, 1943; Lettvin et al., 1959*). Neuronal computation is usually meant as the elaboration of sensory signals - originating from a variety of receptors - their storage and retrieval. Information processing is a major component of neuronal computation and it is primarily based on networks of interacting neurons. Elementary components of neuronal computation are neurons, possibly dendrites (*Koch et al., 1983*) and even spines (*Koch and Poggio, 1983*). Properties of neuronal computation have been investigated thoroughly in experiments, simulations and theoretical analyses often based on information-theoretic approaches (*Dayan and Abbott, 2001*). Parallel processing of elementary operations, such as summation, multiplication and division is at the basis of neuronal computation. The proposed notion of mechanical computation is not based on information-theoretic approaches but stems from the classical notion of computation as developed in Logics and Computer Science.

8.2. MORPHOLOGICAL ANALYSIS OF GROWTH CONES

In order to eliminate discrepancies introduced by the imaging system used, we have introduced and applied two concepts to study the morphology of neuronal growth cones:

- registration of images: the procedure to accurate match corresponding structures in images of biological samples taken with different imaging systems, and
- 0 pN force image: the procedure to reduce possible, if not eliminate, deformations of the surface caused by the AFM tip during scans on the sample under consideration. Thus, it reduces the dependence of the morphology on the force of the scanning tip used.

Further analysis of the 0 pN force image of the growth cone revealed invaginations or holes which are nanometric structures. We used two different fixation procedure to eliminate the fixative used a possible cause of these structures. In order to quantify the smoothness of a surface, we defined and measured a parameter *invagination value*:

$$I = \frac{T}{B \cdot H_{max}}$$

where, T is the total area defined as the area of the entire growth cone, including the hole walls and various invaginations,
B is the base area defined as the area of the growth cone projected on the XY-plane,
H_{max} is the maximum height of the growth cone.

A low value of the parameter, *invagination value* I (around or less than 1) indicates a smooth external surface and a higher value of this quantity is found for growth cones with many holes having a significant height. The *invagination value* for all tested growth cones fixed with either PFA or GLU, varied from 0.5 to 3.

Through polymerization, microtubules grow from the central region towards the peripheral region and where the plus ends interact with the filopodia coordinating cell movement. Comparison with LSCM images showed that more than 80% of the hole area lacks actin filaments or microtubules. Further, the mesh-like network of actin filaments and microtubules is confirmed through statistical analysis of the growth cones. Analyses (Table 5.4) show that regions of the growth cone with a height more than 100 nm exhibiting a significant co-localization with the staining of actin filaments and tubulin, indicating that these proteins act as pillars inside the growth cones, while holes show poor co-localization with actin filaments and microtubules. The tubulin to actin ratio over the entire growth cone tends to fall into two categories (Table 5.4): values around 0.5 indicating an extensive actin network, and values larger than 1 indicating a network composed of a significant microtubule branching. In the region where tubulin staining is present, the mean height is 136±22 nm and the mean height of the region with actin staining is 101±16 nm. Irrespective of the branching of the microtubule network, the ratio of the tubulin height to actin height has an average of 1.36±0.07 over the entire growth cone.

Although there have been many reports on the use of AFM on biological samples, and on neurons in particular (*Parpura et al., 1993; Bonfiglio et al., 1995; Ohshiro et al., 2000; Zhang et al., 2004; Yunxu et al., 2006; Grzywa et al., 2006*), the novel nanometric structures that we observed were not described in previous investigations with AFM. Holes observed in the present investigation are not caused by the AFM tip and are not introduced by the method of cell fixation used. Irrespective of the fixation procedure, these holes typically have a mean height ranging from 2 to 178 nm (Table 5.3), with the base area ranging from 0.01 to 3.5 μm^2 with an average of 0.22±0.20 μm^2 per growth cone. We have not been able to determine why they form, but ongoing work suggests a correlation of the formation of these topographical structures with the exploratory state of the growth cone.

Together, the two procedures described here provide an exceptional approach to explore and study the nanometric world of biological samples. In our studies, the higher vertical resolution offered by AFM revealed structures not observed with conventional imaging systems, while LSCM images allowed us to associate these structures with cytoskeletal components. The combination of two procedures described above is not restricted by the particular imaging system used. Hence, their application can be extended to other modalities such as CCD, SEM, etc. to get a better understanding of the specimen under observation.

9. ADDITIONAL MATERIAL: LIVE CELL IMAGING

The use of different techniques has facilitated our understanding of the complex world of neurons. Neuronal growth cones, consisting of lamellipodia and filopodia, are highly motile sensory structures at the tip of neurites, transducing guidance information into directional movements towards targets. Lamellipodia are made up of microtubules and actin filaments while the filopodia contains primarily actin filaments and only occasionally microtubules. In order to simultaneously follow and quantify the dynamics of these cytoskeletal components, we performed live confocal imaging of growth cones from two types of neurons: DRG neurons and PC12 cells differentiated into neurons. To determine the most efficient method for labeling microtubules and actin filaments, we explored different procedures such as liposome-mediated transfection, microinjection and electroporation. PC12 cells were co-electroporated or co-transfected using Fugene 6 with two plasmids, one coding for the microtubule plus end tracking protein EB1-GFP and the other coding for DsRed-actin.

9.1. MATERIAL AND METHOD

- CELL CULTURE

PC12 cells were grown in RPMI supplemented with 10% horse serum and 5% fetal bovine serum. To induce differentiation, PC12 cells were plated on poly-l-lysine (PLL) and Matrigel-coated glass coverslips in RPMI medium supplemented with 5% horse serum, 2.5% fetal bovine serum, and 100 ng/ml NGF.

DRG neurons were derived from 10-12 days old rats following published procedures and plated on PLL-coated glass coverslips in Neurobasal medium (NBM) supplemented with 10% fetal bovine serum.

- TRANSFECTION PROTOCOLS:

  - FUGENE 6:

It is the process of introducing DNA into cells using lipoposmal action. In our experiments we used Fugene 6 (Roche, Indianapolis, IN, USA).

PC12 cells were induced to differentiate for 24 hours and were then transfected using a 3:1 ratio of Fugene 6:DNA (EB1-GFP and DsRed-Actin). DRG neurons were transfected 24 hours after plating using a 3:1 ratio of Fugene 6:DNA. Confocal microscopy images were acquired after 24-48 hours.

  - MICROINJECTION

It is the process of introducing DNA into cells using an electrode and applying air pressure. The instrument for electroporation used was INJECTMAN NI2 (Eppendorf, Hamburg,

Germany). The DNA was first filled into a electrode with a tip diameter of 1 μm. It was then fitted to the microinjector and air pressure was applied for a short period.

PC12 or DRG neurons were microinjected with 30 μM Alexa 488 Phalloidin and 1 μg/μl Rhodamine Tubulin in injection buffer (100 mM Pipes, 1 mM $MgCl_2$, 1 mM EGTA) using the microinjector. Cells were allowed to recover for one hour and were then imaged at the confocal microscope.

▪ ELECTROPORATION

It is the process of introducing DNA into cells using a high electric field for a short duration. This is possible due to the fact that DNA possesses an overall electric charge and is affected by an external electric field. The instrument for electroporation used was the ElectrSquarePorator ECM 830 (BTX, San Diego, CA, USA).

PC12 cells ($1.5x10^7$ cells/ml in RPMI supplemented with 10% horse serum and 5% fetal bovine serum) were electroporated at 400 V for 8 ms in the presence of 20 μg EB1-GFP and DsRed-Actin DNA. Cells were then plated at the desired density on PLL and Matrigel-coated glass coverslips in RPMI medium supplemented with 5% horse serum, 2.5% fetal bovine serum, and 100 ng/ml NGF.

DRG neurons were electroporated after isolation at 112 V for 5 ms in serum free Neurobasal medium (NBM) supplemented with 1 mM $CaCl_2$ and 5 μg DNA. Cells were then plated at the desired density on PLL-coated glass coverslips in NBM supplemented with 10% fetal bovine serum.

- IMMUNOFLUORESCENCE

PC12 cells and DRG neurons were fixed in 4% paraformaldehyde in phosphate buffer saline (PBS) for 20 min at room temperature (RT), rinsed in PBS, and incubated in blocking solution consisting of 5% fetal bovine serum, 0.3% Triton X-100 in PBS, for 30 min at RT. Cultures were then incubated with the monoclonal antibody TUJ1 (Covance, Berkeley, CA, USA), recognizing the neuron specific Class III β-tubulin, at 1:500 dilution in blocking solution, for 30 min, RT. After washing, cultures were incubated with Alexa Fluor 594 anti-mouse antibody (Molecular Probes, 1:300 dilution) and Alexa Fluor Phalloidin (4 units/coverslip), for 30 min, RT. Nuclei were stained with DAPI. After washing, coverslips were mounted in Vectashield (Vector Labs., Burlingame, CA, USA).

- MICROSCOPY

All time lapse images were acquired using Leica Confocal Microscope LEICA DMIR2, equipped with Diode laser 405nm, Ar/ArKr, He/Ne, He/Ne 633 lasers.

Time lapse recording of the growth cones was performed in XYZT at a frame rate of 200-500 msec. Offline analysis of growth cone motility provided visual information about the dynamics (speed and direction) of motion of the different cytoskeletal components. Three-dimensional structure reconstruction of the growth cone was also performed to quantify actin and microtubule concentrations in the growth cones.

The still images were acquired using LEICA DM600B and AXIOSKOP 2 (ZEISS).

- REAGENTS AND CONSTRUCTS:

ALEXA 488 PHALLOIDIN was purchased from Molecular Probes (Eugene, OR, USA, Cat # A12379).

RHODAMINE LABELED TUBULIN was purchased from Cytoskeleton, Inc. (Denver CO, USA, Catalogue number #TL331M).

EB1-GFP (Plus End Binding Protein 1-Green Fluorescent Protein) was kindly provided by Dr. A. Akhmanova, Department of Cell Biology and Genetics, Erasmus MC, Rotterdam, The Netherlands. The EB1 sequence was cloned into pEGFP-N1 (Clontech, Palo Alto, CA, USA).

DSRED-ACTIN was kindly provided by Dr. F. Vascotto, Marie Curie Institute, Paris, France. The Actin sequence was cloned into pDsRed (Clontech).

9.2. RESULTS

We could successfully transfect PC12 cells using various methods. The plasmids were successfully incorporated into the cytoskeleton network and could be visualised using confocal microscopy. Live stained components, the actin filaments and the microtubule structure, were followed to understand their dynamics. Cells were then fixed and immunofluorescence was performed on the cultures to verify the results.

- LIVE IMAGING OF FLUORESCENT NEURONS IN 3-D

Figures 9.1 and 9.2 show examples of PC12 cells transfected with EB1-GFP and DsRed-Actin using Fugene 6 (Figure 9.1) and by Electroporation (Figure 9.2). Actin filaments are shown in red and microtubules in green. Both forms of transfection showed positive results with high transfection efficiency and high visibility of cytoskeletal components. It was possible to track the motion of the tips using MATLAB, thus the velocity of the tips could be calculated.

- COMPARISON WITH IMMUNOFLUORESCENT ANALYSIS

In order to verify that our plasmids were correctly incorporated into the cytoskeleton, we first transfected the neurons with EB1-GFP and then performed immunohistochemistry using Alexa 594 anti-beta tubulin III on the cells fixed with PFA. Figure 9.3 shows a DRG neuron after such a treatment. EB1-GFP is shown in green and Alexa 594 anti-beta tubulin III is shown in red. Their colocalization proves the success of our transfection.

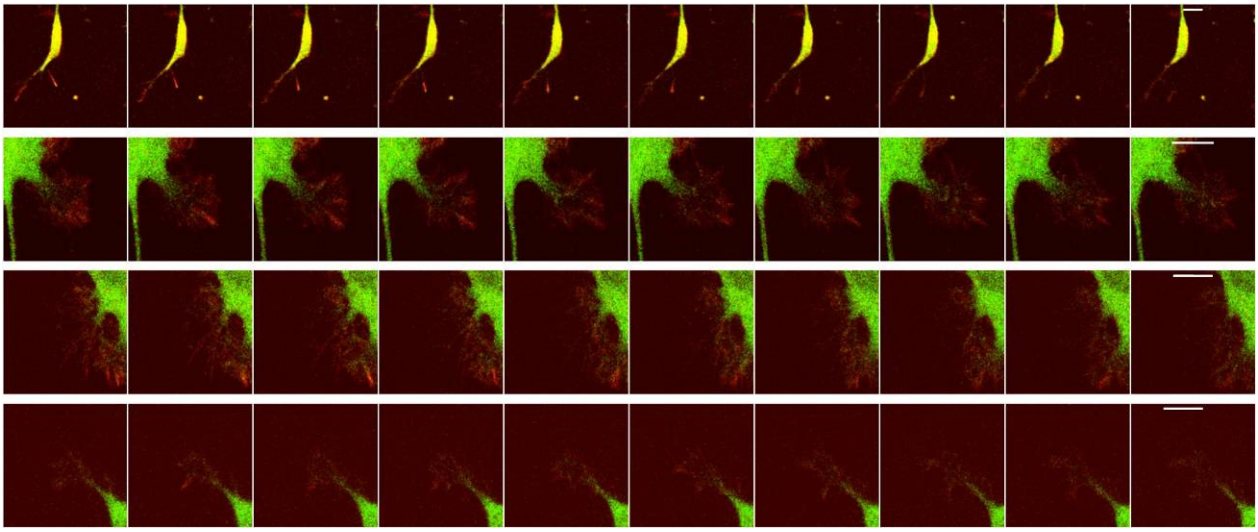

Figure 9.1: PC12 cells transfected with EB1-GFP and DsRed-Actin by Fugene 6. Actin filaments and Microtubules are displayed in red and green, respectively. Time between consecutive images is about 500 msec. Scale bar: 10 µm.

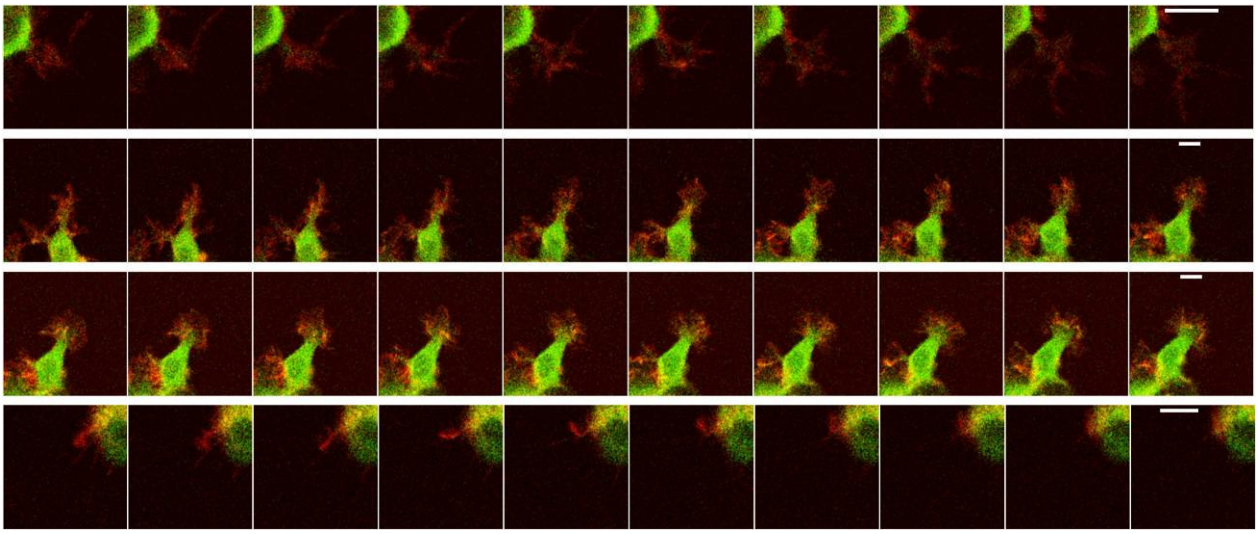

Figure 9.2: PC12 cells transfected with EB1-GFP and DsRed-Actin by Electroporation. Actin filaments are in red and Microtubules in green. Time between consecutive images is about 500 msec. Scale bar: 10 µm.

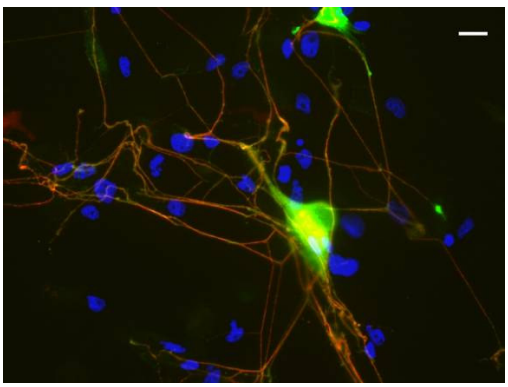

Figure 9.3: Immunofluorescence image of a DRG neuron electroporated with EB1-GFP (in green), subsequently fixed and stained with Alexa 594 anti-beta tubulin III (in red). Scale bar: 10 µm.

Our results indicate that transfection by Fugene 6 is much less toxic to cells than electroporation for DRG neurons. However, the yield of transfected cells is not satisfactory. Electroporation of cells in suspension before plating is by far the more efficient form of transfection in the case of PC12 cells, with a yield of ~25%. While performing electroporation, the most crucial parameter that determines the efficiency of a transfection is the density of the cells in suspension. This issue is easily resolved in the case of PC12 since the cells are actively proliferating before inducing differentiation (by treatment with NGF). DRG neurons are more delicate and the right density is much more difficult to achieve and hence transfection is more tricky. Through trials, we found that DRGs isolated from two rats give the most efficient result.

Transfection by microinjection is not the most suitable form of transfection for small cells such the PC12 cells (with the cell bodies of diameter ~10 μm). DRG neurons on the other hand have comparatively larger cell bodies (with diameter ~15 μm). Hence, it is relatively easier and more effective to use microinjection for these neurons. However, care must be taken while injecting that too much DNA solution is not injected as the cell could start blebbing (*Fackler and Grosse, 2008*). Attention must also be paid while retracting the electrode as sudden retraction could detach the cell from the substrate causing irreparable damage. Further investigation is required to confirm the effectiveness of these procedures.

9.3. CONCLUSION

We have explored different methods to introduce fluorescent material into neurons in order to observe and quantify the dynamics of the cytoskeletal components using confocal imaging of growth cones. Live cell imaging of fluorescent cytoskeletal structures is an interesting approach as:

- it is non-destructive,
- higher temporal resolution than fixation methods,
- use of reagents is maximized,
- quantification is much more straightforward as it is necessary to transfect and observe only a few cells,
- measurements are made in live cells allowing the history and progress of the cell to be followed in real time.

All these features make live cell fluorescence time-lapse imaging an attractive option to study events at the cellular level. It can be applied to follow fascinating phenomenon such as polymerization.

10. APPENDICES

10.1. Manuscript 1:

Mechanical Computation in Neurons

Jummi Laishram, Daniela Avossa, Rajesh Shahapure, Vincent Torre

Under Review

Mechanical Computation in Neurons

Laishram J.[1], Avossa D.[1], Shahapure R.[1] & Torre V.[1,2] *

[1]*International School for Advanced Studies (SISSA-ISAS), Trieste, Italy.* [2]*Italian Institute of Technology, ISAS Unit, Italy.*

* Corresponding author:
Vincent Torre
Scuola Superiore di Studi Avanzati (SISSA)
P1-03b, Ed. Q1, AREA SCIENCE PARK
S.S.14, Km163,5
34012 Basovizza (TS)
ITALY
Email address: torre@sissa.it
Tel: +39 040 3756 513
Fax: +39 040 3756 502 /513

Acknowledgments: We thank Walter Vanzella (Glance Vision Technologies) and Shripad Kondra for computational support.

ABSTRACT

Growth cones are the main motile structures located at the tip of neurites and are composed of a lamellipodium from which thin filopodia emerge. In this manuscript, we analyze the kinetics and dynamics of growth cones with the aim to understand two major issues: firstly, the strategy used by filopodia and lamellipodia during their exploration and navigation; secondly, what kind of mechanical problems neurons need to solve during their operation. In the developing nervous system and in the adult brain, neurons constantly need to solve mechanical problems. Growth cones must decide how to explore the environment and in which direction to grow; they also need to establish the appropriate contacts, to avoid obstacles and to determine how much force to exert. Here we show that in sparse cultures, filopodia grow and retract following statistical patterns, nearly optimal for an efficient exploration of the environment. In a dense culture, filopodia exploration is still present although significantly reduced. Analysis on 1271, 6432 and 185 pairs of filopodia of DRG, PC12 and Hippocampal neurons respectively showed that the correlation coefficient $|\rho|$ of the growth of more than 50% of filopodia pairs was larger than 0.15. From a computational point of view, filopodia and lamellipodia motion can be described by a random process in which errors are corrected by efficient feedback loops. The present manuscript argues that neurons not only process sensory signals, but also solve mechanical problems throughout their entire lifespan, from the early stages of embryogenesis to adulthood.

Keywords: Mechanical computation; growth cone motion; growth cone exploration; obstacle avoidance; obstacle removal

INTRODUCTION

Processing of sensory inputs and its transformation into appropriate motor outputs is a key function of neuronal networks in all living species. A major goal of contemporary neuroscience is to understand this processing at a functional and molecular level. Similarly to electronic devices, neurons process sensory signals and information as electrical signals, but they are also living entities able to move. Indeed, neurons can explore the environment and migrate to destinations that are several microns, even millimeters, away from their original location (Dai and Sheetz, 1995; Atilgan et al., 2006; Solecki et al., 2006; Ghashghaei et al., 2007). Neuronal growth cones are the major motile structures located at the tip of dendrites and axons (Bray et al., 1978; Goodman, 1996; Song and Poo, 2001; Gordon-Weeks, 2004; Duncan et al., 2008), and are composed of a lamellipodium from which thin filopodia emerge (Pollard et al., 2000; Grunwald and Klein, 2002; Guan and Rao, 2003; Huber et al., 2003). The motion of filopodia and lamellipodia plays a major role in morphogenesis and neuronal differentiation: the exploratory motion of filopodia allows neurons to find the correct target and to establish the appropriate synaptic connections. Their motion has been analyzed and characterized to some extent by time lapse microscopy (Aletta and Greene, 1988; Gomez and Letourneau, 1994; Dent and Kalil, 2001; Baker et al., 2003; Baker and Macagno, 2007; Galbraith et al., 2007; Mongiu et al., 2007).

Growth cones contain a variety of adhesion molecules and receptors to guidance molecules–(Bustamante et al., 2000; Yamagata et al., 2003; Huber et al., 2003; Curinga and Smith, 2007; Cline and Haas, 2008); a sophisticated intracellular biochemical machinery couples these receptors to the cytoskeleton (Gallo and Letourneau, 2000; Song and Poo, 2001; Gordon-Weeks, 2004) which is primarily composed of actin filaments and microtubules. Filopodia are usually composed of several bundles of actin filaments and occasionally of some microtubules (Howard, 2001, Schaefer et al., 2002). Growth cone membrane receptors detect guidance molecules (Nicholls et al., 2001) through a process commonly referred to as "pathfinding" which involves growth cone navigation along a gradient of a diffusible factor.

Mechanical properties of cytoskeletal components are usually quantified by measuring their persistence length, λ_p, defined as the length over which correlations of the motions between the tip and the end are lost (Howard, 2001). Cytoskeletal components with a length L such that $L/\lambda_p << 1$, move like rigid sticks and the motions of their tip and base are highly correlated. The value λ_p of actin filaments is 18±1 μm when stabilized with phalloidin and 9±0.5 μm in non-stabilized conditions (Isambert et al., 1995), while microtubules are more rigid with values of λ_p varying from 110 to 5035 μm (Pampaloni et al., 2006).

In this manuscript, we analyze the kinetics and dynamics of growth cones with the aim to understand two major issues: firstly, the strategy used by filopodia and lamellipodia during their exploration and navigation; secondly, what kind of mechanical problems neurons need to solve during their operation. In the developing nervous system - during neuronal differentiation and migration -, and in the adult brain - during memory formation and consolidation - , neurons have the constant necessity to solve mechanical problems: growth cones need to explore the environment, establish the appropriate contacts, avoid obstacles, decide in which direction to grow and how much force to exert. The present manuscript argues that neurons not only process information, but continuously solve mechanical problems throughout their entire lifespan, from the early stages of embryogenesis to adulthood.

METHODS

CELL CULTURE

Dorsal Root Ganglia (DRG) neurons were prepared from Wistar rats (P10-P12), anesthetized with CO_2 and sacrificed by decapitation (in accordance with the Italian Animal Welfare Act and approved by the Local Authority Veterinary Service) as previously described in Cojoc et al., (2007). Dissociated cells were plated on poly-L-lysine (PLL, 0.5 μg/ml, Sigma) and Matrigel (BD Biosciences, Bedford, MA, USA) -coated coverslips in Neurobasal medium (Invitrogen) containing 10% fetal bovine serum (FBS, Sigma) and 100 ng/ml nerve growth factor (NGF, Alomone, Israel) at a density of 10^4 cells/ml (corresponding to ~2000 cells/cm^2).

PC12 cells were grown in RPMI (Invitrogen) supplemented with 10% horse serum (Sigma) and 5% FBS. The cells were plated on PLL and Matrigel coated glass coverslips in RPMI medium supplemented with 5% horse serum (Sigma) and 2.5% FBS at a density of 10^4 cells/ml (corresponding to ~2000 cells/cm^2). To induce differentiation into sympathetic neurons, 100 ng/ml NGF was added to the culture.

Hippocampal neurons were isolated from P0-P2 rats as previously described in Bonifazi et al., (2005). Cells were plated on polyornithine (Sigma)/matrigel-coated coverslips at a density of 8×10^5 cells/cm^2 and maintained in Minimal Essential Medium with Earle's salts (Invitrogen) supplemented with 5% fetal calf serum, 0.5% D-glucose, 14 mM Hepes, 0.1 mg/ml apo-transferrin, 30 μg/ml insulin, 0.1 μg/ml D-biotin, 1 mM Vit.B12, and 2 μg/ml gentamycin (all supplements were purchased from Sigma). 48 hours after plating, 5 μM cytosine-β-D-arabinofuranoside (Ara-C) was added to the culture medium, in order to block glial cell proliferation. Medium change was performed twice a week.

All neuronal cultures were kept in an incubator providing a controlled level of CO_2 (5%), temperature (37°C) and moisture (95%). DRG and PC12 neuronal cultures were used for imaging 20-30 hours after plating, while hippocampal cultures were used after two weeks in culture.

LIVE IMAGING, CELL TRANSFECTION

Differential interference contrast (DIC) images of moving DRG growth cones were obtained with a Leica DMIR2 confocal microscope (Leica Microsystems GmbH, Germany), equipped with a Diode laser emitting at 405 nm, and Ar/ArKr (at 488 nm), He/Ne (at 543/594 nm), and He/Ne (at 633 nm) lasers. Coverslips were placed into a chamber and kept at 37ºC and 5% CO_2 to minimize cell damage or death during live recording. The Ar/ArKr laser was used as a light source set at 11% of its maximal power so to reduce neuronal damage. Stacks of four images (set in DIC configuration) at different focal planes (0, 1, 2 and 3 μm above the glass where the neurons were plated) were acquired with a 63×, 1.4 NA oil immersion objective every 5-10 seconds, for 12 to 35 minutes. Time lapse movies of acquired images are shown in the Supplementary Information material: exploring filopodia in SI 1 and a moving lamellipodium in SI 2. The growth cone is a 3D structure because filopodia and lamellipodia can move by some microns along the z-axis and their three dimensional (3D) motion was recovered using an operator assisted program (see below).

Hippocampal neurons were transfected with pEGFP-N1 (CloneTech, Palo Alto, CA, USA), a plasmid encoding for enhanced green fluorescent protein (EGFP), after 8 to 11 days *in vitro* (DIV) using the Ca^{2+}-phosphate method (Köhrmann et al., 1999) and live imaging of moving growth cones was performed 2-5 days after transfection. To determine the cell density, sister hippocampal cultures were immunolabeled with the anti-β tubulin III antibody TUJ (Covance, USA; 1:750 dilution) and counterstained with DAPI (Boehringer Mannheim GmBH, Germany; 1:1000 dilution) as previously described (Bonifazi et al., 2005). At the time point

chosen for live imaging of growth cones, the total cell density was 9.60±1.1 × 10^4 cells/cm^2 and the neuron density was 5.70±0.8 × 10^4 neurons/cm^2.

DATA ANALYSIS

Filopodia were tracked by an operator assisted program and data were analyzed using MATLAB 7.1 (The MathWorks Inc. http://www.mathworks.com). For each filopodium i and for each frame n (n=1,…,N) of a growth cone, we determined the location of its base or starting point $s_i(x,y,z,n)$ and the location of its tip or end point $e_i(x,y,z,n)$. Figure 1A illustrates a 3D rendering of the set of $s_i(x,y,z,n)$ in red and the set of $e_i(x,y,z,n)$ in black for a DRG growth cone. When these points are projected on the (x,y) plane, they are distributed over a portion of a circular sector with inner and outer radii R and R+A respectively and a central angle θ (Fig. 1B). The z resolution was equal to the distance between different focal planes, i.e. 1 μm. A suitable program combined the information obtained at each focal plane and the 3D backbone of each filopodium was recovered for all frames so that it was possible to follow its motion in the 3D space. The distance D at frame n, was defined as the distance between $s_i(x,y,z,n)$ and $e_i(x,y,z,n)$, and the filopodial length L, as the sum of distances between consecutive points making up the filopodium backbone. A filopodium emerging from a point where another one had previously disappeared was considered as a new filopodium. With this procedure, the length and orientation of all filopodia were recovered.

ESTIMATION OF EXPLORABLE AND EXPLORED SPACE

In order to quantify the exploratory behavior of growth cones in culture, we define two quantities: the explorable and the explored 3D free space around growth cones. The explorable 3D free space is an estimation of the 3D space that the growth cone could potentially explore and the explored 3D space is the 3D space which is actually explored by the growth cone at a given frame n.

As shown in Figures 1A-B, the starting and ending points of all filopodia of DRG usually lie on the perimeter of a circular sector with inner radius R and an outer radius R+A, where R corresponds approximately to the radius of the growth cone and A is the maximal length of filopodia. If C is the centre of this circular sector, (see Fig. 1B), filopodia starting and ending points cover approximately an angle θ. Therefore, the volume of the explored 3D space at frame n is defined as:

$$Free(n) = h \cdot \pi((R+A)^2 - R^2) \cdot \frac{\theta(n)}{2\pi}$$

where h is the maximal height to which the filopodium tip can arise, estimated to be 3 μm (Figs. 1-2). $\theta(n)$ depends on the frame n whereas R and A are assumed to be constant. The explorable 3D space *ExplFree* is the maximum value of *Free(n)* over the entire image sequence n=1,…,N and the fraction of explored free space at frame n is
Free(n)/ExplFree.

For Hippocampal neurons, the volume of the explorable free space around a growth cone is assumed to be

$$ExplDense = \frac{4}{3}\pi((R+A)^3 - R^3)$$

i.e. the volume of a sphere of radius R+A minus the volume of the sphere of radius R. In these cultures, the explored space $Dense_{cyl}(n)$ at frame n is defined in the following way: for each filopodia i, we consider the segment S_{in} joining the starting $s_i(x,y,z,n)$ and ending point $e_i(x,y,z,n)$ and draw the cylinder Cyl_{in} with axis S_{in} and radius R_{cyl}. The radius R_{cyl} is assumed to be the standard deviation of lateral filopodia fluctuations corresponding to approximately 1 μm as

measured by video microscopy. The explored space at frame n, $Dense_{cyl}(n)$, is defined as $U_i\ Cyl_{in}$, where U is the union operator of Set Theory. Thus, the fraction of explorable free space at frame n is the ratio of the two volumes $Dense(n)$ and $ExplDense$.

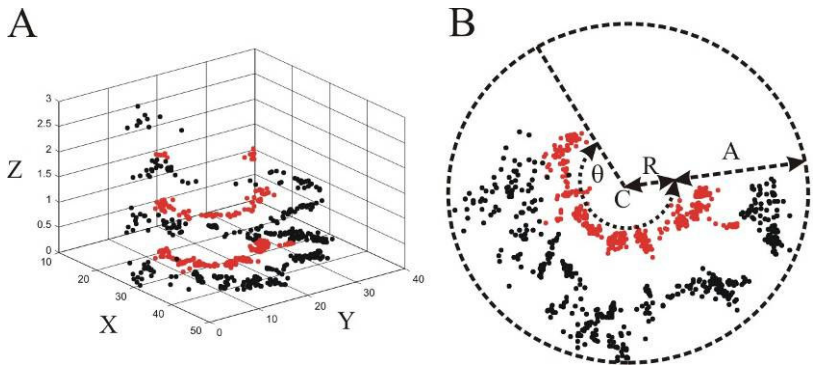

Fig. 1. Determination of the explorable and explored space around a growth cone. **A**: Red and black points are the starting $s_i(x,y,z,n)$ and end points $e_i(x,y,z,n)$ respectively of DRG filopodia identified during 10 minutes of observation. **B**: Determination of the explored free space by filopodia of a growth cone in a free environment, i.e. in a diluted culture.

CORRELATED AND ANTI-CORRELATED GROWTH

Given the 3D backbone of filopodia i and j at frame n, their mean lengths μ_i and μ_j over all frames were computed. If x_i is the set of lengths (at frames 1,…,N) of filopodium i and y_j is the set of corresponding lengths of filopodium j, the correlation coefficient ρ_{ij} between the length of filopodia i and j was computed as:

$$\rho_{ij} = \frac{E[(x-\mu_i)(y-\mu_j)]}{\sqrt{E[(x-\mu_i)^2]\cdot E[(y-\mu_j)^2]}}$$

where, E[·] is the average value of · computed over all frames 1,…,N; and μ_i and μ_j are the mean values of the lengths x_i and y_j over all frames 1,…,N.

ρ_{ij} could be positive or negative indicating correlated and anticorrelated growth respectively. In order to establish the existence of correlated or anticorrelated growth, two thresholds corresponding to ±0.15 and ±0.5 were considered (see Table 1). If the absolute value of ρ_{ij} was less than 0.15, the motion of filopodia was considered uncorrelated.

CONTACT FORMATION

Contact formation between neighboring growth cones was quantified by considering the number of formed contacts, lifetime and persistence. A contact between the two endpoints $e_i(x,y,z,n)$ and $e_j(x,y,z,n)$ of filopodia i and j is established at frame n if $e_i(x,y,z,n)$ and $e_j(x,y,z,n)$ coincided at frame n and for at least 10 subsequent frames. A previously formed contact was lost at frame m if $e_i(x,y,z,m)$ and $e_j(x,y,z,m)$ no longer coincided at frame m and for at least 10 subsequent frames.

OPTICAL TWEEZERS AND FORCE MEASUREMENTS

The optical tweezers setup was built as described in Cojoc et al., (2007). The dish containing the differentiating neurons and beads (1 μm diameter, PSI-1.0NH2; G.Kisker GbR, Steinfurt Germany) was placed on the inverted microscope stage which could be moved with a 3 axis piezoelectric nanocube (17 MAX 301, Melles Griot Inc., USA). The temperature of the dish

was maintained at 37° C by a Peltier device. The bead position $\mathbf{x}$= (x,y,z) was determined in the x,y plane with an accuracy of 10 nm using back focal plane (BFP) detection, which relies on the interference between forward scattered light from the bead and unscattered light. The BFP of the condenser was imaged onto a quadrant position detector (QPD) and the light was converted to differential outputs digitized at 20 kHz and low pass filtered at 5 kHz. Bead z position was determined using the Gouy phase shift effect (Neuman and Block, 2004; Rohrbach et al., 2004). The trap stiffness $\boldsymbol{\kappa}_{x,y}=(k_x,k_y,k_z)$ and the detector sensitivity were calibrated using the power spectrum method. Detector sensitivity was also checked by measuring voltage signals originating from displacements of a bead stuck to the bottom of the coverslip with a nanopositioning device (the nanocube). The force exerted by the neurite $\mathbf{F}_{\mathbf{neu}}$ was taken as equal to $-\mathbf{F}_{\mathbf{trap}}$. When the absolute displacement of the bead $\mathbf{d}=(d_x,d_y,d_z)$ from its equilibrium position inside the trap was less than 400 nm, $\mathbf{F}_{\mathbf{trap}}=(F_x,F_y,F_z)$ was calculated as $F_x=d_xk_x$, $F_y=d_yk_y$ and $F_z=d_zk_z$.

The velocity was obtained by numerical differentiation of the sampled position (x(n),y(n),z(n)) where n=1,…,N. Numerical differentiation was computed by convolution of the position with the derivative of a Gaussian filter $A\exp(-t^2/\sigma^2)$ with the unit area (Gaussian filtering).

RESULTS

The present manuscript is divided into two sections: an experimental section and a computational section. In the experimental section, we analyze several properties of the kinetics and dynamics of filopodia and lamellipodia motion. We have used three different types of neurons grown in culture: hippocampal neurons from the central nervous system, DRG neurons from the peripheral nervous system and PC12 cells differentiated into sympathetic neurons. In the present manuscript we show that, despite well-established differences (Joshi et al., 1985; Dennerll et al., 1989; Heidemann and Wirtz, 2004), all these neurons explore the surrounding environment in a similar fashion.

In the computational section, we model many of the results presented in the experimental section, with the aim of clarifying the notion of *mechanical computation* and formalize it in simple pseudo-codes.

EXPERIMENTAL SECTION

DRG neurons and PC12 cells were plated at low densities (2000 cells/cm^2) and were used after 20-30 hours in culture so to analyze growth cone motion in an environment where filopodia and lamellipodia could freely move. Hippocampal neurons, on the contrary, were plated at high densities (8×10^5 cells/cm^2) and cultivated for two weeks so to form a highly connected network.

KINETICS OF FILOPODIA MOTION

DRG and PC12 neurons were plated on glass coverslips and after 20-30 hours, neurites growing in different directions were observed. The kinetics of filopodia emerging from growth cones was analysed with time lapse DIC imaging (Fig. 2A). Images were taken at four optical sections corresponding to the plane of the coverslip (height of 0 μm) and to three other planes at a height of 1, 2 and 3 μm above the bottom of the coverslip (Fig. 2B). A stack of four images was acquired every 5-10 seconds for a total observation time varying from 8 to 30 minutes. DIC images acquired from 19 growth cones were analysed off line by an operator assisted program able to reconstruct the 3D profile of moving filopodia (see Methods). Filopodia lifted up and

often appeared in focus some μm above the bottom of the coverslip (see Fig. 2B and SI 1 in Supplementary Information) and their tips visited locations at distances up to 16 μm from the lamellipodium edge.

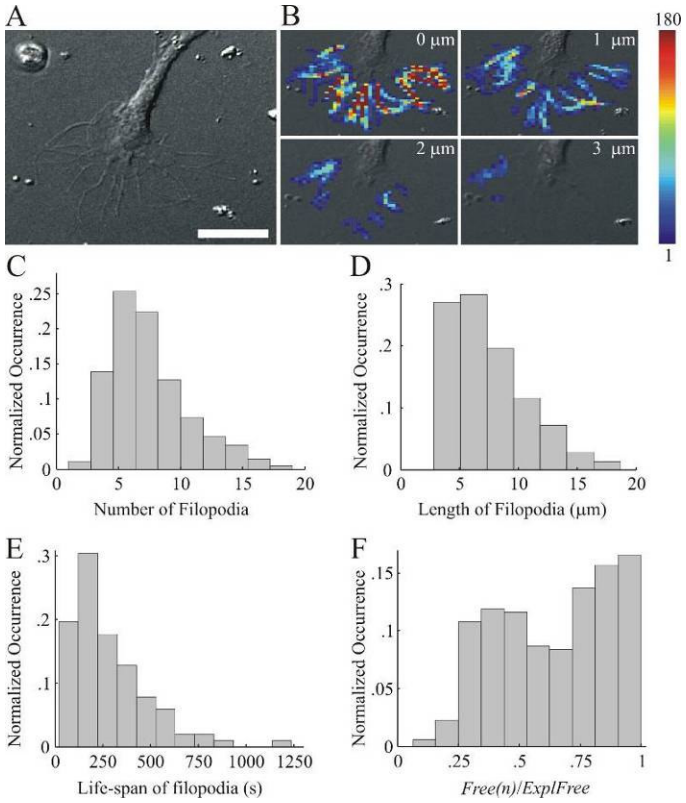

Fig. 2. Kinetics of filopodia from DRG growth cones. **A-B**: Density map of the region explored by filopodia from a DRG growth cone. In the color scale, red indicates highly visited voxels (180 times) whereas blue indicates less visited voxels (1 time). Scale bar: 10 μm. **C**: Normalized occurrence of the total number of filopodia from DRG growth cones. **D**: Normalized occurrence of length of DRG filopodia. **E**: Normalized occurrence of the life-span of DRG filopodia. **F**: Normalized occurrence fraction of the volume explored by a growth cone in a free environment calculated as *Free(n)/ExplFree*. Collected data from 19 DRG neuronal growth cones.

We analyzed the kinetics of filopodia from 19 DRG growth cones. Collected data show that the number of filopodia emerging from DRG growth cones was 7.3±3.4 filopodia per growth cone (range from 2 to 18 filopodia per growth cone) (Fig. 2C) and their length had an average value of 7.5±3.2 μm (range from 2.9 to 18.1 μm, n=19) (Fig. 2D). During the observation time, we identified several filopodia starting to grow and subsequently retracting completely. Exploring filopodia had a life time varying from just 1 to about 20 minutes (Fig. 2F). Other filopodia, after a period of exploration, stopped moving and appeared to stably adhere to the substrate.

We divided the space around a growth cone in cubic voxels of 1 μm. We computed how often each voxel was visited by a filopodium so to reconstruct the 3D profile of the space visited by filopodia: almost all voxels were visited at least once. As shown in Figure 2B, voxels at a height of 3 μm above the coverslip were occasionally visited by some filopodia.

The explorable free *ExplFree* and explored *Free(n)* 3D space around growth cones of DRG neurons was determined as described in the Methods. The value of *ExplFree* ranged from 1272 to 4671 μm^3 (n=19) with an average value of 3084±990 μm^3. At any time, the volume explored by the filopodia, *Free(n)*, varied from 187 to 4671 μm^3, with an average value of 1971±866 μm^3 . The fraction of the explored 3D space *Free(n)/ExplFree* had an average value of

66±24% (range from 6 to 100%, n=19) indicating that growth cones explored a significant fraction of the surrounding free space (Fig. 2F).

We reconstructed and tracked the 3D profile of each filopodium (see Methods), and calculated the ratio D/L, where D is defined as the distance between the filopodium tip and its base and L is the total filopodium length, computed as the sum of the distances between consecutive points making up the backbone of the filopodium. When the ratio D/L is close to 1, the filopodium is rigid, whereas values of D/L smaller than 1 characterize bending filopodia.

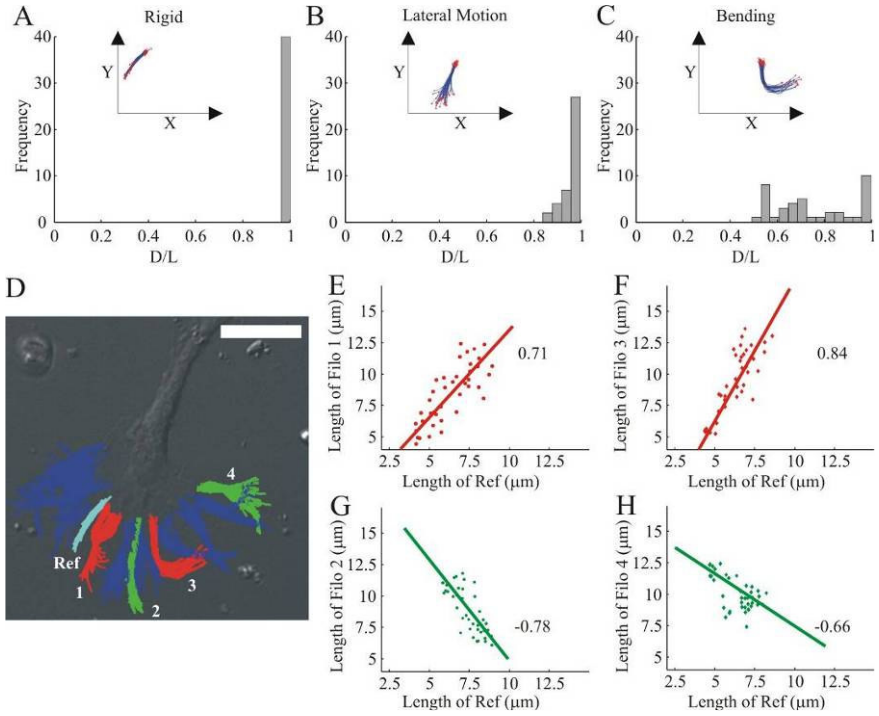

Fig. 3. Filopodia properties and correlated growth and retraction. **A-C**: Frequency distribution of the ratio D/L for three classes of filopodia respectively. Insets show the projection on the (X,Y) plane of a representative filopodium. **D**: 2D profile of filopodia emerging from a DRG growth cone superimposed to a DIC image of the growth cone. The filopodium marked in cyan is taken as reference. Scale bar: 10 µm. **E-H**: Cross-correlation between the length of the reference filopodium (in cyan) and the length of the two red filopodia indicated by 1 and 3 (E and F) and the length of the two green filopodia indicated by 2 and 4 (G and H). Changes in length of red and green filopodia were positively and negatively correlated to the changes in length of the filopodium marked in cyan, respectively. Changes in length of blue filopodia were not correlated.

The ratio D/L for several filopodia (29%) was very close to 1. These filopodia grew and/or retracted without changing the ratio D/L and behaved as rigid sticks emerging from the peripheral region of the growth cone (Fig. 3A). For other filopodia (18%) the ratio D/L varied between 0.8 and 1 and moved their tip laterally as if shaken at their base, possibly by shearing movements of the underlying actin filament network (Fig. 3B). For other filopodia (32%) the ratio D/L was less than 0.8, indicating a significant bending (Fig. 3C). Filopodia had at the most one bend and the ratio D/L did not change significantly during the observation time. The remaining filopodia (21% of all filopodia) could not be categorized into any of these classes because of their short lifespan. The average ratio computed over all filopodia fluctuated in time around 0.9 for all investigated growth cones.

During the recording time, new filopodia emerged and others completely retracted, therefore we investigated whether growth and retraction of neighboring filopodia were correlated

(Fig. 3D-H). In all growth cones, a specific filopodium was taken as reference such as that shown in cyan (Fig. 3D) and we analyzed whether other filopodia retracted or grew in synchrony. In the example shown in Figure 3D when the cyan filopodium retracted, some neighboring filopodia (indicated in red) also retracted while other filopodia (indicated in green) grew. The correlation coefficient ρ between the length of the reference filopodium and the length of the red filopodia was 0.71 and 0.84 respectively, whereas the value of ρ between the reference filopodium and the two green filopodia was -0.78 and -0.66 respectively.

Table 1: Percentage of correlated filopodial growth in different neuronal growth cones

Type of neuron	Percentage of filopodia with (ρ is correlation coefficient) (A = Anticorrelated; C = Correlated)		
	Uncorrelated $\|\rho\|<0.15$	Moderately correlated $0.15\leq\|\rho\|\leq0.5$	Correlated $\|\rho\|<0.50$
DRG (n=19; 1271 pairs)	18.3	42.9 20.9 (A) + 22 (C)	38.8 14.1 (A) + 24.7 (C)
PC12 (n=6; 6432 pairs)	43.3	43.3 25.7 (A) + 17.6 (C)	13.4 1.4 (A) + 12 (C)
Hippocampal (n=7; 185 pairs)	38.4	39.8 28.2 (A) + 11.6 (C)	21.8 1.5 (A) + 20.3 (C)

We investigated the degree of correlated growth and retraction in 19 DRG, 6 PC12 and 7 hippocampal neuronal growth cones. Analysis on 1271, 6432 and 185 pairs of filopodia of DRG, PC12 and hippocampal neurons respectively showed that the correlation coefficient |ρ| of the growth of more than 50% of filopodia pairs was larger than 0.15 (see Table 1). In DRG growth cones, 38.8% of these pairs had a value of |ρ| larger than 0.5 and were classified as correlated, out of which 14.1% were anticorrelated and 24.7% correlated. 42.9% of the filopodia pairs were classified as moderately correlated (with correlation coefficient $0.15\leq|\rho|\leq0.5$), with 20.9% of the filopodia being moderately anticorrelated and 22% moderately correlated. The remaining 18.3% of these pairs had a correlation coefficient $|\rho|<0.15$ and were classified as not correlated. A similar degree of correlated growth was observed also in filopodia pairs of PC12 and hippocampal growth cones. These results indicate that growth and retraction of filopodia from the same growth cone are - to some extent - correlated, and when one filopodium grows, the other filopodium retracts.

Having established that growth and retraction of filopodia from the same growth cone could be correlated and anti-correlated, we analysed in detail the degree of correlation between 197 pairs of neighboring filopodia from the same DRG growth cone. Two neighboring filopodia could grow simultaneously almost doubling their length within a minute (Fig. 4A). We also observed the opposite behavior (Fig. 4B): when one filopodium grew, a neighboring filopodium retracted (43/197) and in some occasions (18/197), it retracted completely.

Data collected from 197 pairs of neighboring filopodia in DRG neuronal growth cones (Fig. 4C) indicated a variable degree of correlated growth, with values of ρ ranging from -0.8 to 1. The fraction of pairs of neighboring filopodia showing a correlated growth with a value of |ρ| larger than 0.5 was 44.2%, similar to what observed in pairs of filopodia - not necessarily neighboring - from the same growth cone, as shown in Table 1. Therefore, correlated growth or retraction does not necessarily depend on the proximity to the reference filopodium and often, distant filopodia could be correlated or anticorrelated.

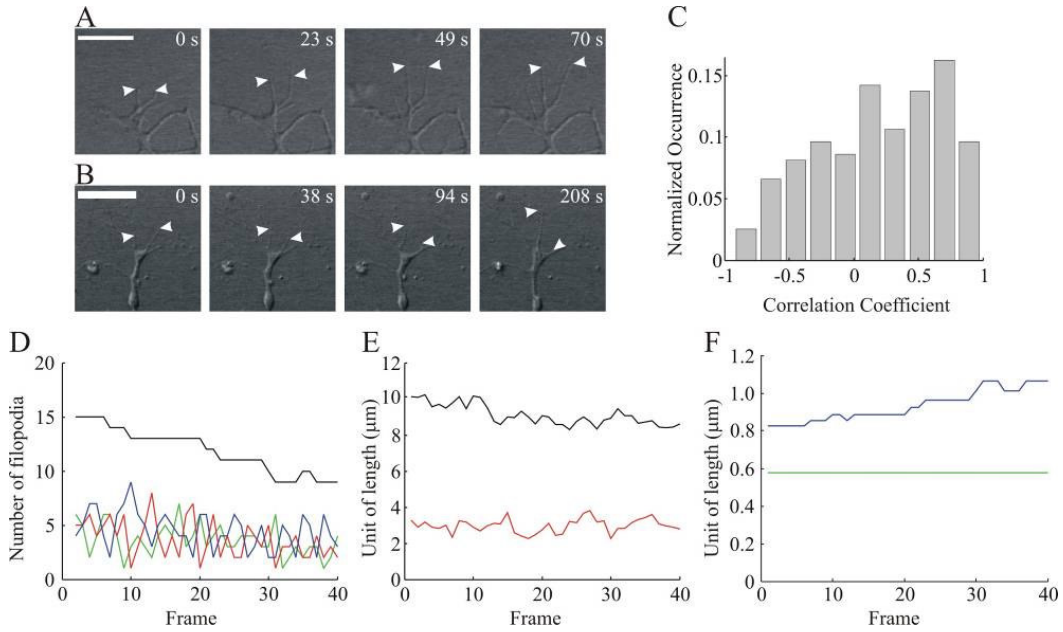

Fig. 4. Correlation between lengths of neighboring filopodia. **A-B:** Selected frames of a growth cone with two filopodia (indicated by white arrows) growing in a correlated way (**A**) and in an anti-correlated way (**B**). Scale bar: 10 µm. **C**: Distribution of the coefficient of correlation ρ between 197 pairs of neighboring filopodia. +1 indicates maximum correlation while -1 indicates maximum anti-correlation. The percentage of neighboring filopodia pairs with $|\rho|>0.5$ is 44.2%. **D**: Number of filopodia (black) emerging from the growth cone (shown in Fig. 2) at each frame. Green, red and blue traces indicate the number of growing, retracting and stationary filopodia respectively. **E**: Mean $\langle l \rangle_n$ (black) and standard deviation σ_l (red) of filopodia length at each frame. **F**: Comparison between $\sigma_l / \sqrt{N(n)}$ (blue) and $\sigma_{\langle l \rangle n}$ (green).

The observed patterns of correlation and anticorrelation of Figures 4A-C could be caused by random fluctuations of filopodia length and not by an orchestrated growth and retraction. Indeed if filopodia grow and retract in a random independent way, there will be pairs of filopodia whose growth is correlated and other pairs being anticorrelated. In order to verify the existence of an orchestrated behavior of filopodia emerging from the same growth cone, we performed the following statistical test:

let us suppose that at frame n there are N(n) filopodia emerging from the same growth cone and that their average length is $\langle l \rangle_n$. If growth and retraction of these filopodia are completely independent - and therefore there is no correlation or orchestrated pattern - and if σ_l is the standard deviation of their length, the standard deviation of $\langle l \rangle_n$ - computed over all frames n - $\sigma_{\langle l \rangle n}$ is expected to be equal to $\sigma_l / \sqrt{N(n)}$. This is a simple consequence of statistical properties of independent random variables. If $\sigma_{\langle l \rangle n}$ is consistently less than $\sigma_l / \sqrt{N(n)}$, then the growth and retraction of filopodia are not independent but have a global orchestration of correlations and anticorrelations.

Figure 4D reproduces the total number of filopodia (black trace) emerging from the growth cone shown in Figure 2 at frame n (n=1,…,40) and the number of growing (green), retracting (red) and stationary filopodia (blue). As shown by the black trace in Figure 4E, the value of $\langle l \rangle_n$ (black) was stable around the mean value of 9.1 µm and its standard deviation $\sigma_{\langle l \rangle n}$ was equal to 0.6 µm. The value of σ_l computed over all filopodia present at frame n varied around 3.2 µm (red line in Fig. 4E) in agreement with the value of the standard deviation computed over all filopodia emerging from the 19 considered growth cones (see Fig. 2). The value of $\sigma_{\langle l \rangle n}$

(green trace in Fig. 4F) was significantly less than the value of $\sigma_l/\sqrt{N(n)}$ (blue trace in Fig. 4F) which varied between 0.8 and 1.1 μm. The same statistical analysis performed on all growth cones (n=19) indicated that the value of $\sigma_{<l>n}$ was less than the value of $\sigma_l/\sqrt{N(n)}$ in 18/19 growth cones. The growth cone in which $\sigma_{<l>n}$ was larger than $\sigma_l/\sqrt{N(n)}$ had a consistent correlated growth of its filopodia and $<l>_n$ steadily increased from 6.7 to 10.8 μm during the observation time.

These results show that growth and retraction of filopodia follow an orchestrated pattern, by which the average filopodia length is stable, more than what expected from simple independent fluctuations. This orchestrated motor plan also minimizes collisions between adjacent filopodia and provides an even exploration of the surrounding environment both in time and space. In addition, this motor plan allocates necessary metabolic resources - such as ATP molecules - in an efficient way and provides a possible recycling of G-actin monomers between polymerizing and depolymerizing actin filaments in neighboring filopodia. These observations allow us to understand the fine orchestration of filopodial motion underlying their mechanical computation.

FILOPODIA MOTION AND CONTACT FORMATION

Filopodia emerging from growth cones explore the environment in search of neurons in order to establish a physical contact. Therefore, we looked for pairs of neighboring growth cones and followed their exploratory motion and kinetics of contact formation. We observed two cases of contact formation between neighboring PC12 neuronal growth cones.

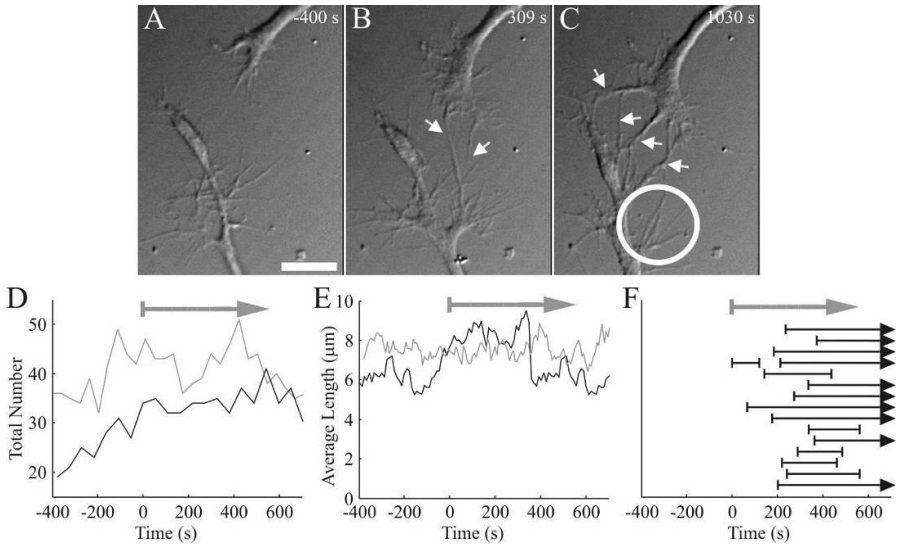

Fig. 5. Contact formation between two neighboring exploring PC12 growth cones. **A-C**: DIC images during contact formation. Time zero corresponds to the formation of the first contact. Scale bar: 10 μm. **D**: Total number of filopodia from the two growth cones during contact formation. The grey horizontal arrow indicates the period during which the contacts between growth cones were established. **E**: Time evolution of the average filopodia length. Data from two experiments. **F**: Time course of contact formation for one pair of growth cones. Arrows indicate the timing of the formation of physical contact and the arrow head indicates that the contact was also present at the end of the observation time.

Growth cones had between 20 and 50 exploring filopodia (Fig. 5A) and seven minutes after the start of the recording, two filopodia - from different growth cones - collided and established a permanent contact (Fig. 5B). Subsequently, several additional contacts were made (Fig. 5C) and then one growth cone retracted (shown within the white circle) without destroying the established contacts. Established contacts were usually stable and could be seen for several hours after image recording. Before establishing the contact, the total number of filopodia slightly increased (Fig. 5D) and after the formation of 2-5 contacts (white arrows), the total number of filopodia decreased. During the exploratory phase, contact formation and retraction, the average filopodia length remained stable with a value of 7.2±1.1 μm (range 3.5 to 9.5 μm, n=6) (Fig. 5E).

In one observation (see Fig. 5F), the number of contacts reached a maximum value of 15 contacts 400-650 seconds after the first contact was established, and 4 contacts were subsequently lost, but 11 out of 15 were present at the end of the observation time (10 minutes). One contact was interrupted but then quickly reformed. A large portion of exploring filopodia had a life time varying from 1 to 6 minutes, but other filopodia explored for a longer time, up to 10-20 minutes.

FILOPODIA MOTION IN A DENSE CULTURE

Cultures of hippocampal neurons derived from neonatal rats were plated at high densities (8×10^5 cells/cm^2), and were grown for two weeks *in vitro* in serum-containing medium (see Methods section). In these conditions, glial cells rapidly proliferated and formed a cell monolayer on top of which neurons grew and became richly innervated (Goslin and Banker, 1998). To visualize neuronal growth cones, cultures were transfected with EGFP at 11 DIV and analyzed with time lapse confocal microscopy two days later (Fig. 6). To determine the cell density and the percentage of neurons, sister cultures were fixed and immunolabeled with the TUJ antibody which recognizes β tubulin III, a specific marker for neurons and DAPI staining for nuclei. The density of hippocampal cultures was quantified by counting the number of cells in an area of 100×100 μm^2 at the time of plating (n_{cover}) and after cultivation and DAPI staining (n_{DAPI}). In our experimental conditions, n_{cover} was 80±12 and n_{DAPI} was 25±15. The measured value of n_{DAPI} was about 2-8 times lower than n_{cover} because of cell death during cultivation. The total thickness of the culture was 50±15 μm. The average radius of the soma of these neurons was 7.4±2.2 μm and the measured volume of the dendritic tree was 5.4±1.3 times that of the cell body (unpublished data). Hence, the fraction of the volume occupied by the cells is between 37 to 79% and the free space around the growth cones is limited.

Also in dense hippocampal cultures, filopodia grew and retracted within minutes (Figs. 6A-D). The motion of filopodia, however, was more restricted compared to that of filopodia from DRG neurons and filopodia primarily moved along specific directions (Fig. 6E) less occupied by other biological structures. The explorable free space $Dense_{cyl}$ and explored space *ExplDense* were estimated as described in the Methods section. *ExplDense* was estimated by assuming the radius of the growth cones to be 5 μm and the filopodia length, 3 μm (Fig. 6H). The average value of *ExplDense* was 682±202 μm^3 (range from 514 to 944 μm^3; data from 7 hippocampal neuronal growth cones). As shown in Figure 6I, the fraction of explored free space ($Dense_{cyl}(n)/ExplDense$) was, on average, 4±4% ranging from 0 to 14% (n=7). The fraction of explored free space was significantly smaller than for DRG growth cones in culture where filopodia could move freely (Fig. 2D), indicating that filopodia exploration in dense hippocampal cultures is highly restricted.

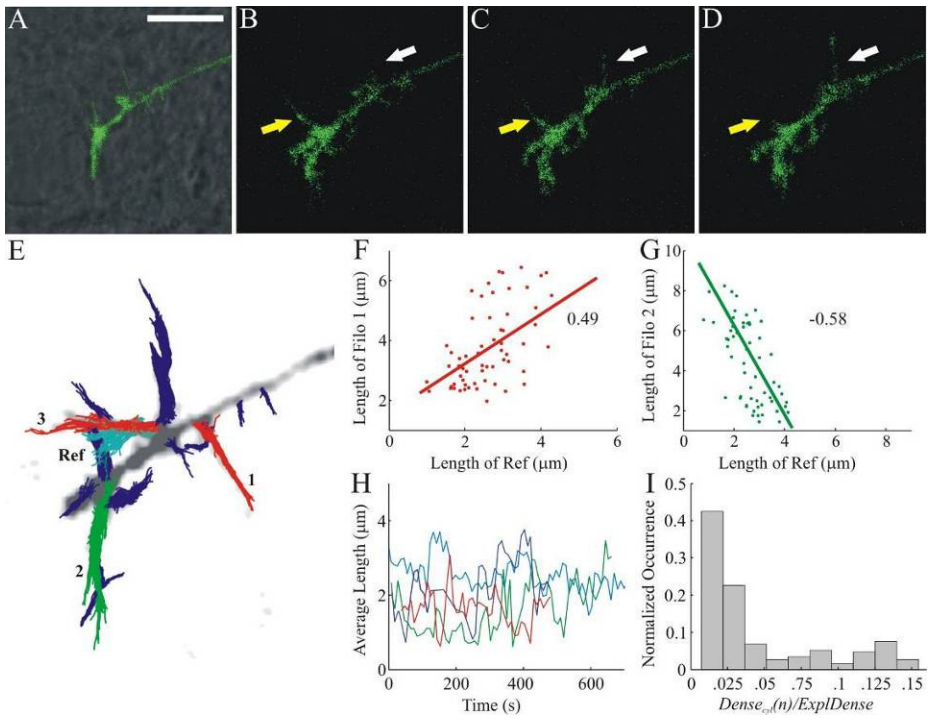

Fig. 6. Filopodia motion in dense neuronal cultures. **A-D**: Time lapse images of a growth cone from a hippocampal neuron transfected with EGFP. **A**: Overlay of a transmitted and fluorescent image. Scale bar: 10 µm. **B-D**: Example of negatively correlated growth: the filopodium indicated by the yellow arrow retracted whereas the filopodium indicated by the white arrow grew. **E**: 2D profile of filopodia emerging from the same growth cone. The filopodium indicated in cyan is taken as the reference filopodium, 'Ref'. **F-G**: Cross-correlation between the length of filopodia indicated by the corresponding numbers in panel **E** and the reference filopodium, 'Ref' indicated in cyan. Each point indicates the length of the two filopodia at different observation times. The length of filopodia marked in red and green are positively and negatively correlated respectively to the length of the filopodium marked in cyan. The length of blue filopodia is not significantly correlated to the length of the reference filopodium. **H**: Time evolution of the average filopodia length for four hippocampal growth cones. **I**: Percentage of explored free space by filopodia in dense hippocampal cultures computed as $Dense_{cyl}(n)/ExplDense$. Data from 7 hippocampal neuronal growth cones.

The average tip velocity of hippocampal filopodia was 0.06±0.04 µm/s (n=7) for hippocampal neurons vs. 0.4±0.3 µm/s (n=19) for DRG neurons. The total number of filopodia emerging from growth cones of DRG neurons varied from 2 to 18, rarely exceeding 15; while in hippocampal growth cones, the total number of filopodia varied from 2 to 8, rarely exceeding 5. The length of filopodia varied between 1 and 11 µm and their average length was around 3 µm (3.1±0.9 µm, range from 1.5 to 6.4 µm) (Fig. 6H). Similarly to what was observed for DRG growth cones, growth and retraction of neighboring filopodia was correlated: as shown in Figures 6B-D, when one filopodium retracted (yellow arrow), a neighboring filopodium grew (white arrow). The correlation coefficient ρ between the length of the reference filopodium (cyan in Fig. 6E) and that of the two red filopodia was 0.48 and 0.49 (Fig. 6F) whereas the value of ρ between length of the cyan filopodium and the length of the green filopodium was -0.58 (Fig. 6G). The growth of blue filopodia was not correlated to that shown in cyan.

We investigated the degree of correlated growth and retraction in 185 pairs of neighboring filopodia from 7 growth cones (see Table 1). Of all these pairs, 21.8% had a correlation coefficient higher than 0.5 suggesting a strong correlated behavior (1.5% were anticorrelated and 20.3% were correlated) while 39.8% were moderately correlated (28.2% were moderately anticorrelated while 11.6% were moderately correlated). The remaining 38.4% had a value of

$|\rho|<0.15$ and were considered not correlated. Therefore, we can conclude that filopodia growth and retraction is correlated also in dense hippocampal cultures. Correlated or anticorrelated growth or retraction was observed in pairs of filopodia emerging from the same growth cone and not necessarily from neighboring filopodia, as shown in Figures 6B-D.

DYNAMICS OF FILOPODIA AND LAMELLIPODIA MOTION

When a filopodium collides with an obstacle, it probes its chemical properties and mechanical resistance. Exploring filopodia can collide with an obstacle during their protrusion when polymerizing actin filaments push the membrane forward. Filopodia can also hit the obstacle from the side leading to a lateral collision. By using optical tweezers and appropriate detectors, it is possible to measure the bead position $\mathbf{x}=(x,y,z)$, its velocity $\mathbf{v}=(v_x,v_y,v_z)$ and the force $\mathbf{F}=(F_x,F_y,F_z)$ exerted on it by growth cones (Cojoc et al., 2007). Figure 7A shows the three components F_x, F_y and F_z of the exerted force $\mathbf{F}$ and Figure 7B the trajectory of the displaced bead in the 3D space. The force exerted by an isolated filopodium never exceeded 2 pN, neither during lateral collisions nor during protrusions.

While exploring, lamellipodia could displace encountered obstacles. During some collisions, the force developed primarily in one direction but, more often, the force $\mathbf{F}$ changed in all three orthogonal directions (Fig. 7A) and the bead described a complex trajectory (Fig. 7B). In these experiments (n=13), it was possible to measure simultaneously the force $\mathbf{F}$ exerted by the lamellipodium on the bead and its velocity $\mathbf{v}$. From these two vectorial quantities, the exerted power was obtained by their scalar product $\mathbf{F}\cdot\mathbf{v}$ (Fig. 7C) and the instantaneous power per unit area of the bead could reach values close to 10^{-17} Watt μm^{-2} as in the experiment analysed in Figure 7. When data were considered at a bandwidth up to 30 Hz, we measured power up to 10^{-16} Watt μm^{-2} in lamellipodia which were moving vigorously.

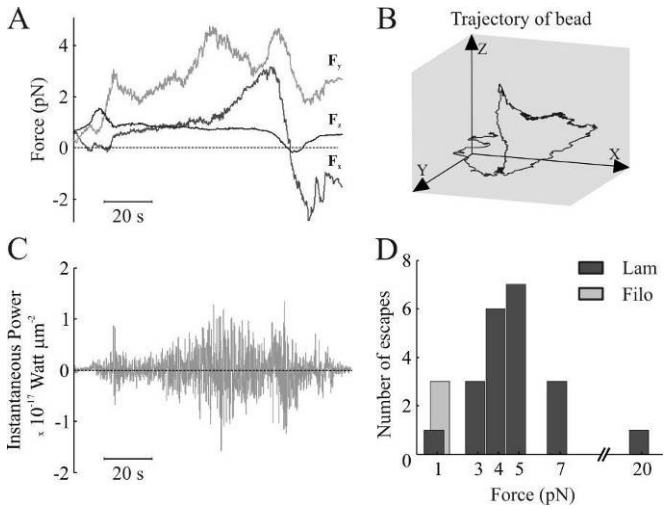

Fig. 7. Force exerted by filopodia and lamellipodia of DRG growth cones. **A**: The three components of the force F_x, F_y and F_z exerted by a lamellipodium during a collision with a trapped bead smoothed at 10 Hz. Forces measured with an optical tweezer (see Methods). **B**: Trajectory of the bead during its collision with the lamellipodium. The bead coordinates are detected using a quadrant position detector positioned on the back focal plane (see Methods). **C**: Instantaneous power produced by the lamellipodium per unit area of the bead during the collision, computed as $\mathbf{F}\cdot\mathbf{v}$, where $\mathbf{F}=(F_x,F_y,F_z)$ is the force exerted on the bead and $\mathbf{v}=(v_x,v_y,v_z)$ is the bead velocity. **D**: Histogram of collisions between trapped beads and filopodia (pale grey) and lamellipodia (dark grey) resulting with the displacement of the bead out of the optical trap, as a function of maximal trapping force. (Lam=lamellipodia, Filo=filopodia).

We counted the number of collisions (N= 24) in which filopodia and lamellipodia displaced the bead out of the optical trap. Beads were trapped with different laser powers so to vary the stiffness of the encountered obstacles and almost one hundred collisions were observed. Filopodia are less suitable than lamellipodia to displace obstacles: indeed only occasionally (3/24), an isolated filopodium was able to move a bead out of its trap: in all these cases, the maximal trapping force F_{max} was 1 pN (Fig. 7D). A trapping force of 1 pN is very small and corresponds to an almost negligible stiffness. When F_{max} was increased to 3 pN, we never observed a filopodium displacing a bead out of its trap and we concluded that isolated filopodia cannot efficiently displace obstacles even those with a low stiffness. In contrast, lamellipodia could displace beads from the trap even when the maximum trapping force was 20 pN (Fig. 7D). In these experiments, the bead diameter was 1 μm and therefore the measured maximal pressure and power per unit area of the bead was 20 pN μm^{-2} and 10^{-16} Watt μm^{-2}. If lamellipodia exert maximal pressure of the order of 20 pN μm^{-2}, the total force exerted by a lamellipodium on an obstacle, such as debris or a cell intruding in the path towards its desired destination will depend on its size. Therefore, lamellipodia are expected to exert larger forces on larger obstacles, possibly up to hundreds of pN.

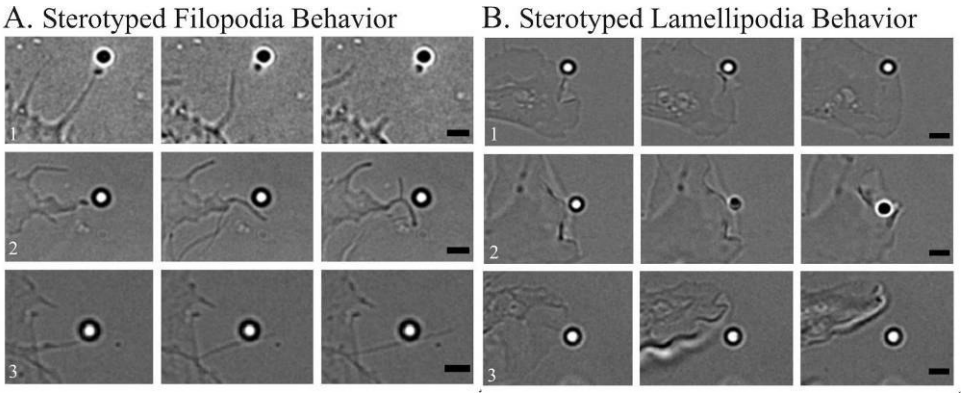

Fig. 8. Stereotyped filopodia (**A**) and lamellipodia (**B**) behaviors in the presence of an obstacle mimicked by a silica bead of 1 μm diameter trapped with an optical tweezers. See text for an illustration of these behaviors. Scale bar: 2 μm.

When filopodia and lamellipodia encounter obstacles, they seem to follow stereotyped patterns. An isolated filopodium colliding with an obstacle exhibits three possible behaviors illustrated in Figure 8A: 1) it can collide with the obstacle and then fully retract (Fig. 8A1); 2) after the initial collision the filopodium partially retracts branching new filopodia in one and even two different directions (Fig. 8A2); 3) a light collision with the obstacle, after which the filopodium continues its growth or exploration (Fig. 8A3). We have analysed the probability of these three different behaviors as a function of the obstacle stiffness, i.e. its resistance to an exerted force. Data collected from 98 experiments show that strong collisions with a stiff obstacle were usually followed by a retraction. Similarly, when a lamellipodium encounters an obstacle, it reacts in three possible ways: 1) it collides with the obstacle but continues its motion by growing underneath it (Fig. 8B1); 2) it can collide with the obstacle in a “shovel like” fashion, displacing it rearwards (Fig. 8B2); 3) it can retract (Fig. 8B3). We have analysed the probability of these three different behaviors as a function of the obstacle stiffness, but we could not find any clear correlation between stiffness and lamellipodium behavior.

The results illustrated in Figures 7 and 8 show several dynamical properties of filopodia and lamellipodia. Firstly, filopodia cannot displace obstacles and act primarily as exploring sensors but lamellipodia, in contrast, are able to efficiently displace obstacles. Secondly, lamellipodia can develop a power per unit area up to 10^{-16} Watt μm^{-2} and this power must be properly used and maintained. Thirdly, when encountering obstacles, filopodia and lamellipodia react displaying a stereotyped behavior. In the next section, it is argued that these stereotyped reactions are essential components of mechanical computation.

COMPUTATIONAL SECTION

This section aims to establish a computational framework in order to understand the kinetics and dynamics of filopodia and lamellipodia. We follow the classical view that a computation is the solution to a problem, which can be solved by the most general and simple computing device, i.e. the Turing Machine (Hopcroft et al., 2006). Therefore, we will use a computational approach by creating a pseudo-code (a program) able to solve mechanical problems.

As we have seen in the previous section, randomness is a major feature of filopodia and lamellipodia kinetics and dynamics. In growth cones, however, the random exploration of the environment is coupled to a variety of feedback loops. These feedback loops are formed by: i) the factors controlling axon growth and guidance molecules, such as neurotrophins, morphogens and molecules of extracellular matrix (Curinga and Smith, 2007); ii) the receptors present on the growth cone membrane which detect these factors; iii) the consequent activation of a signaling cascade within the growth cone. These loops are responsible for the rapid formation of physical contacts when two filopodia tips with appropriate receptors meet (Fig. 5) or for the rapid retraction of a filopodium when a stiff obstacle is encountered (Fig. 8). They have been optimized by billions of years of evolution making the random search and exploration "smart" and "efficient".

The combination of a random exploration with efficient feedback loops that continuously correct errors provides the basis of what we propose to be *mechanical computation,* by which neurons establish their appropriate physical and chemical contacts, migrate to their final destinations, enlarge and/or prune spines and synapses. Let us see some examples of mechanical computations and how the combination of a random search and feedback loops can lead to the efficient solution of mechanical problems. Mechanical computations will be described as pseudo-codes for a probabilistic Turing Machine (Hopcroft et al., 2006), mixing random searches with feedback loops.

MECHANICAL COMPUTATION: OBSTACLE AVOIDANCE

For simplicity, let us consider an idealized filopodium tip moving on a square grid, with the origin (0,0) in the upper left corner. The filopodium tip starts at an initial point on line 0 (which in the example of Figure 9A is (9,0)) and its goal is to reach any point on line 20 avoiding the obstacles shown in Figure 9A. The pseudo-code able to perform this mechanical computation is:

1 ***Move from (m,k) to (m+j,k+1)***
with p=½ if j=0 or with p=¼ if j=±1
If an obstacle is encountered, retract to (m,k)
and move with p=½ to to (m-1,k) or to (m+1,k)
Go to 1

The program is composed of one simple reaction, i.e., the instruction to advance and one feedback loop, i.e., the instruction to retract if an obstacle is encountered (indicated by the bold lines) and by random searches (indicated by the underlined line).

A filopodium tip following this program avoids obstacles and is able to reach its final destination (Fig. 9) following a simple trajectory with a limited number of retractions (Fig. 9A) or with a large number of growths and retractions (Fig. 9B). Black circles and white squares represent growth and retraction respectively while the black star represents the final destination in Figures 9A-B. The program - or the computation - is intrinsically probabilistic: the number of retractions (grey trace in Fig. 9C) and the number of steps (black trace in Fig. 9C) necessary to reach the final destination vary significantly from trial to trial from 20 to 100. As shown in Figure 9D, the distribution of number of growths (black) and of retractions (grey) had a long tail corresponding to the trials in which the filopodium tip did not find immediately its way through the obstacles and retracted before reaching its final destination (Fig. 9B). The computation can be made faster and more efficient by introducing a gradient of guidance molecules, as it will be shown in the next example.

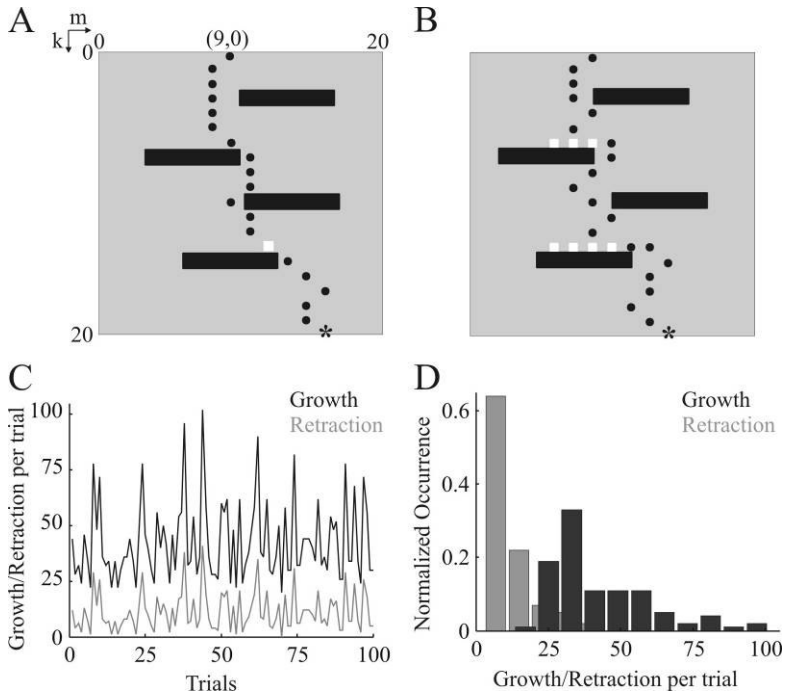

Fig. 9. Mechanical computation: Obstacle Avoidance. **A-B**: Two trajectories of a filopodium tip avoiding obstacles (black bars) and reaching the final destination (black star). **A** reproduces a fast trajectory with a low number of moves, whereas **B** reproduces a slow trajectory with several retractions and a high number of moves. Moves and retractions are denoted by black circles and white squares respectively. **C**: Number of growths (black trace) and retractions (grey trace) required to reach destination per trial. **D**: Normalized distribution of number of growths (black) and retractions (grey) per trial.

MECHANICAL COMPUTATION: FORMATION OF PHYSICAL CONTACTS

Let us now consider two idealized growth cones each formed by two filopodia (Fig. 10A) so that when one filopodium grows the other one retracts (see Figs. 3 and 6). This correlated behavior can be formalized by assuming that the length of the two filopodia l_1 and l_2 satisfies the relation $l_1+l_2=L$ where L is a fixed length. We assume also that one filopodium has at its tip a receptor R_1, able to form a physical contact with the tip of a different filopodium with the same receptor R_1.

Another filopodium has at its tip a different receptor R_2 which can form a physical contact with filopodia bearing at their tips the same receptor R_2. The exploratory motion of all these four filopodia is random but it is constrained by the condition that $l_1+l_2=L$. The mechanical computation to be solved is the formation of a physical contact between the filopodia tips with the same receptor R_i. The pseudo-program able to perform this mechanical computation is:

1 *The tip of filopodium 1 of growth cone 1 moves from (n_1,m_1) to (n_1+i,m_1+j) with probability $p_{i,j}$*
The tip of filopodium 2 of growth cone 1 moves from (k_1,h_1) to (k_1+i,h_1+j) so that $l_{1,1}+l_{2,1}=L$
The same for growth cone 2
If filopodia tips with the same receptors meet in the same location go to 2
Go to 1

2 Formation of a physical contact
Stop

where, the parameters "i" and "j" are constrained to single grid jumps, i.e. i and j=[-1,0,1] so that single step horizontal, vertical and diagonal moves are allowed. The simple reactions/feedbacks and random searches are indicated in the same style as in the previous pseudo-program.

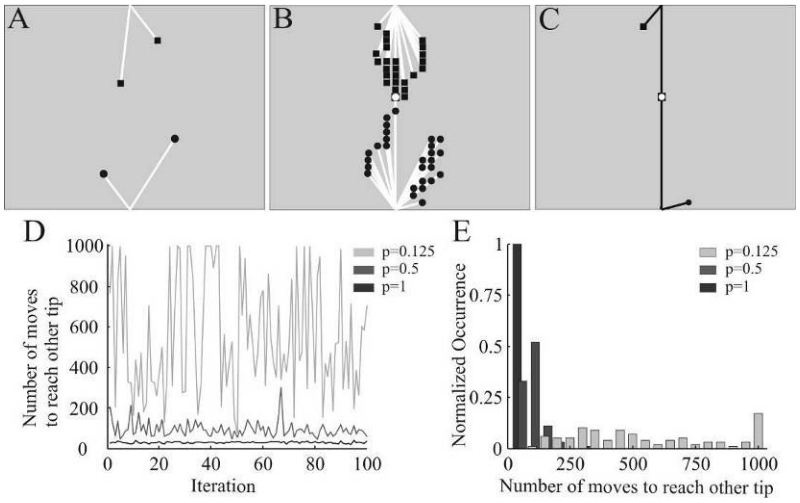

Fig. 10. Mechanical computation: Formation of Physical Contacts. **A**: Initial configuration of two idealized growth cones (black square and black circles) with two filopodia each. **B**: Representative configurations of the two growth cones before the formation of a physical contact. The total length of filopodia in each growth cone is constant. **C**: Final configuration, in which filopodia tips meet (white circle coinciding with black square). **D**: Number of steps required for formation of physical contact in different trials. When p=0.125, the search is completely random and the number of steps necessary to establish a physical contact is highly variable. When p=0.5, the search is biased by a chemical cue in the correct direction. When p=1, the search is completely deterministic and tips move straight towards each other. **E**: Normalized distribution of number of steps for p=0.125 (pale grey), p=0.5 (dark grey) and p=1 (black).

Given the initial configuration of two growth cones (Fig. 10A), the tips of the two filopodia in each growth cone move randomly (Fig. 10B) and after some iterations, a physical contact can be established (Fig. 10C). Also in this case, the number of necessary steps varies significantly from trial to trial (Fig. 10D). When the search is completely probabilistic - i.e., there are no guidance molecules present and the probability $p_{i,j}$ is equal in all directions (p=1/8=0.125) - a physical contact is established after a high number of moves. The number of moves, however,

can be substantially decreased by introducing guidance cues i.e, helping the two filopodia with the same receptors to meet more often. At each step, the probability $p_{i,j}$ of the filopodium tip bearing receptor R_i moving towards the tip of the filopodium bearing the same receptor R_i can be increased by introducing a guidance molecule. From a computational point of view, this is equivalent to increasing the probability to move towards the correct direction from p to p*, while the probability to move towards the other seven directions is reduced to (1-p*)/7. As shown in Figures 10D-E, the total number of moves required to establish a physical contact is substantially decreased when p*=1 (black trace) and p*=1/2 (dark grey trace) in comparison to the case where all p_{ij} are equal to 1/8 (pale grey trace). When p*=1, the search is completely deterministic and the physical contact is formed in a limited number of moves.

MECHANICAL COMPUTATION: OBSTACLE REMOVAL

Let us now consider a slightly more complicated mechanical computation: a lamellipodium besides retracting or avoiding obstacles also displaces them. At each cycle, the lamellipodium can exert a force $F_1<F_2<...F_i<\ldots<F_n$. Obstacles have varying stiffness $S_1<S_2<\ldots S_j<...<S_n$ (indicated by the numbers on the black/grey bars in Fig. 11A) and can be displaced when the lamellipodium exerts a force $F_i>S_j$. For this task, when an obstacle is encountered, the lamellipodium has to choose between two options: to retract or to advance while exerting a force F_i and see whether it will displace the obstacle. If the maximum force exerted by the lamellipodium is not strong enough to displace the obstacle, the lamellipodium will retract.

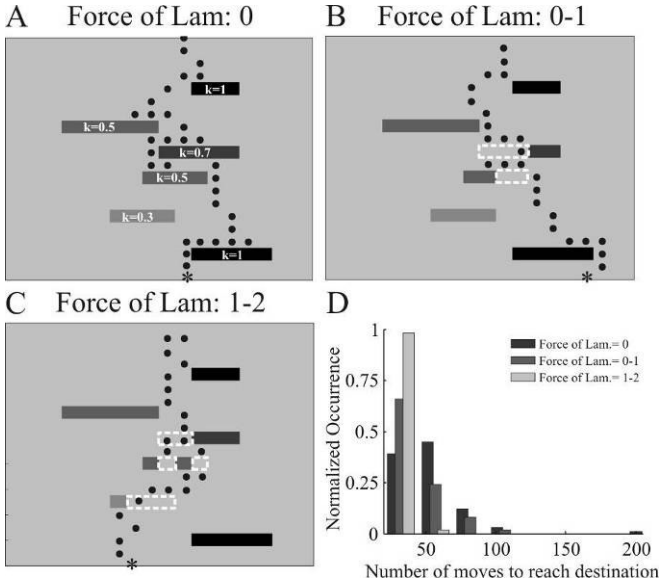

Fig. 11. Mechanical computation: Obstacle Avoidance and Removal (Lam stands for lamellipodium). **A**: Trajectory of a lamellipodium avoiding obstacles (represented by black bars) and reaching the final destination (black star), corresponding to line 20. Each obstacle has a stiffness ranging from 0 to 1, as indicated. **B-C**: Trajectories of a lamellipodium able to displace obstacles. The lamellipodium can exert forces varying from 0 to 1 (**B**), and from 1 to 2 (**C**). Force and stiffness are in the same arbitrary units. The lamellipodium can displace an obstacle and then it could retract, see some cases in **B** and **C**. Removed obstacles are shown as dotted white boxes. **D**: Normalized distribution of number of moves/steps necessary to reach the final destination when the lamellipodium does not exert a force (black), when it exerts a force varying from 0 to 1 (grey) and from 1 to 2 (pale grey).

As shown in Figure 11A, if the lamellipodium cannot exert any force, it has to navigate its way through the obstacles before finding its final destination. When the lamellipodium can exert forces up to 1 will displace objects with a stiffness lower than 1 (where the force and the stiffness

are in the same arbitrary unit).Therefore the lamellipodium is able to reach its final destination by avoiding or displacing obstacles (Fig. 11B). When the lamellipodium can exert forces up to 2, it can displace all obstacles and it will reach its final destination with a lower number of moves. Figure 11D shows the distribution of moves required to reach the final destination: as expected, a lamellipodium able to exert large forces will reach its final destination more rapidly.

DISCUSSION

Anatomical, biochemical and functional properties of growth cones and of their major components, lamellipodia and filopodia, have been thoroughly investigated (Aletta and Greene, 1988; Gomez and Letourneau, 1994; Baker and Macagno, 2007). The present work has two major aims: firstly, to examine in detail the kinetics and dynamics of filopodia and lamellipodia in an almost free environment and in a dense tissue; secondly, to provide a computational framework to rationalize the observed kinetics and dynamics.

Neurons process and compute information very efficiently, but during their entire lifespan, from the early stages of embryogenesis to adult neurogenesis, they also move, migrate and exert forces. Therefore, neurons not only process information but they also continuously perform and solve mechanical computations. In what follows, we will review several properties of the kinetics and dynamics of filopodia and lamellipodia and we will introduce and discuss the notion of mechanical computation.

EXPLORATION IN A FREE ENVIRONMENT

Growth cones explore the surrounding space through filopodia motion. Filopodia cannot exert forces larger than 2-3 pN (Kovar and Pollard, 2004; Footer et al., 2007; Cojoc et al., 2007) and therefore sense the environment in a gentle and delicate way. An optimal exploration requires an even sampling of the environment in space and time. As shown in Figure 2, filopodia explore the free space evenly, within 10 μm from the peripheral zone of the lamellipodium laterally and within 2-3 μm vertically. As shown in Figure 4, growth and retraction of filopodia emerging from the same growth cone are not completely independent, but are orchestrated in such a way to keep the filopodia average length more stable than expected from a complete statistical independence. This orchestrated behavior and the ability of filopodia to lift up (Fig. 2) allows a nearly optimal exploration of the surrounding environment. This orchestration of filopodia growth and retraction constitutes also an optimization of the available resources in which actin monomers are recycled from one filopodium to a neighboring one (Dent and Gertler, 2003; Medeiros et al., 2006) and consumption of ATP does not undergo large fluctuations with an excessive demand at specific times.

Filopodia have an average length of about 7 μm, occasionally extending up to 18 μm (Figs. 2 and 6) and are primarily composed by actin filaments. If the length between the tip and the base of an actin filament is significantly longer than its persistence length λ_p, then the tip and base will act almost independently and it will be nearly impossible to control the motion of the tip by acting on the base. In order to have a good control over the tip of a filopodium, its length must be comparable to λ_p, which for actin filaments in non-stabilized condition is around 9 μm (Isambert et al., 1995). These considerations suggest that the average length of exploring filopodia is close to λ_p, as experimentally observed (7.5±3.2 μm for DRG growth cones; 7.2±1.1 μm for PC12 growth cones).

EXPLORATION AND NAVIGATION IN A DENSE TISSUE

It is well known that spines are continuously formed and pruned in the developing and mature brain (Engert and Bonhoeffer, 1999; Maletic-Savatic et al., 1999; Ahmari and Smith, 2002; Fonseca et al., 2006) and it is not surprising that filopodia growth and retraction can also occur in a dense medium, such as a dense neuronal culture (Fig. 6). Hippocampal filopodia move at a speed (0.06±0.04 μm/s) approximately 5-8 times slower than DRG filopodia in a free environment (0.4±0.3 μm/s). Filopodia exploration in a dense tissue is restricted along specific paths where the local density of biological material is less pronounced.

When two exploring growth cones come close, they quickly establish several contacts (Fig. 5), which are maintained even when one growth cone retracts. These contacts are likely to be primarily mediated by adhesion molecules, such as the neuroligins and their binding partners, the neurexins, the B ephrins and their partners EphR, etc (Yamagata et al., 2003; Cline and Haas, 2008). These contacts are only structural and not yet functional: the formation of synapses is a much longer process occurring on a time scale of several hours (Nagerl et al., 2007; Cline and Haas, 2008). During long term potentiation, a sophisticated biochemical and genetic program is activated, but the insertion of new biological structures in synapses and dendrites requires a careful mechanical computation performed by the actin network and controlling proteins (Cingolani and Goda, 2008).

The migration of neurons in the developing brain or during adult neurogenesis necessitates the generation of larger forces: the force generated by a migrating keratocyte is of the order of 1-2nN (Prass et al., 2006), i.e. 10-100 times larger than the maximal force measured in a differentiating neuron (Cojoc et al., 2007). During morphogenesis, neuronal precursor cells migrate from the zone where they were born to their final destinations, which are often several millimeters away (Solecki et al., 2006; Ghashghaei et al., 2007) and in doing so, they must produce a substantial force and power. The dynamics of filopodia and lamellipodia are particularly interesting in densely packed tissue and it will be important to determine whether they show similar behaviors as those observed in our analysis *in vitro*, and whether mechanical forces of the same magnitude are generated and play an important role in the insertion of new cells into, for example, the hippocampus or the cortex. It is difficult to measure with optical tweezers and/or Atomic Force Microscopy the force exerted by exploring filopodia in a dense tissue. As the molecular mechanisms controlling force generation in isolated neurons and in neurons embedded in a tissues are expected to be the same or similar, forces per unit area exerted by filopodia and lamellipodia in the brain are expected to be of the order of tens pN μm^{-2}.

The fraction of the volume explored by hippocampal filopodia in a dense culture (Fig. 6) is about 10 times less than that explored by DRG filopodia (Fig. 2) in an almost free environment. This difference could be due to the fact that DRG are peripheral sensory neurons while hippocampal neurons are from the central nervous system and have different membrane receptors and motor proteins. In addition, DRG neurons are plated on a glass coated with poly-L-lysine while hippocampal neurons grow on top of other cells, hence their growth cones move on or within the extracellular matrix.

INTERACTION WITH OBSTACLES

When exploring, filopodia and lamellipodia often encounter obstacles and their reaction appears to follow stereotyped patterns (Fig. 8). After collision, an isolated filopodium either completely retracts, or partially retracts and branches new filopodia, or lightly collides with the obstacle and continues its growth. Similarly, a lamellipodium either collides with the obstacle and continues its motion by growing underneath it, or removes it in a “shovel like” fashion, or retracts. We have not been able to determine when and how a given reaction is chosen or decided and we propose that the choice is the result of a random process leading to a trial and error

procedure. These reactions are likely to be mediated by receptors located at the filopodia and lamellipodia tips, such as the integrins, which are coupled to the cytoskeleton acting as signaling transducers and also helping the neuron to attach to the extracellular matrix or to other cells (Hynes, 2002).

MECHANICAL COMPUTATION: A PERSPECTIVE

The specific examples of mechanical computation illustrated in this manuscript can be addressed and studied from a molecular perspective. This requires a careful identification of all proteins and enzymes involved and a detailed analysis of the metabolic consumption occurring at each step (Mogilner and Oster, 1996; Carlsson, 2001&2003; Janson et al., 2003; Mogilner and Rubinstein, 2005; Mogilner, 2006; Kerssemakers et al., 2006), which is beyond the scope of this article. Besides, it is also essential to understand the global computational plan in a more abstract form, as illustrated in Figures 9-11. Two factors seem to be at the basis of mechanical computation: an exploratory search relying on a trial and error strategy and a set of efficient feedback loops and/or simple reactions mediated by a variety of receptors and local protein networks, as discussed in the previous sections. The overall computation will not be deterministic and its accuracy, timing and performance will depend on the efficiency of the feedback loops, as illustrated in Figure 10.

Fundamental functions of the nervous system, such as parallel and information processing, require the solution of mechanical problems, which have not yet been addressed from a computational point of view. Let us consider, for instance, neuronal plasticity and memory formation, which are at the basis of higher brain functions. One of the simplest mechanisms underlying memory formation is spine enlargement and the insertion of new receptors in its membrane. The motion of these receptors is primarily driven by random fluctuations (Triller and Choquet, 2008) caused by Brownian collisions with water molecules. In this case, the diffusive dynamics is constrained by specific molecular interactions so that molecules find their targets in a time scale compatible with the appropriate occurrence of biological events. Spine enlargement and the insertion of new receptors require the assembly of actin filaments, the transportation of new proteins from their synthesis sites, the generation of forces to open the way to the growing spine and many other steps. These biological events occur in a physical environment where forces are exerted and energy is consumed and these events necessitate the solution of mechanical problems that require sophisticated timing and planning. The understanding of these issues from a computational perspective is one of the aspects of mechanical computation.

Many problems of mechanical computation can be addressed with well known tools from Complexity Theory and Computational Geometry (Hopcroft et al., 2006) and are likely to be very similar to those addressed in Robotics (Xie, 2003). The exploration of an unknown environment by a random search is a strategy that is found very often in nature: indeed, it is used by insects and worms for food search, navigation, homing (Poggio and Reichardt, 1973; Valente et al., 2007) and also by mammals such as mice during maze exploration and other behavioral tasks (Drai et al., 2000). Finally, it is important to remember that random searches are also used in Computer Science to solve very difficult issues, such as finding global minima in optimization problems (Kirkpatrick et al., 1983) and finding approximate solutions for NP-complete problems (Boseniuk and Ebeling, 1988; Accardi and Ohya, 2004).

REFERENCES

Accardi L, Ohya M, 2004. A stochastic limit approach to the SAT problem. Open Sys & Information Dyn 11:219-233.

Ahmari SE, Smith SJ. 2002. Knowing a nascent synapse when you see it. Neuron 34:333-336.

Aletta JM, Greene LA. 1988. Growth cone configuration and advance: a time-lapse study using video-enhanced differential interference contrast microscopy. J Neurosci 8:1425-1435.

Atilgan E, Wirtz D, Sun SX. 2006. Mechanics and dynamics of actin-driven thin membrane protrusions. Biophys J 90:65-76.

Baker MW, Kauffman B, Macagno ER, Zipser B. 2003. *In vivo* dynamics of CNS sensory arbor formation: a time-lapse study in the embryonic leech. J. Neurobiol 56:41-53.

Baker MW, Macagno ER. 2007. *In vivo* imaging of growth cone and filopodial dynamics:evidence for contact-mediated retraction of filopodia leading to the tiling of sibling processes. J Comp Neurol 500:850-862.

Bonifazi P, Ruaro ME, Torre V. 2005. Statistical properties of information processing in neuronal networks. Eur J Neurosci 22(11):2953-2964.

Boseniuk T, Ebeling W. 1988. Optimization of NP-Complete problems by Boltzmann-Darwin strategies including life cycles. Europhys Lett 6:107-112.

Bray D, Thomas C, Shaw G. 1978. Growth cone formation in cultures of sensory neurons. Proc Natl Acad Sci USA 75:5226-5229.

Bustamante C, Macosko JC, Wuite GJ. 2000. Grabbing the cat by the tail: manipulating molecules one by one. Nat Rev Mol Cell Biol 1:130-136.

Carlsson AE. 2001. Growth of branched actin networks against obstacles. Biophys J 81:1907-1923.

Carlsson AE. 2003. Growth velocities of branched actin networks. Biophys J 84:2907-2918

Cingolani LA, Goda Y. 2008. Actin in action: the interplay between actin cytoskeleton and synaptic efficacy. Nat Rev Neurosci 9(5):344-356.

Cline H, Haas K. 2008. The regulation of dendritic arbor development and plasticity by glutamatergic synaptic input: a review of the synaptotrophic hypothesis. J Physiol 586:1509-1518.

Cojoc D, Difato F, Ferrari E, Shahapure RB, Laishram J, Righi M, Di Fabrizio EM, Torre V. 2007. Properties of the force exerted by filopodia and lamellipodia and the involvement of cytoskeletal components. PLoS ONE 2(10):e1072. doi:10.1371/journal.pone.0001072.

Curinga G, Smith GM. 2007. Molecular/genetic manipulation of extrinsic axon guidance factors for CNS repair and regeneration. Exp Neurol 209(2):333-342.

Dai J, Sheetz MP. 1995. Mechanical properties of neuronal growth cone membranes studied by tether formation with laser optical tweezers. Biophys J 68:988-996.

Dennerll TJ, Lamoureux P, Buxbaum RE, Heidemann SR. 1989. The cytomechanics of axonal elongation and retraction. J Cell Biol 109(6):3073-3083.

Dent EW, Kalil K. 2001. Axon branching requires interactions between dynamic microtubules and actin filaments. J Neurosci 21:9757-9769.

Drai D, Benjamini Y, Golani I. 2000. Statistical discrimination of natural modes of motion in rat exploratory behavior. J Neurosci Meth 96(2):119-31.

Duncan M, Fothergil T, Pujic Z, Richards LJ, Goodhill GJ. 2008. Growth cone chemotaxis. Trends Neurosci 31:90-98. doi:10.1016/j.tins.2007.11.008.

Engert F, Bonhoeffer T. 1999. Dendritic spine changes associated with hippocampal long-term synaptic plasticity. Nature 399:66-70.

Fonseca R, Nagerl UV, Bonhoffer T. 2006. Neuronal activity determines the protein synthesis dependence of long-term potentiation. Nat Neurosci 9:478-480.

Footer MJ, Kerssemakers JW, Theriot JA, Dogterom M. 2007. Direct measurement of force generation by actin filament polymerization using an optical trap. Proc Natl Acad Sci USA 104:2181-2186.

Galbraith CG, Yamada KM, Galbraith JA. 2007. Polymerizing actin fibers position integrins primed to probe for adhesion sites. Science 315:992-995.

Gallo G, Letourneau PC. 2000. Neurotrophins and the dynamic regulation of the neuronal cytoskeleton. J Neurobiol 44:159-173.

Ghashghaei HT, Lai C, Anton ES. 2007. Neuronal migration in the adult brain: are we there yet? Nat Rev Neurosci 8:141-151.

Goodman CS. 1996. Mechanisms and molecules that control growth cone guidance. Annu Rev Neurosci 19:341-377.

Gomez TM, Letourneau PC. 1994. Filopodia initiate choices made by sensory neuron growth cones at laminin/fibronectin borders *in vitro*. J Neurosci 14:5959-5972.

Gordon-Weeks PR. 2004. Microtubules and growth cone function. J Neurobiol 58:70-83.

Goslin K, Banker G. 1998. Culturing nerve cells. 2nd ed. Cambridge, MA: MIT Press. Rat hippocampal neurons in low-density culture, p 339-370.

Grunwald IC, Klein R. 2002. Axon guidance: receptor complexes and signaling mechanisms. Curr Opin Neurobiol 12:250-259.

Guan KL, Rao Y. 2003. Signalling mechanisms mediating neuronal responses to guidance cues. Nat Rev Neurosci 4:941-956.

Heidemann SR, Wirtz D. 2004. Towards a regional approach to cell mechanics. Trends Cell Biol 14(4):160-166. doi:10.1016/j.tcb.2004.02.003

Hopcroft, JE, Motwani R & Ullman JD. 2006. Introduction to Automata Theory, Languages and Computation. 3rd ed. Addison-Wesley Eds. New York.

Howard J. 2001. Mechanics of Motor Proteins and the Cytoskeleton. Sinauer Associates, Inc., Sunderland, MA. 384 pages.

Huber AB, Kolodkin AL Ginty DD, Cloutier JF. 2003. Signaling at the growth cone: ligand-receptor complexes and the control of axon growth and guidance. Annu Rev Neurosci 26:509-563.

Hynes R, 2002. Integrins: Bidirectional, Allosteric Signaling Machines. Cell 110(6):673-687.

Isambert H, Venier P, Maggs AC, Fattoum A, Kassab R, Pantaloni D, Carlier MF. 1995. Flexibility of actin filaments derived from thermal fluctuations. Effect of bound nucleotide, phalloidin, and muscle regulatory proteins. J Biol Chem 270:11437-11444.

Janson ME, de Dood ME, Dogterom M. 2003. Dynamic instability of microtubules is regulated by force. J Cell Biol 161:1029-1034.

Joshi HC, Chu D, Buxbaum RE, Heidemann SR. 1985. Tension and compression in the cytoskeleton of PC12 neurites. J Cell Biol 101:697 - 705.

Kerssemakers JW, Munteanu EL, Laan L, Noetzel TL, Janson ME, Dogterom M. 2006. Assembly dynamics of microtubules at molecular resolution. Nature 442:709-712.

Kirkpatrick S, Gelatt CD Jr & Vecchi MP. 1983. Optimization by Simulated Annealing. Science 220:671-680.

Köhrmann M, Haubensak W, Hemraj I, Kaether C, Leβmann VJ, Kiebler MA. 1999. Fast, convenient, and effective method to transiently transfect primary hippocampal neurons. J Neurosci Res 58:831-835.

Kovar DR, Pollard TD. 2004. Insertional assembly of actin filament barbed ends in association with formins produces piconewton forces. Proc Natl Acad Sci USA 101:14725-14730.

Maletic-Savatic M, Malinow R, Svoboda K. 1999. Rapid dendritic morphogenesis in CA1 hippocampal dendrites induced by synaptic activity. Science 283:1923-1927.

Medeiros NA, Burnette DT, Forscher P. 2006. Myosin II functions in actin-bundle turnover in neuronal growth cones. Nat Cell Biol 8:215-226.

Mogilner A, Oster G. 1996. Cell motility driven by actin polymerization. Biophys J 71:3030-3045.

Mogilner A, Rubinstein B. 2005. The physics of filopodial protrusion. Biophys J 89:782-795.

Mogilner A. 2006. On the edge: modeling protrusion. Curr Opin Cell Biol 18(1):32-9.

Mongiu AK, Weitzke EL, Chaga OY, Borisy GG. 2007. Kinetic-structural analysis of neuronal growth cone veil motility. J Cell Sci 120:1113-1125.

Nagerl UV, Kostinger G, Anderson JC, Martin KA, Bonhoffer T. 2007. Protracted synaptogenesis after activity-dependent spinogenesis in hippocampal neurons. J Neurosci 27(30): 8149-56.

Neuman KC, Block SM. 2004. Optical trapping. Rev Sci Instrum 75:2787-2809.

Nicholls JG, Martin AR, Wallace BG, Fuchs PA. 2001. From Neuron to Brain. 4th ed. Washington: Sinauer Associates, Inc.

Pampaloni F, Lattanzi G, Alexandr Jonas A, Surrey T, Frey E, Florin E-L. 2006. Thermal fluctuations of grafted microtubules provide evidence of a length-dependent persistence length. PNAS 103;10248-10253. doi:10.1073/pnas.0603931103.

Poggio T, Reichardt W. 1973. A theory of the pattern induced flight orientation of the fly Musca domestica. Kybernetyk 12(4):185-203.

Pollard TD, Blanchoin L, Mullins RD. 2000. Molecular mechanisms controlling actin filament dynamics in nonmuscle cells. Annu Rev Biophys Biomol Struct 29:545-576.

Prass M, Jacobson K, Mogilner A, Radmacher M. 2006. Direct measurement of the lamellipodial protrusive force in a migrating cell. J Cell Biol 174:767-772.

Schaefer AW, Kabir N, Forscher P. 2002. Filopodia and actin arcs guide the assembly and transport of two populations of microtubules with unique dynamic parameters in neuronal growth cones. J Cell Biol 158:139-152.

Solecki DJ, Govek EE, Hatten ME. 2006. mPar6 alpha controls neuronal migration. J Neurosci 26:10624-10625.

Song H, Poo M. 2001. The cell biology of neuronal navigation. Nat Cell Biol 3:E81-E88.

Rohrbach A, Tischer C, Neumayer D, Florin E-L, Stelzer EHK. 2004. Trapping and tracking of a local probe with the photonic force microscope. Rev of Sci Instr 75(6):2197-2210.

Triller A, Choquet D. 2008. New concepts in Synaptic Biology Derived from Single-Molecule Imaging. Neuron 59:359-374.

Valente D, Golani I, Mitra PP. 2007. Analysis of the trajectory of *Drosophila melanogaster* in a circular open field arena. PLoS ONE. Oct 24; 2(10):e1083.

Yamagata M, Sanes JR, Weiner JA. 2003. Synaptic adhesion molecules. Curr Opin Cell Biol 15(5):621-632.

Xie M. 2003. Fundamentals of robotics: linking perception to action. (Series in Machine Perception and Artificial Intelligence). World Scientific. ISBN-13:9789812383358.

10.2. Manuscript 2:

A morphological analysis of growth cones of DRG neurons combining Atomic Force and Confocal Microscopy

Jummi Laishram, Shripad Kondra, Daniela Avossa, Elisa Migliorini,
Marco Lazzarino, Vincent Torre

Under Review

A morphological analysis of growth cones of DRG neurons combining Atomic Force and Confocal Microscopy

Jummi Laishram[a], Shripad Kondra[a], Daniela Avossa[a], Elisa Migliorini[c], Marco Lazzarino[b,c], Vincent Torre[a,d]*

[a]*International School for Advanced Studies (SISSA-ISAS), 34012, Trieste, Italy.*
[b]*CBM-Area Science Park - Basovizza 34012 Trieste, Italy.*
[c]*CNR-INFM laboratorio TASC Area Science Park - Basovizza 34012 Trieste, Italy.*
[d]*Italian Institute of Technology, ISAS Unit, Italy.*

*Author for correspondence:
Vincent TORRE
International School for Advanced Studies (SISSA/ISAS),
Ed. Q1 AREA SCIENCE PARK, S.S.14 Km 163,5,
34012 Basovizza (TS), Italy.
Tel.: +39 040 3756513
Fax: +39 040 3756502.
E-mail address: torre@sissa.it

Abstract

We have analyzed the morphology of growth cones of differentiating neurons from rat dorsal root ganglia (DRG) with conventional Laser Scanning Confocal Microscopy (LSCM) and Atomic Force Microscopy (AFM). Images of immunofluorescent DRG growth cones colabeled for actin and tubulin were superimposed to images obtained with AFM at different scanning forces. In order to reduce changes of the image surface caused by the pressure of the AFM tip, we have developed a procedure to obtain 0 pN AFM images. Further analysis of these images revealed topographical structures with nanoscale dimensions, referred to as "invaginations" or "holes". These holes had an area varying from 0.01 to 3.5 μm^2 with a depth varying from 2 to 178 nm. Comparative analysis with LSCM images showed that these holes correspond to regions where staining of both actin and tubulin was negligible. Filopodia height varied from 40 to 270 nm and their diameter from 113 to 887 nm. These results show that the combination of LSCM and AFM reveal structural details with a nanoscale dimension of DRG growth cones, difficult to resolve with conventional microscopy.

Key words: invagination, cytoskeleton, growth cone, AFM, holes

1. Introduction

The cellular membrane separates and isolates internal organelles and the nucleus from the external environment, while allowing specific ions and compounds to permeate through it (Kandel et al., 2000). Its mechanical properties determine the way in which the membrane wraps the cell interior: when the cellular membrane is rigid the cell interior will be wrapped as an inflated balloon and the external surface will be minimal. In contrast, if the membrane is flexible then the cellular membrane will have several invaginations and its total surface will be larger than when it is rigid. Mechanical properties of cells and neurons depend on the elastic properties of the membrane, usually characterized by its Young modulus (Howard, 2001) and by its interactions with the cytoskeleton (Hofmann et al., 1997), primarily composed of actin filaments and microtubules. Measurements of the Young' modulus obtained with the cantilever tip of Atomic Force Microscope in cells provide values ranging from 0.1 up to 400 kPa, i.e. values varying by 3 orders of magnitude (Kuznetsova et al., 2007). This large variability can be ascribed - to some extent - to different experimental procedures and also to an intrinsic variability of mechanical properties of cells and neurons, which could change significantly in different phases of their cycle and according to the functions which have to be performed. For instance, it is expected that cellular mechanical properties change when cells or neurons move and migrate and when they retract or undergo pruning or other endocytotic processes. Indeed, it has been reported that migrating cells can leave tracks of a small size in the order of 50-100 nm (Kirfel et al., 2004). Similarly, growth cones of axons entering the "decision zone" can pause and holes can appear in their lamellipodium (Godement et al., 1994; Mason and Erskine, 2000).

Atomic Force Microscopy (AFM) can provide a precise measurement with a nanometer resolution of the shape - size, height and degree of invagination - of cellular membranes and in particular of growth cones and its constituents, i.e. lamellipodia and filopodia. The advantages of using AFM lie in the nanometer resolution that it offers. Using this technique, we can obtain precise information of the shape, size, and height of a biological sample. The process by which AFM obtains the topographical information of the sample under investigation is via the interaction i.e., the repulsion or attraction between the probe and the sample. The probe is typically a tip at the free end of a silicon cantilever and scans the region of interest. A small laser, focused on the cantilever, detects small deflection of its tip, providing therefore a precise measurement of the distance between the tip and the sample. The result is an image of interaction values providing a three-dimensional (3D) map of the sample height. This information provides a precise characterization of the surface topography of the sample under investigation.

Early investigations using AFM (Parpura et al., 1993; Bonfiglio et al., 1995) have shown that filopodia height was in the 100 nanometers (nm) range, but they have also shown that the cantilever tip of the microscope, which has been also used to perform nanosurgery, can damage neurons. AFM has already been used to image live hippocampal neurons (Yunxu et al., 2006) and to explore adhesion of neurons on silicon wafer (Ma et al., 2005 & 2007, Young and Chen, 2006). Ohshiro et al. (2000), Zhang et al. (2004) and Ricci et al. (2004) have visualized dendrites and growth cones in a variety of cultures and co-cultures. It is also possible to functionalize the cantilever tip with Nerve Growth Factor (Reddy et al., 2004) or appropriate antibodies (Li et al., 2006) and to localize specific molecules on the neuron with a high resolution.

In the present manuscript, we have investigated the shape and degree of invagination of the external surface of differentiating neurons from dorsal root ganglia (DRG) after 20-30 hours of culture. We have combined Laser Scanning Confocal Microscopy (LSCM) imaging of cytoskeletal components stained with antibodies to high resolution imaging of the external surface with AFM (Kondra et al., 2009). Many growth cones had a fragmented shape composed of several nanoscale microstructures. Such studies can lead to a better understanding of

neurodegeneration where the mechanical and morphological properties of neurons and of growth cones change; and studies on these changes can be of paramount importance.

2. Materials and Methods

2.1. DRG Neuron Culture

DRG neurons were prepared from P10-12 Wistar rats as previously described in Cojoc et al. (2007). Briefly, Wistar rats were anesthetized with CO_2 and sacrificed by decapitation in accordance with the Italian Animal Welfare Act and approved by the Local Authority Veterinary Service. DRGs were incubated with 0.5 mg/ml trypsin, 1 mg/ml collagenase, and 0.1 mg/ml DNase (all from Sigma-Aldrich) in 5 ml Neurobasal medium (Invitrogen) in a shaking bath at 37°C for 35-40 minutes. They were mechanically dissociated, centrifuged at 300 rpm, resuspended in culture medium, and plated on 0.5 μg/ml poly-L-lysine (PLL; Sigma-Aldrich) and Matrigel (BD Biosciences, Bedford, MA, USA) - coated 24 mm coverslips in Neurobasal medium (Invitrogen) containing 10% fetal bovine serum (FBS; Sigma-Aldrich) and 100 ng/ml nerve growth factor (NGF; Alomone, Israel) at a density of 10^4 cells/ml (corresponding to ~2000 cells/cm^2). Cells were then fixed 20-30 hours after differentiation.

2.2. Cell Fixation

Before imaging with LSCM and AFM, DRG neurons were fixed. In order to verify that the observed structural details were not caused by the specific fixation method, two fixation procedures were used and compared: with Paraformaldehyde and Glutaraldehyde.

Fixation with Paraformaldehyde (PFA): DRG neurons were fixed by incubating in 4% PFA (Sigma-Aldrich) containing 0.15% picric acid in phosphate-buffered saline (PBS) for 20 minutes at room temperature (RT), rinsed in PBS, and incubated in blocking solution (consisting of 5% fetal bovine serum, 0.3% Triton X-100 in PBS) for 30 minutes at 37°C.

Fixation with Glutaraldehyde (GLU): DRG neurons were perfused 3 times with 0.25% GLU (Sigma-Aldrich) in buffer solution (consisting of 100 mM Cacodylate (pH 7.4), 5 mM $CaCl_2$ and 10 mM $MgCl_2$) and incubated in buffer solution for 10 minutes at 37°C (Rochlin et al., 1995).

2.3. Immunofluorescence

After fixation, cultures were washed 4X with PBS and then incubated for 30 minutes at RT with the monoclonal antibody TUJ1 (1:500 dilution in blocking solution; Covance, Berkeley, CA, USA), which recognizes the neuron specific Class III β-tubulin. After washing 2X, cultures were incubated for another 30 minutes at RT with Alexa Fluor 594 anti-mouse antibody (1:300 dilution; Molecular Probes) and Alexa Fluor 488 Phalloidin (1:10 dilution; Sigma-Aldrich). Nuclei were stained with DAPI (1:1000 dilution; Boehringer Mannheim GmbH, Germany). After washing 3X with PBS, the coverslips were mounted in Vectashield (Vector Labs., Burlingame, CA, USA).

2.4. Confocal Imaging

Cells were imaged using a confocal (Leica DMIR2) microscope, equipped with Diode laser (emitting at 405 nm), Ar/ArKr (at 488 nm), He/Ne (at 543/594 nm) and He/Ne (at 633 nm) lasers. A stack of 4-7 images, 400 to 700 nm apart, were collected with a 40X magnification and 1.44 NA oil- immersion objective. The averaged image of the stack was used to compare with the images acquired using AFM.

2.5. AFM Imaging

Atomic Force Microscopy (AFM) was performed using a commercial AFM (Nanowizard II, JPK Berlin) combined with an inverted optical microscope (Zeiss Axiovert 200), and a fluorescence set-up (Zeiss X-cite). Neurons fixed on 24 mm diameter glass coverslips were mounted on the AFM liquid cell, filled with PBS solution and mounted onto the AFM microscope. After laser alignment and tip calibration, the system was left to settle for 30 minutes with laser and microscope condenser switched on to minimize thermal and force drift during image acquisition. AFM was operated in contact mode in liquid medium and the contact force of the cantilever tip was adjusted during imaging to minimize the force exerted by the tip on the sample during scanning. Soft tips from VEECO with low force constant (OBL, 0.03 N/m) were utilized and forces were kept between 100 pN and 1 nN during scanning. AFM scanner position sensors detect the position of the tip with an accuracy of 2-3 nm and AFM images were acquired using the commercial Software (DirectOverlay, JPK, Berlin).

2.6. Registration of Confocal and AFM Images

AFM and LSCM images contain different information: every pixel at location $(x,y)_{AFM}$ in the AFM images provides a direct measurement in nm of the sample height while fluorescence images characterize the emitted fluorescence at location $(x,y)_{LSCM}$ by a labeled biological structure. In order to integrate these different pieces of information, it is important to properly align or superimpose these images. This problem has been extensively studied in Computer Vision, where it is referred to as "*Registration*" of different images. The word *Registration* is used with two different meanings (Hill et al., 2001). The first meaning is to determine a transformation of one image so that features in the sensed image can be put in a one-to-one correspondence to features in the reference image. The second meaning of *Registration* enables also the comparison of the intensity at corresponding positions. It incorporates the concepts of re-sampling and interpolation. We will use the first meaning of *Registration*. The Registration Protocol by which LSCM and AFM images were superimposed is discussed in detail in Kondra et al. (2009) and in Appendix A. In brief, if (x,y) is the system of reference of image A and (x',y') and the system of reference of image B, the transformation from one system of reference to the other can be described by a simple multiplication with x' and y' as the coordinates of the transformed point.

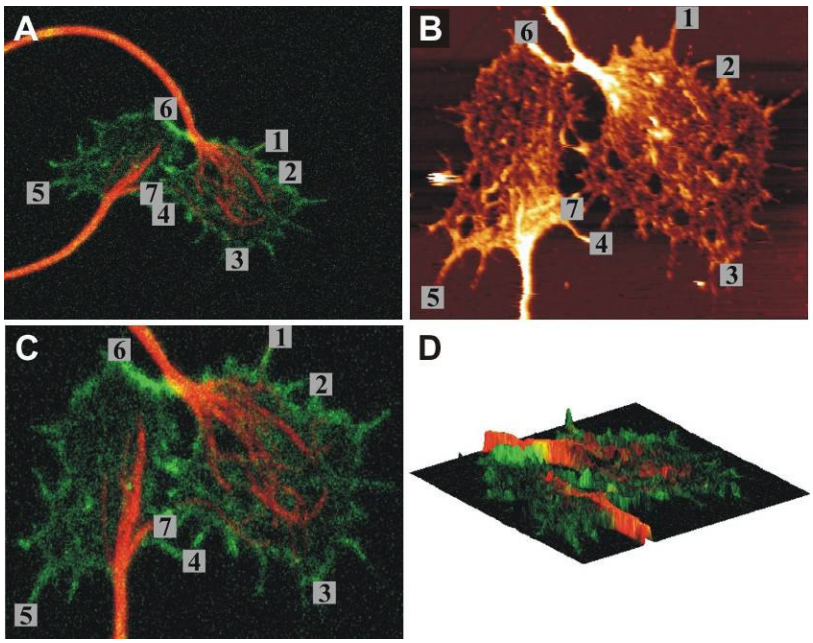

Fig. 1: Registration of LSCM Image with respect to AFM image. **A**: Original Confocal Image of a growth cone with Alexa488 Phalloidin for Actin and anti-β tubulin III, followed by Alexa594 anti-mouse IgG. **B**: AFM scanning of the same growth cone. **C**: Confocal image after registration with AFM scan. **D**: 3D view of the information from the two images superimposed.

2.7. Determination of the *0 pN AFM Image*

The operation of an AFM requires the application of a force to its cantilever. The minimal force required to acquire a stable height map of a sample is of the order of 100 pN. In order to verify whether properties of growth cones measured with AFM are affected by the force applied by the AFM cantilever on the sample, we obtained a series of AFM images of the same growth cone at increasing scanning forces, from 100 to 2000 pN, and then repeated with the lowest scanning force to confirm that the growth cone has not been destroyed by the multiple scans. As shown in Figs. 2A-C & E-G, very similar AFM images were obtained with low (100 pN) and high (2000 pN) scanning forces and the morphology is not destroyed. But it must be pointed out that higher scanning forces tend to press the more flexible structures (Fig. 2I). In order to eliminate this problem, we developed a procedure to obtain *0 pN AFM Images* by extrapolation.

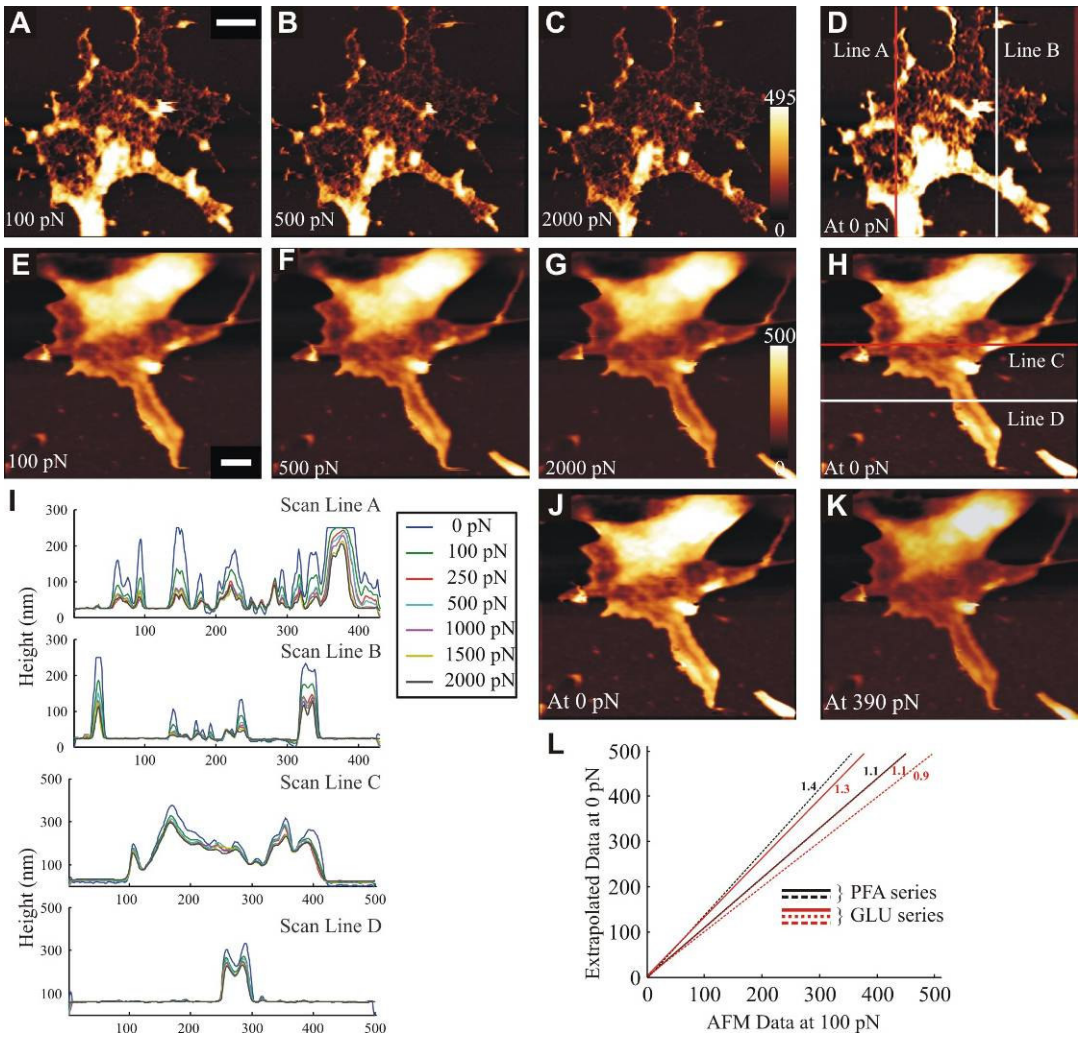

Fig. 2: AFM images at 0 pN scanning force: **A-C** and **E-G**: AFM series of growth cones fixed using PFA (**A-C**) and GLU (**E-G**) taken with different scanning forces. Color bar indicates height in nanometers. Scale bar: 2 µm. **D and H:** AFM images estimated for zero scanning force using Spline Interpolation on each AFM image series. **I:** Corresponding line profiles of the scan lines shown in **D** and **H**. **J**: *0 pN AFM Image* by extrapolation of the series. **K:** Interpolation at an arbitrary scanning force, in the figure, 390 pN. **L**: Relation between the AFM images at 100 pN and at 0 pN of different image series. Numbers indicate the slope of the line that fits the distribution of data points.

Once the AFM images are obtained at scanning forces varying from 100 to 2000 pN, they are registered with the image taken at the lowest force. The AFM image at *0 pN AFM Image* is obtained using *spline* interpolation of the pixel intensities obtained at different forces and is discussed in detail in Appendix C. Following this procedure, we obtain a database for different series of AFM images taken with different scanning forces of growth cones fixed using different fixation procedures. Using this database, we can find the corresponding AFM image at 0 pN for an AFM image of another sample taken with an arbitrary scanning force. Figs. 2D,H show two examples of the growth cones at 0 pN scanning force. In addition to obtaining images at 0 pN scanning force, this procedure can used to obtain the height map of a growth cone by interpolating for any desired scanning force (Fig. 2K). This procedure was repeated for the 5 growth cones fixed using either PFA or GLU. This provided us with a database to extrapolate or

interpolate AFM images to any scanning force. Fig. 2L shows the relation between the AFM images at 100 pN and at 0 pN of different image series, and suggests that we can estimate the 0 pN AFM image for an image scanned at any arbitrary force using either database.

2.8. Morphometric characterization of Holes in DRG Growth Cones

As will be shown in the Results section, the outer membrane of DRG growth cones when imaged with AFM often exhibit significant invaginations and holes. We have characterized these holes by measuring the depth and size of these holes by using tools inspired by Computer Vision, such as snake algorithms (Kass et al., 1987; Xu and Prince, 1998). An approximating closed region Γ around the growth cone is selected by the user (Fig. 3B green trace), and then a snake algorithm is applied, which drives Γ to the boundary of the growth cone. (Fig. 3B blue trace). The surface of an arbitrary surface can be approximated by Delaunay triangulation (Barber et al., 1996). Holes are detected and analyses were performed following the protocol described in Appendix B by using a graphical interface written in Matlab 7.1 (The MathWorks Inc. http://www.mathworks.com).

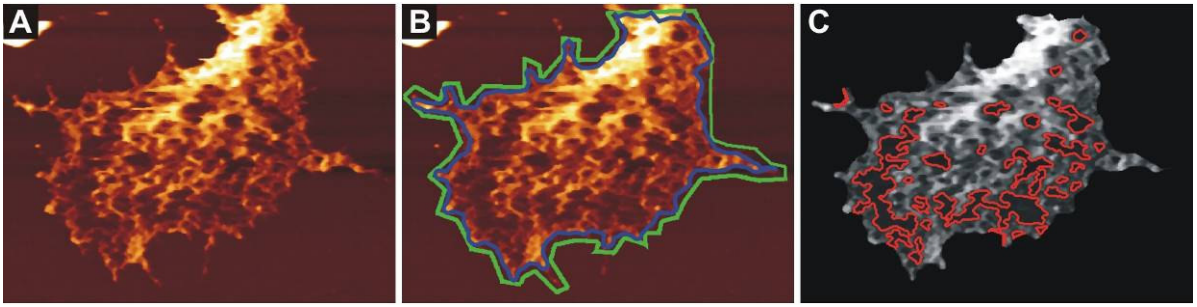

Fig. 3: Calculation of area of holes: **A**: Original AFM image. **B**: Selection of growth cone for calculation by Snake Map. **C**: holes found after calculation (i.e., below threshold).

For each growth cone, we measured:

i. the *total area* (T), defined as area of the entire growth cone, including the hole walls and various invaginations (i.e., sum of area of the triangles representing the surface approximated by Delaunay triangulation);

ii. the *base area* (B), defined as the area of the growth cone projected on the XY-plane;

iii. the *invagination value* I, a parameter defined as: $I = \frac{T}{B \cdot H_{max}}$, where H_{max} is the maximum height of the growth cone.

If the growth cone is more invaginated, it has more folds on the surface and thus this ratio is high. Collected data from the 13 analyzed growth cones are reproduced in Table 1. All AFM images shown in Fig. 3 are extrapolated images for 0 pN scanning force (see previous section).

3. Results

Neuronal growth cones have been usually imaged and characterized with conventional optical microscopes which have a spatial resolution not exceeding 200-400 nm. Therefore structures with a nanometric size will be very poorly resolved. The aim of the present work is to

investigate the shape of DRG growth cones with a nm resolution and to compare possible nanometric structures with the underlying content of actin filaments and microtubules. Therefore, we have combined AFM and LSCM imaging of the same growth cones.

Fixed growth cones were usually first imaged with AFM and then were inspected with a confocal microscope. When the cantilever tip of an AFM is advanced towards a biological sample, it could modify and even damage the cellular membrane of imaged neurons. In order to check for possible distortions introduced by the AFM tip, an image of a growth cone labeled for actin and tubulin was acquired with LSCM first (tubulin channel shown in Fig. 4A), then an AFM image of the same growth cone was acquired (Fig. 4B) and the same growth cone was imaged again with the LSCM (tubulin channel shown in Fig. 4C).

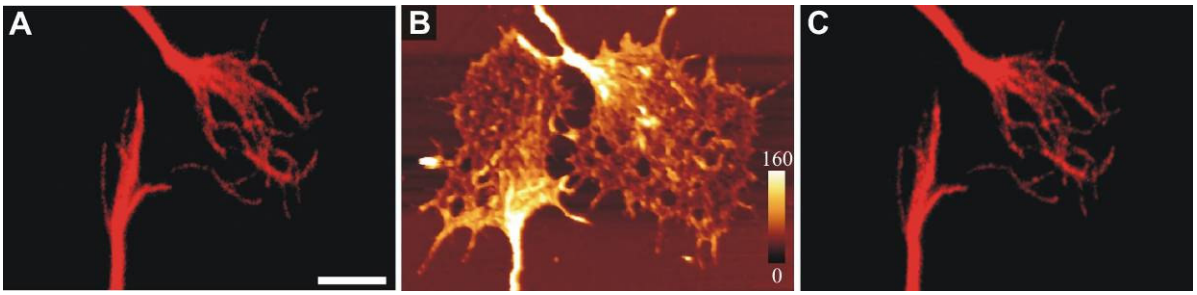

Fig 4: Comparison of Immunofluorescent Images of a growth cone labeled with anti-β tubulin III, followed by Alexa594 anti-mouse IgG taken before and after AFM scanning. **A**: Confocal image of microtubules in the cytoskeleton of the growth cone before AFM. Scale bar: 5 μm. **B**: AFM image of the same growth cone. Color bar indicates height in nanometers. **C**: Confocal image after AFM scanning.

As shown in Fig. 4, the LSCM images of microtubules before and after AFM imaging were indistinguishable suggesting that in our experimental conditions, the cantilever tip did not modify the growth cone. These results show that imaging growth cones first with AFM and then with LSCM provide results very similar when the reverse procedure is used, i.e. LSCM is used before AFM.

In order to analyze the relative distribution of actin filaments and microtubules in DRG growth cones, DRG neurons were fixed 20-30 hours after plating and immunostained with Alexa594 anti-β tubulin III to label neuronal microtubules and Alexa488 phalloidin to label actin filaments (Fig. 5). Two different types of growth cones were observed: one type (19 out of 40 growth cones) had an extensive lamellipodium from which 1-5 short filopodia (with lengths between 1.3 and 7 μm) protruded (Fig. 5A-C). The growth cone area stained with phalloidin was 1400±355 μm^2. Actin filaments were distributed throughout the lamellipodium and filopodia and were often clustered around lamellipodium edges. Tubulin, on the contrary, was present only in the central region of the growth cone where it formed an extensive network of microtubules (Figs. 5B,E). The second type (21 out of 40 growth cones) of growth cone (Fig. 5D-F) had smaller dimensions with an average area of 60±7 μm^2, containing many filopodia (>10) with lengths between 1.5 and 12.5 μm, some of which (22%) contained both actin and tubulin (arrow in Fig. 5G-I). Of the total filopodia population, 23% were bent (a filopodium is considered bent if it has an angle <165º) and 31% of these bent filopodia contained tubulin, compared to 20% straight filopodia containing tubulin. Very often, tubulin staining in filopodia, both straight and bent, was interrupted, either because the fluorescent signal was below threshold or because the microtubule was indeed broken (arrow in Fig. 5H).

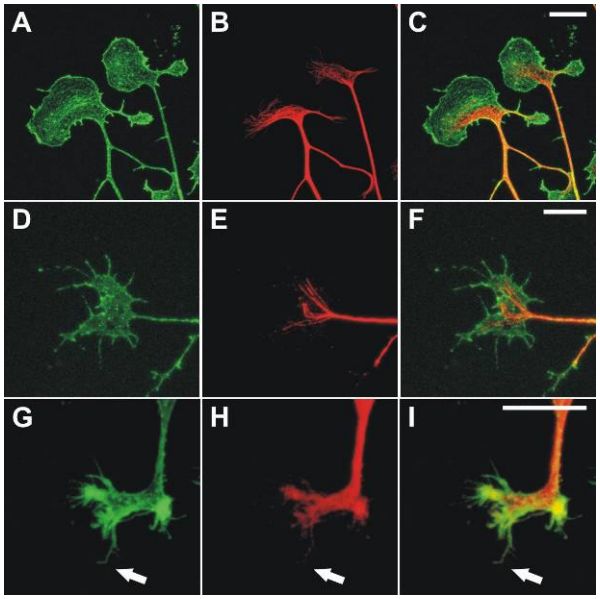

Fig. 5: Immunofluorescent images of DRG growth cones labeled with Alexa488 phalloidin (**A, D, G**) and anti-β tubulin III, followed by Alexa594 anti-mouse IgG (**B, E, H**). **C, F, I** show merged images. Scale bar: 10 µm.

These results indicate a significant variability in the cellular distribution of actin filaments and microtubules in growth cones, but are consistent with the view that microtubules are primarily distributed in the central region of growth cones, while actin filaments can extend into the peripheral region and in filopodia (Kalil and Dent, 2005).

3.1. AFM images of Growth Cones reveal Nanosize Holes

In order to understand whether the fixation procedure affects morphological properties of the growth cone, we used two different fixation procedures, one using PFA and the other using GLU. As these two chemicals fix the cell through different processes (Cross and Williams Jr., 1991) it is useful to verify whether detected nanometer dimensional structures are introduced by treatment with these chemicals. We analyzed growth cones with AFM using scanning forces from 100 pN up to 2000 pN so to obtain 0 pN AFM images, representing the outer surface of the growth cone with a minimal distortion introduced by the cantilever tip. The outer surface of 13 over 15 imaged growth cones was not smooth, but instead was highly corrugated and had a significant number of holes.

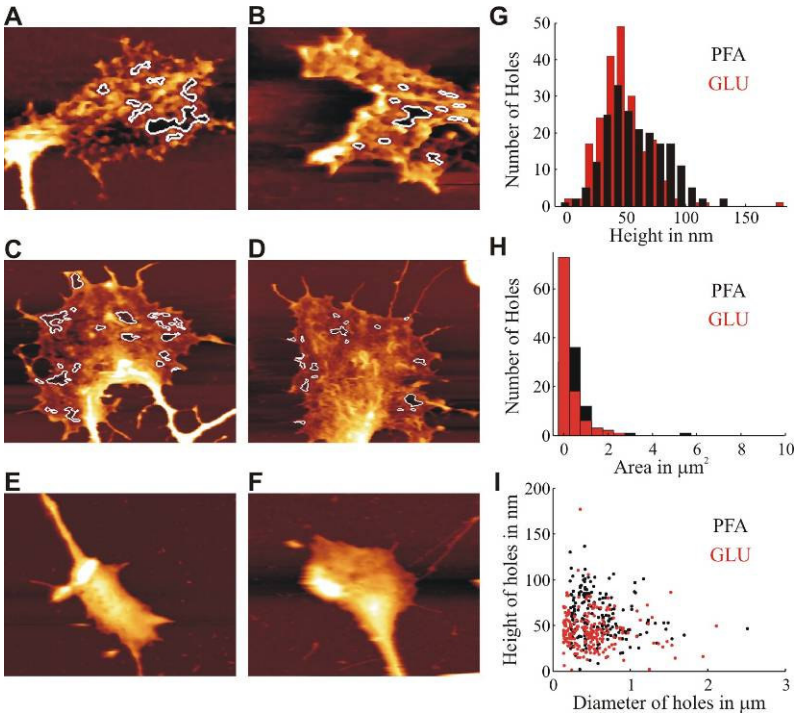

Fig. 6: Comparison of different fixation procedures using statistics obtained from holes: **A-D**: AFM images (interpolated for 0 pN) after fixing with PFA (**A, B**) and GLU (**C, D**). White contours indicate holes. **E-F**: Examples of growth cones without holes. **G-I**: Distribution of height (**G**) and area (**H**) of holes observed in the growth cones after fixation using PFA and GLU. **I**: Plot of height against diameter of holes after using the two different fixatives. Black denotes PFA and Red GLU.

As shown in Fig. 6, holes were observed when growth cones were fixed both using PFA (6 growth cones) and GLU (7 growth cones). Having observed an invaginated surface with holes, we attempted to quantify their properties and therefore we measured the height of a hole as the difference between the mean height of the "hill" surrounding the hole and the threshold used to find the holes (see Methods); and other parameters such as their area. The distributions of height and area of detected holes are shown in Figs. 6G,H respectively and are very similar for both fixation procedures. Properties of holes varied significantly among individual growth cones, as shown in Table 1 and Fig.6. The number of detected holes varied from just 9 holes (image-13 and image-15) to 70 holes in image-16. The height of holes varied from just 2 nm up to 178 nm and their average height was about 51 nm (see Table 2). The area of their base was rather varying with a range from 0.01 to 3.5 μm^2.

Table 1: Comparison of parameters from growth cones fixed using the two different Protocols:

Fixation Method	AFM Image	Total Surface Area (μm^2)	Total Hole Area (μm^2)	Base Area (μm^2)	Total Area/ Base Area	Number of Holes	Maximum Height of Holes (nm)	Invagination Value
PFA	Image-1	599	14	132	4.2	55	200	2.1
	Image-2	136	7	33	4.1	16	140	3
	Image-3	603	51	143	4.2	29	160	2.6
	Image-4	765	108	187	4.1	20	160	2.6
	Image-5	520	46	127	4.1	19	150	2.7
	Image-6	245	10	55	4.5	60	250	1.8
	Average	478±239	39.3±23	112.8±57	4.2±0.16			
GLU	Image-11	1137	30	270	4.2	59	400	1.1
	Image-12	965	144	232	4.2	37	250	1.7
	Image-13	280	17	62	4.5	9	500	0.9
	Image-14	187	9	41	4.6	10	500	0.9
	Image-15	395	62	93	4.3	9	450	1
	Image-16	161	19	37	4.4	70	400	1.1
	Image-17	670	43	159	4.2	16	800	0.5
	Image-18	95	0	19	5	No holes	650	0.8
	Image-19	144	0	32	4.5	No holes	650	0.7
	Average	448.2±285	36.1±23	105±45	4.4±0.3			

Table 2: Hole statistics:

Parameters	PFA (n = 6)	GLU (n = 7)	Both fixation protocols (n = 13)
Height Range	2 to 128 nm	2 to 178 nm	2 to 178 nm
Average Height	57 ± 23 nm	45 ± 21 nm	51 ± 23 nm
Base Area of Holes Range	0.04 to 2.3 μm^2	0.01 to 3.5 μm^2	0.01 to 3.5 μm^2
Average Base Area	0.19 ± 0.17 μm^2	0.26 ± 0.24 μm^2	0.22 ± 0.20 μm^2

These results show that growth cones fixed with either GLU or PFA do not always have a smooth external surface but often have holes with nanometric dimensions, which cannot be seen by conventional optical microscopes.

3.2. Characterization of growth cones outer surface

As AFM provides a rather accurate 3D representation of imaged growth cones, we characterized several geometrical properties of its surface. Three quantities were computed, i.e. *total area*, *base area* and *hole area* (see Methods and Appendix 2), providing a characterization of the outer surface of growth cones. Collected data from the 15 analyzed growth cones are reproduced in Table 1. All measurements are based on the extrapolated 0 pN AFM images. In order to quantify the smoothness of a surface, we have introduced the parameter, *invagination value,* I (for definition see Methods): a low value of I (around or less than 1) indicates a smooth external surface and a higher value of this quantity is found for growth cones with many holes

having a significant height. The *invagination value* for all tested growth cones fixed with either PFA or GLU, varied from 0.5 to 3.

In order to correlate the measured height with the cytoskeletal components of the analysed growth cones, we applied immunofluorescent techniques where actin is fluorescently label with Alexa488 phalloidin and tubulin with anti-β tubulin III, followed by Alexa594 anti-mouse IgG. This enabled us to visualize the correspondence of the observed invaginations with the internal cytoskeletal structure and in particular with the presence or absence of actin filaments and/or tubulin. LSCM scanning were performed first on the fluorescently labeled growth cone. 4-7 slices of fluorescence images were acquired with a step size of 500 nm. The stack of these images was then averaged and used for further analysis. AFM was then performed on the same growth cone. Acquired AFM and averaged LSCM images were registered as described in Kondra et al. (2009) and briefly in the Methods section. Images in Fig. 7 show regions of the growth cone with a height more than 100 nm exhibiting a significant co-localization with the staining of actin filaments and tubulin, indicating that these proteins act as pillars inside the growth cones. In contrast, holes (area within white contours, Fig. 7) show poor co-localization with actin filaments and microtubules.

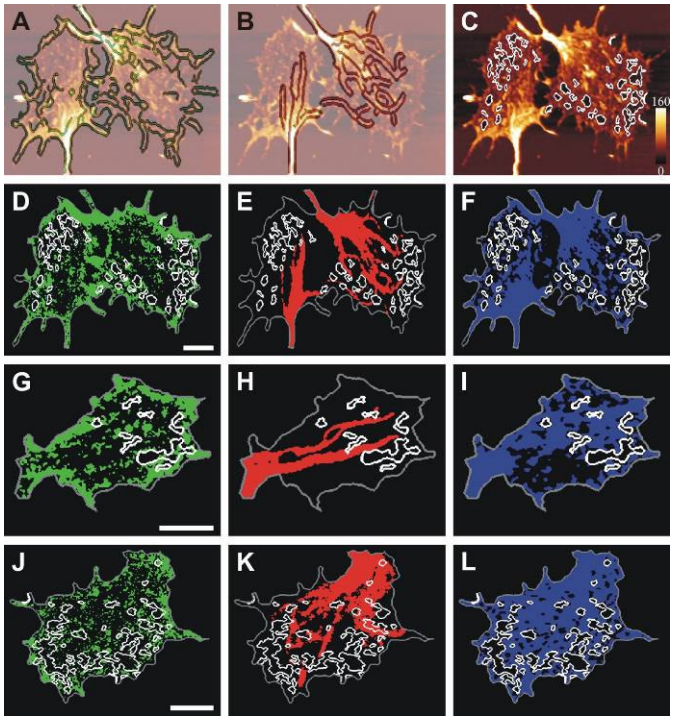

Fig. 7: Superposition of AFM image with Actin edges (**A**), Tubulin edges (**B**) and holes (**C**). White contours indicate holes. See text for further explanation. **D-L:** Binarization of Confocal and AFM Images: Actin (green; **D,G,J**), tubulin (red; **E,H,K**), AFM (dark blue; **F,I,L**). Scale bar: 5 μm.

In order to verify whether holes in AFM images correspond to absence of major cytoskeletal components, we binarized fluorescent actin and tubulin images as well as AFM images (green, red and blue regions respectively in Fig. 7). Using a simple AND operation, we computed the number of pixels which are common to binarized tubulin or binarized actin and the holes. Table 3 shows the result of our analysis of the correspondence of the topography of the growth cone to the presence (or absence) of actin and tubulin through AFM scanning and subsequent confocal imaging.

Table 3: Comparison of Actin Tubulin Ratio in growth cones:

Parameters	Image-1	Image-3	Images-4	Image-5	Average ± Standard Deviation
Tubulin inside holes (%)	18	2	6	3	7 ± 7
Actin inside holes (%)	13	18	19	15	16 ± 3
Actin + Tubulin outside holes (%)	55	60	64	62	60 ± 4
Tubulin/Actin ratio of entire growth cone	1.47	0.57	1.05	0.67	
Tubulin Height (nm)	146	162	109	127	136 ± 22
Actin Height (nm)	115	112	79	94	101 ± 16
Tubulin Height /Actin Height	1.27	1.44	1.37	1.35	1.36 ± 0.07

Holes rarely coincide with tubulin staining (2 to 18% of the total area of the holes) or actin staining (13 to 19% of the total area of the holes), which indicates that more than 80% of the hole area lacks actin filaments or microtubules. Outside the holes, 55 to 64% of the total area coincides with tubulin and actin staining, indicating the existence of a mesh-like network throughout the growth cone with gaps in between, instead of a densely packed structure. This agrees with the view that the central region of growth cones is rich in microtubules and the peripheral region is occupied by a mesh of actin filaments (Kalil and Dent, 2005). The tubulin to actin ratio over the entire growth cone tends to fall into two categories: values around 0.5 indicating an extensive actin network, and values larger than 1 indicating a network composed of a significant microtubule branching. In the region where tubulin staining is present, the mean height is 136±22 nm and the mean height of the region with actin staining is 101±16 nm. Irrespective of the branching of the microtubule network, the ratio of the tubulin height to actin height has an average of 1.36±0.07 over the entire growth cone.

These results, taken together, show that holes observed in AFM images of DRG growth cones, colocalize with regions of poor density of major cytoskeletal components, such as actin and microtubules.

3.3. Filopodia properties

In order to analyze the properties of the filopodia that are seen present in the AFM scans, we characterized the length, mean diameter, base area and height of the filopodia. As can be seen in Fig. 8, the base area of observed filopodia in either PFA or GLU fixed growth cones ranged from 0.1 to 3.22 μm^2 (Fig. 8B). The distance between the base and the tip of a filopodium ranged from 0.5 to 8.6 μm (Fig. 8C). The mean diameter of the filopodia varied from 113 to 887 nm (Fig. 8D), while the mean height varied from 40 to 270 nm (Fig. 8E). The total length of the filopodia varied from 0.5 to 8.9 μm (Fig. 8F). In Fig. 8G, the height of a filopodium is plotted against its width, and there is no correlation between these two parameters (correlation coefficient=0). On the other hand, the plot of the area of a filopodium against its width (Fig.8H) shows a positive

correlation with the value of the correlation coefficient being 0.5. Fig. 8I shows the plot of the area against the height where there is a clustering at around the 100-200 nm range.

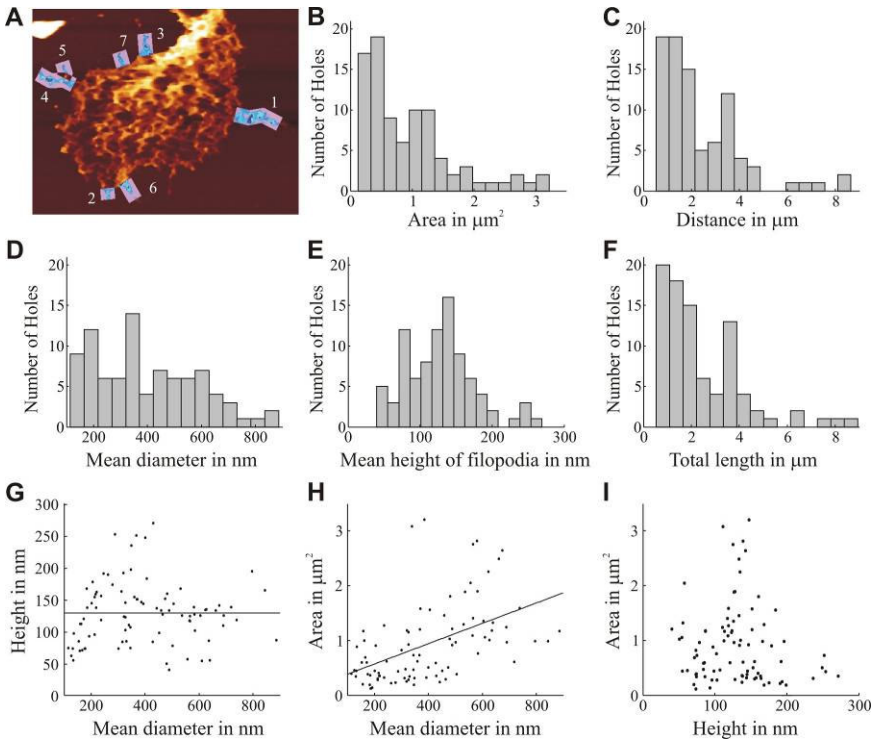

Fig. 8: Filopodia characterization. **A**: AFM image with filopodia. **B**: Distribution of the area (in μm^2) of the filopodia. **C**: Distribution of distance between the starting point and the ending point (in μm). **D**: Distribution of the mean diameter (in nm) of the filopodia. **E**: Distribution of the mean height of the filopodia (in nm) from the AFM scan. **F**: Distribution of the total length of filopodia (in μm). **G**: Relation between the height (in nm) and the mean diameter (in nm) of the filopodia. **H**: Relation between the area (in μm^2) and the mean diameter (in nm) of the filopodia. **I**: Relation between the area (in μm^2) and the height (in nm) of the filopodia.

4. Discussion

The present investigation of the shape and morphology of growth cones of differentiating DRG neurons reveals topographical structures with nanoscale dimensions which we refer as "invaginations" or "holes". These nanometric structures cannot be seen by conventional optical microscopes and are revealed by AFM.

The advantages of using Atomic Force Microscopy on biological samples have been extensively explored (Bonfiglio et al., 1995; Fotiadis et al., 2002; Reddy et al., 2004; McNally et al., 2005; Yunxu et al., 2006; Grzywa et al., 2006). Information obtained from AFM provides an accurate description of the surface topography of the sample under investigation. We developed a procedure to reduce possible deformations of the surface caused by the AFM tip during scans (Sen et al., 2005). This procedure has been referred to as the determination of the *0 pN AFM Image* of a sample. Using this method, it is possible to extrapolate an AFM image of a growth cone acquired at 0 pN scanning force as well as at any other desired force, if necessary, for comparison of AFM images acquired at different scanning forces.

Although there have been many reports on the use of AFM on biological samples, and on neurons in particular (Parpura et al., 1993; Bonfiglio et al., 1995; Ohshiro et al., 2000; Zhang et al., 2004; Yunxu et al., 2006; Grzywa et al., 2006), we found novel structures with nanometric dimensions, which could not be seen with conventional optical microscopes and were not described in previous investigations with AFM. These novel nanometric structures are referred to as "invaginations" or "holes" in this report. These holes are reminiscent of those described by Godement et al. (1994) and Mason and Erskine (2000) in in vivo retinal ganglion axons, presumably originating from the fusion or contact of lamellar extensions of the growth cone with glial processes. Holes observed in the present investigation are not caused by the AFM tip and are not introduced by the fixation procedure. Irrespective of the fixation procedure, these holes typically have a mean height ranging from 2 to 178 nm, with the base area ranging from 0.01 to 3.5 μm^2 with an average of 0.22 ± 0.20 μm^2 per growth cone.

Through polymerization, microtubules grow from the central region towards the peripheral region and where the plus ends interact with the filopodia coordinating cell movement. Comparison with LSCM images showed that more than 80% of the hole area lacks actin filaments or microtubules. Further, the mesh-like network of actin filaments and microtubules is confirmed through statistical analysis of the growth cones.

Ongoing work from our laboratory (personal communication: Ban, J., Di Foggia, V., Migliorini, E., Lazzarino, M., Torre, V. and Ruaro, M. E.) on embryonic stem cells derived neurons in vitro suggests a correlation between the presence of these holes and the exploratory state of the growth cone. Growth cones of immobile isolated neurons or of retracting neurons display significant topological irregularities and holes. In contrast, actively exploring growth cones and those having established a contact with another growth cone rarely contain holes and have a smooth surface. Fragmentation seems a characteristic step during the physiological cycle of growth cones for example, when they stop actively exploring the environment. It is well known that cytoskeletal abnormalities are one of the hallmarks of neurodegenerative diseases (Goldman and Yen, 1986; McMurray, 2000) and it is possible that the kind of fragmentation described here for DRG growth cones also occurs during neurodegeneration or spinal cord injury (Tom et al., 2004). Thus, it would be rather crucial to examine growth cones from neurons with hallmarks of neurodegeneration by using the techniques described here.

Acknowledgements: We thank Diana Bedolla and Rajesh B. Shahapure for valuable discussion and suggestion during the preparation of this article. This work was supported by the EU projects: NEURO Contract n. 012788 (FP6-STREP, NEST) and NanoScale Contract n.214566 (FP7-NMP-2007-SMALL-1). In addition, we acknowledge the financial support of a FIRB grant D.M.31/03/05 from the Italian Government, Contr. RICN no.011936 BINASP from the European Community, funds from the Istituto Italiano di Tecnologia (Research Unit IIT) and of the GRAND Grant from CIPE/FVG, Friuli Venezia Giulia region. SK's work was supported by EU Marie Curie Training Network: Visiontrain Contract n. MRTN-CT-2004-005439.

Appendix A: Registration

If (x,y) is the system of reference of image A and (x',y') the system of reference of image B, the transformation T from A to B is defined as:

$$\begin{bmatrix} a1 & a2 & t_x \\ a3 & a4 & t_y \\ c1 & c2 & 1 \end{bmatrix} \quad (1)$$

where,

$\begin{bmatrix} a1 & a2 \\ a3 & a4 \end{bmatrix}$ is a rotation matrix which defines the kind of the transformation that will be performed, which in our case consists of scaling, rotation, and translation, $\begin{bmatrix} t_x \\ t_y \end{bmatrix}$ is the translation vector (which simply moves the points), and $\begin{bmatrix} c1 & c2 \end{bmatrix}$ is the projection vector, used for projective transformations. For affine transformations, as those used here, c1 and c2 are zero.
If x and y are the coordinates of a point, the transformation can be done by the simple multiplication:

$$\begin{bmatrix} a1 & a2 & t_x \\ a3 & a4 & t_y \\ c1 & c2 & 1 \end{bmatrix} \times \begin{bmatrix} x \\ y \\ 1 \end{bmatrix} = \begin{bmatrix} x' \\ y' \\ 1 \end{bmatrix} \quad (2)$$

Here, x' and y' are the coordinates of the transformed point.

The unknown parameters in the transformation matrix can be estimated either by matching a selected number of points or landmarks in the two images or by matching entire contours in the two images. The first method (*Points selection Method*) is used when it is possible to identify enough points in the two images corresponding to the same physical structure, such as the tip of a dendrite, or a small vesicle. The second method (*Procrustes Analysis*) is used when rounded biological structures are present, with no obvious marks and it is more convenient to put in correspondence two contours and not isolated points. These two methods are described in detail in Kondra et al. (2009).

Appendix B: Holes Estimation

To determine the holes, we use the following algorithm implemented in MATLAB 7.1:

1. Display AFM image where the intensity corresponds to height.

2. Choose threshold *Th*. Th *is usually set to 15% of the maximum intensity value of the image.*

3. Define a region *R* of the AFM image as a hole if the following conditions are fulfilled:
    a. Intensity averaged over *R (Int(R))* is less than Th. As AFM images intensity corresponds to height, this procedure is equivalent to set a threshold on its average height,
    b. Area of *R* is less than 5% of the total area of the base of the growth cone,
    c. *R* is completely surrounded by a non-hole (hilly) region.

    False positives are eliminated using these conditions. True holes are shown in Fig. 3C.

4. Repeat Step 2 and 3 with increasing values of *Th* till no holes can be found.

5. Merge all the holes found with all the different values of the threshold.

6. Calculate *base area*. Scale to real dimension (μm^2 in our case).

7. Calculate *height* of the 'hill' as the height of a sector of width of 5 pixels surrounding the hole. *This gives the depth of the hole.* Scale to real dimension (nm in our case).

8. Calculate *height* of the hole as the difference between the mean height of the 'hill' surrounding the hole and the mean height of the hole i.e., the threshold used to find the holes.

9. Perform triangulation of surface/height given by the AFM image and find area of each triangle. The sum gives *total area* of the surface. Scale to real dimension (μm^2 in our case).

10. Ratio of *total area* to *base area* indicates the texture of the surface: if close to 1, surface is flat and devoid of holes, whereas higher values indicate a surface with many holes.

11. Determine other parameters as required.

If *R* has been classified as a hole, we consider a sector *S* of width of 5 pixels surrounding *R* and the depth or height of the hole *R* is defined as *Int(S)- Int(R)*. *Hole area* is calculated as the area of the region *R*, scaled to real dimensions.

Appendix C: Estimation of Images at scanning force 0 pN

Procedure to obtain *0 pN AFM Images* by extrapolation:

1. AFM Images for growth cone 'A' at forces ranging from 100 pN to 2000 pN are obtained.

2. AFM images are registered and a stack is assembled from all the registered images.

3. Using the stack of growth cone 'A', we obtain two images one extrapolated at 0 pN and another at 390 pN using *interp3* command in Matlab (*spline* interpolation of the pixel intensities obtained at different forces is used internally in this function).

4. Using these two images, we obtain a 4^{th} degree polynomial function which maps the height values at 390 pN to the one at zero force for growth cone 'A' (Fig. C1).

5. Using this function, the *0 pN AFM Image* for growth cone 'B' is obtained.

This procedure can also be used to obtain the height map at any desired scanning force. In that case, one should interpolate between the available scanning force and the desired one (at step 3).

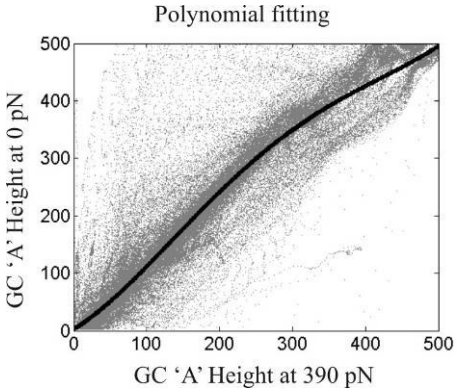

Fig. C1: Data fitting to obtain a relation between values of AFM height of growth cone 'A' taken at 0 pN and at 390 pN of the image series.

References

Barber, C. B., Dobkin, D. P., Huhdanpaa, H. T., 1996. The Quickhull Algorithm for Convex Hulls. ACM T Math Software. 22(4) p. 469-483.

Bonfiglio, A., Parodi, M. T., Tonini, G. P., 1995. Subcellular details of early events of differentiation induced by retinoic acid in human neuroblastoma cells detected by atomic force microscope. Exp. Cell Res. 216(1):73-79.

Cojoc, D., Difato, F., Ferrari, E., Shahapure, R. B., Laishram, J., Righi, M., Di Fabrizio, E. M., Torre, V., 2007. Properties of the force exerted by filopodia and lamellipodia and the involvement of cytoskeletal components. PLoS ONE. 2(10):e1072.

Cross, A. R., Williams Jr., R. C., 1991. Kinky Microtubules: Bending and Breaking Induced by Fixation In Vitro With Glutaraldehyde and Formaldehyde. Cell Motil Cytoskel. 20:272-278.

Fotiadis, D., Scheuring, S., Müller, S. A., Engel, A. and Müller, D. J. (2002). Imaging and manipulation of biological structures with the AFM. Micron 33(4):385-397.

Godement, P., Wang, L-C., Mason, C. A., 1994. Retinal axon divergence in the optic chiasm: Dynamics of growth cone behaviour at the mideline. J. Neurosci. 14:(7024-7039).

Goldman, J. E., Yen, S-H., 1986. Cytoskeletal protein abnormalities in neurodegenerative diseases. Ann. Neurol. 19(3):209-223.

Grzywa, E. L., Lee, A. C., Lee, G. U., Suter D. M., 2006. High-resolution analysis of neuronal growth cone morphology by comparative atomic force and optical microscopy. J. Neurobiol. 66(14):1529-1543.

Hill, D. L., Batchelor, P. G., Holden, M., Hawkes, D. J., 2001. Medical image registration. Phys. Med. Biol. 46:R1-R45.

Hofmann, U. G., Rotsch, C., Parak, W. J., Radmacher, M., 1997. Investigating the cytoskeleton of chicken cardiocytes with the atomic force microscope. J. Struct. Biol. 119(2):84-91.

Howard, J., 2001. Mechanics of Motor Proteins and the Cytoskeleton. Sinauer Associates, Inc., Sunderland, MA. 384 pages.

Kalil, K., Dent, E. W., 2005. Touch and go: guidance cues signal to the growth cone cytoskeleton. Curr. Opin. Neurobiol. 15:521-526.

Kandel, E. R., Schwartz, J. H., Jessell, T. M., 2000. Principles of Neural Science. McGraw Hill, 4/e.

Kass, M., Witkin, A., Terzopoulos, D., 1987. Snakes: active contour models. Int. J. Comput. Vision. 1(4):321-331.

Kirfel, G., Rigort, A., Borm, B., Herzog, V., 2004. Cell migration: mechanisms of rear detachment and the formation of migration tracks. Eur. J. Cell Biol. 83:717-724.

Kondra, S., Laishram, J., Ban, J., Migliorini, E., Di Foggia, V., Lazzarino, M., Torre, V., Ruaro, M. E., 2009. Integration of confocal and atomic force microscopy images. J. Neurosci. Methods. 177(1):94-107. Epub 2008 Oct 18.

Kuznetsova, T. G., Starodubtseva, M. N., Yegorenkov, N. I., Chizhik, S. A., Zhdanov, R. I., 2007. Atomic force microscopy probing of cell elasticity. Micron. 38(8):824-833.

Li, G., Xi, N., Wang, D.H., 2006. Probing membrane proteins using atomic force microscopy. J. Cell Biochem. 97(6):1191-1197.

Ma, J., Liu, B. F., Xu, Q. Y., Cui, F. Z., 2005. AFM study of hippocampal cells cultured on silicon wafers with nano-scale surface topograph. Colloids Surf. B. Biointerfaces. 44(2-3):152-157.

Ma, J., Cui, F. Z., Liu, B. F. and Xu, Q. Y. (2007). Atomic force and confocal microscopy for the study of cortical cells cultured on silicon wafers. J. Mater Sci: Mater Med. 18:851-856.

Mason, C, Erskine, L., 2000. Growth cone Form, Behavior, and Interactions in Vivo: Retinal Axon Pathfinding as a Model. J. Neurobiol. 44(2), pp 260-270.

McMurray, C.T., 2000. Neurodegeneration: diseases of the cytoskeleton? Cell Death Differ. 7:861-865.

McNally, H. A., Rajwa, B., Sturgis, J., Robinson, J.P., 2005. Comparative three-dimensional imaging of living neurons with confocal and atomic force microscopy. J. Neurosci. Methods. 142(2):177-84.

Ohshiro, H., Suzuki, R., Furuno, T., Nakanishi, M., 2000. Atomic force microscopy to study direct neurite-mast cell (RBL) communication in vitro. Immunol. Lett. 74(3):211-214.

Parpura, V., Haydon, P. G., Henderson, E., 1993. Three-dimensional imaging of living neurons and glia with the atomic force microscope. J. Cell Sci. 104:427-432.

Reddy, C.V., Malinowska, K., Menhart, N., Wang, R., 2004. Identification of TrkA on living PC12 cells by atomic force microscopy. Biochim. Biophys. Acta. 1667(1):15-25.

Ricci, D., Grattarola, M., Tedesco, M., 2004. Growth cones of living neurons probed by atomic force microscopy. Methods Mol. Biol. 242:125-140.

Rochlin, M. W., Itoh, K., Adelstein, R. S., Paul, C., Bridgman, P. C., 1995. Localization of myosin II A and B isoforms in cultured neurons. J. Cell Sci.108:3661-3670.

Sen, S., Subramanian, S., Discher, D. E., 2005. Indentation and Adhesive Probing of a Cell Membrane with AFM: Theoretical Model and Experiments. Biophys. J. 89:3203-3213.

Tom, V. J., Steinmetz, M. P., Miller, J. H., Doller, C. M., Silver, J., 2004. Studies on the Development and Behavior of the Dystrophic Growth Cone, the Hallmark of Regeneration Failure, in an In Vitro Model of the Glial Scar and after Spinal Cord Injury. J. Neurosc. 24(29):6531-6539.

Xu, C., Prince, J. L., 1998. Snakes, shapes, and gradient vector flow. IEEE Trans Image Process. 7(3):359-369.

Young, T. H., Chen, C. R., 2006. Assessment of GaN chips for culturing cerebellar granule neurons. Biomaterials. 27(18):3361-3367.

Yunxu, S., Danying, L., Yanfang, R., Dong, H., Wanyun, M., 2006. Three-dimensional structural changes in living hippocampal neurons imaged using magnetic AC mode atomic force microscopy. J. Electron Microsc(Tokyo). 55(3):165-172.

Zhang, R. Z., Zhu, W. Y., Xia, M. Y., Feng, Y., 2004. Morphology of cultured human epidermal melanocytes observed by atomic force microscopy. Pigment Cell Res. 17(1):62-65.

11. BIBLIOGRAPHY

Ahmari SE, Smith SJ. 2002. Knowing a nascent synapse when you see it. Neuron 34:333-336.

Aletta JM, Greene LA. 1988. Growth cone configuration and advance: a time-lapse study using video-enhanced differential interference contrast microscopy. J Neurosci 8:1425-1435.

Al-Kofahi KA, Lasek S, Szarowski DH, Pace CJ, Nagy G, Turner JN, Roysam B. 2002. Rapid automated three-dimensional tracing of neurons from confocal image stacks. IEEE Trans Inf Technol Biomed. 2002 Jun;6(2):171-87.

Bentley D, Toroian-Raymond A.1986. Disoriented pathfinding by pioneer neurone growth cones deprived of filopodia by cytochalasin treatment. Nature. 1986 Oct 23-29;323(6090):712-5.

Betz T, Koch D, Stuhrmann B, Ehrlicher A, Kas J. 2007. Statistical analysis of neuronal growth: edge dynamics and the effect of a focused laser on growth cone motility. New J Phys 2007;9:426.

Bonfiglio, A., Parodi, M. T., Tonini, G. P., 1995. Subcellular details of early events of differentiation induced by retinoic acid in human neuroblastoma cells detected by atomic force microscope. Exp. Cell Res. 216(1):73-79.

Bray D., and Chapman, K. 1985. Analysis of microspike movements on the neuronal growth cone. J. Neurosci. 5, 3204–3213

Capowski EE, Wells JM, Harrison GS, Karrer KM. 1989. Molecular analysis of N6-methyladenine patterns in Tetrahymena thermophila nuclear DNA. Mol Cell Biol. 1989 Jun;9(6):2598-605.

Challacombe JF, Snow DM, Letourneau PC. 1996. Actin filament bundles are required for microtubule reorientation during growth cone turning to avoid an inhibitory guidance cue. J Cell Sci. 1996 Aug;109 (Pt 8):2031-40.

Chi W. Pak, Kevin C. Flynn and James R. Bamburg. 2008. Actin-binding proteins take the reins in growth cones. Nature february 2008; volume 9; p136

Chien CB, Rosenthal DE, Harris WA, Holt CE. 1993. Navigational errors made by growth cones without filopodia in the embryonic Xenopus brain. Neuron. 1993 Aug;11(2):237-51.

Cingolani LA, Goda Y. 2008. Actin in action: the interplay between actin cytoskeleton and synaptic efficacy. Nat. Rev. Neurosci. 9:5, 344-56.

Cojoc D, Difato F, Ferrari E, Shahapure RB, Laishram J, Righi M, Di Fabrizio EM, Torre V. 2007. Properties of the force exerted by filopodia and lamellipodia and the involvement of cytoskeletal components. PLoS ONE 2(10):e1072. doi:10.1371/journal.pone.0001072.

Desai A, Mitchison TJ. 1997. Microtubule polymerization dynamics. Annu Rev Cell Dev Biol. 1997;13:83-117.

Endo M, Ohashi K, Sasaki Y, Goshima Y, Niwa R, Uemura T, Mizuno K. 2003. Control of growth cone motility and morphology by LIM kinase and Slingshot via phosphorylation and dephosphorylation of cofilin. J Neurosci. 2003 Apr 1;23(7):2527-37.

Endo M, Ohashi K, Mizuno K. 2007. LIM kinase and slingshot are critical for neurite extension. J Biol Chem. 2007 May 4;282(18):13692-702. Epub 2007 Mar 13.

Engert F, Bonhoeffer T. 1999. Dendritic spine changes associated with hippocampal long-term synaptic plasticity. Nature 399:66-70.

Fackler OT, Grosse R. 2008. Cell motility through plasma membrane blebbing. J Cell Biol. 2008 Jun 16;181(6):879-84. Epub 2008 Jun 9.

Fonseca R, Nagerl UV, Bonhoffer T. 2006. Neuronal activity determines the protein synthesis dependence of long-term potentiation. Nat. Neuroscience 9:478-480.

Gallo G, Letourneau PC. 1998. Axon guidance: GTPases help axons reach their targets. Curr Biol. 1998 Jan 29;8(3):R80-2.

Gallo G, Pollack ED. 1995. Cyclic remodelling of growth cone lamellae and the effect of target tissue. Brain Res Dev Brain Res. 1995 Mar 16;85(1):140-5.

Gallo G, Pollack ED. 1997. Temporal regulation of growth cone lamellar protrusion and the influence of target tissue. J Neurobiol. 1997 Dec;33(7):929-44.

Ghashghaei HT, Lai C, Anton ES. 2007. Neuronal migration in the adult brain: are we there yet? Nat Rev Neurosci 8:141-151.

Godement P., Wang L-C, Mason CA. 1994. Retinal Axon Divergence in the Optic Chiasm: Dynamics of Growth Cone Behavior at the Midline. The Journal of Neuroscience, November 1994, 74(11): 7024-7039.

He W, Hamilton TA, Cohen AR, Holmes TJ, Pace C, Szarowski DH, Turner JN, Roysam B. Microsc. Microanal. 9, 296–310, 2003 Automated Three-Dimensional Tracing of Neurons in Confocal and Brightfield Images

Hill, D. L., Batchelor, P. G., Holden, M., Hawkes, D. J., 2001. Medical image registration. Phys. Med. Biol. 46:R1-R45.

Huber AB, Kolodkin AL Ginty DD, Cloutier JF. 2003. Signaling at the growth cone: ligand-receptor complexes and the control of axon growth and guidance. Annu Rev Neurosci 26:509-563.

Isambert H, Venier P, Maggs AC, Fattoum A, Kassab R, Pantaloni D, Carlier MF. 1995. Flexibility of actin filaments derived from thermal fluctuations. Effect of bound nucleotide, phalloidin, and muscle regulatory proteins. J. Biol. Chem. 270: 11437-11444.

Ishikawa R, Kohama K. 2007. Actin-binding proteins in nerve cell growth cones. J Pharmacol Sci. 2007 Sep;105(1):6-11. Epub 2007 Sep 8.

Jay DG. 2000 The clutch hypothesis revisited: ascribing the roles of actin-associated proteins in filopodial protrusion in the nerve growth cone. J Neurobiol. 2000 Aug;44(2):114-25.

Jin Z, Strittmatter SM. 1997. Rac1 mediates collapsin-1-induced growth cone collapse. J Neurosci. 1997 Aug 15;17(16):6256-63

Kandel ER, Schwartz JH, Jessell TM. 2000. Principles of Neural Science. McGraw Hill, 4/e.

Kuhn TB, Brown MD, Wilcox CL, Raper JA, Bamburg JR. 1999 Myelin and collapsin-1 induce motor neuron growth cone collapse through different pathways: inhibition of collapse by opposing mutants of rac1. J Neurosci. 1999 Mar 15;19(6):1965-75.

Kuhn TB, Meberg PJ, Brown MD, Bernstein BW, Minamide LS, Jensen JR, Okada K, Soda EA, Bamburg JR. 2000. Regulating Actin Dynamics in Neuronal Growth Cones By ADF/Cofilin and Rho Family GTPases

Kuznetsova TG, Starodubtseva MN, Yegorenkov NI, Chizhik SA, Zhdanov RI. 2007. Atomic force microscopy probing of cell elasticity. Micron. 38(8):824-833.

Lee H, Van Vactor D.2003. Neurons take shape. Curr Biol. 2003 Feb 18;13(4):R152-61.

Letourneau PC, Shattuck TA, Ressler AH. 1987. "Pull" and "push" in neurite elongation: observations on the effects of different concentrations of cytochalasin B and taxol. Cell Motil Cytoskeleton. 1987;8(3):193-209.

Letourneau PC. 1996. The cytoskeleton in nerve growth cone motility and axonal pathfinding. Perspect Dev Neurobiol. 1996;4(2-3):111-23.

Lin CH, Forscher P. 1993. Cytoskeletal remodeling during growth cone-target interactions. J Cell Biol. 1993 Jun;121(6):1369-83.

Lin SX, Pfister KK, Collins CA. 1996 Comparison of the intracellular distribution of cytoplasmic dynein and kinesin in cultured cells: motor protein location does not reliably predict function. Cell Motil Cytoskeleton. 1996;34(4):299-312

Loisel TP, Boujemaa R, Pantaloni D, Carlier MF. 1999. Reconstitution of actin-based motility of Listeria and Shigella using pure proteins. Nature. 1999 Oct 7;401(6753):542-3.
Luo L. 2002. Actin cytoskeleton regulation in neuronal morphogenesis and structural plasticity. Annu. Rev. Cell Dev. Biol. 18: 601–635.

Luo L, Jan LY, Jan YN. 1997. Rho family GTP-binding proteins in growth cone signalling. Curr Opin Neurobiol. 1997 Feb;7(1):81-6.

Maletic-Savatic M, Malinow R, Svoboda K. 1999. Rapid dendritic morphogenesis in CA1 hippocampal dendrites induced by synaptic activity. Science 283:1923-1927.

Mallavarapu A, Mitchison T. 1999. Regulated actin cytoskeleton assembly at filopodium tips controls their extension and retraction. J Cell Biol. 1999 Sep 6;146(5):1097-106.
Marsh and Letourneau, 1984; Growth of neurites without filopodial or lamellipodial activity in the presence of cytochalasin B.

Mason C., Erskine L. 2000. Growth Cone Form, Behavior, and Interactions in Vivo: Retinal Axon Pathfinding as a Model

McNally HA, Rajwa B, Sturgis J, Robinson JP. 2005. Comparative three-dimensional imaging of living neurons with confocal and atomic force microscopy. J. Neurosci. Methods. 142(2):177-84.

Meijering E, Sarria J-CF, Steiner P, Hirling H, Unser M. 2004. Design and Validation of a Tool for Neurite Tracing and Analysis in Fluorescence Microscopy Images. Cytometry Part A 58A:167–176 (2004)

Mitchison T, Kirschner M. 1988. Cytoskeletal dynamics and nerve growth. Neuron. 1988 Nov;1(9):761-72.

Mongiu AK, Weitzke EL, Chaga OY, Borisy GG. 2007. Kinetic-structural analysis of neuronal growth cone veil motility. J Cell Sci 120:1113-1125.

Parpura V, Haydon PG, Henderson E. 1993. Three-dimensional imaging of living neurons and glia with the atomic force microscope. J. Cell Sci. 104:427-432.

Schaefer et. al., 2001; Kabir N, Schaefer AW, Nakhost A, Sossin WS, Forscher P. 2001. Protein kinase C activation promotes microtubule advance in neuronal growth cones by increasing average microtubule growth lifetimes. J Cell Biol. 2001 Mar 5;152(5):1033-44.

Solecki DJ, Govek EE, Hatten ME. 2006. mPar6 alpha controls neuronal migration. J Neurosci 26:10624-10625.

Stossel TP. 1993. On the Crawling of Animal Cells. Science, Vol. 260, No. 5111 (May 21, 1993), pp. 1086-1094

Suter DM and Forscher P. 1998. An emerging link between cytoskeletal dynamics and cell adhesion molecules in growth cone guidance. . Curr. Opin. Neurobiol. 8:106-116

Suter DM, Forscher P. 2000 Substrate-cytoskeletal coupling as a mechanism for the regulation of growth cone motility and guidance. J Neurobiol. 2000 Aug;44(2):97-113.

Rochlin MW, Dailey ME, Bridgman PC. 1999 Polymerizing microtubules activate site-directed F-actin assembly in nerve growth cones. Mol Biol Cell. 1999 Jul;10(7):2309-27.

Yong Zhang, Xiaobo Zhoua, Alexei Degterev, Marta Lipinski, Donald Adjeroh, Junying Yuan, Stephen T.C. Wong. 2007. A novel tracing algorithm for high throughput imaging Screening of neuron-based assays. Journal of Neuroscience Methods 160 (2007) 149–162

Yunxu, S., Danying, L., Yanfang, R., Dong, H., Wanyun, M., 2006. Three-dimensional structural changes in living hippocampal neurons imaged using magnetic AC mode atomic force microscopy. J. Electron Microsc(Tokyo). 55(3):165-172.

Zitova B, Flusser J. 2003. "Image registration methods: a survey," Image and Vision Computing, vol. 21, no. 11, pp. 977-1000, Oct.2003.

Zhou FQ, Cohan CS. 2004. How actin filaments and microtubules steer growth cones to their targets.J Neurobiol. 2004 Jan;58(1):84-91.

12. ACKNOWLEDGMENTS

I would like to thank my supervisor, Prof. Vincent Torre, for all the guidance and support he has given me over the years, academically and otherwise. Without him, the work in this thesis would not be in its present form.

My most sincere gratitude goes to Dr. Dan Cojoc, Dr. Enrico Ferrari and Dr. Franceso Difato for helping in a big way in the beginning of my Ph.D.

I would also like to thank all the secretaries and the technical assistants in the Neurobiology sector especially Tullio for being ever helpful.

By no means can I forget Daniela on whose shoulders fell the unpleasant task of teaching me molecular and cell biology. Her patience and willingness to answers my silly questions encouraged me to enjoy working with bugs, immunos and microscopes; her culinary prowess also proved exceptional. Thank you babe, you are the best.

The early days of my Ph.D. would have been a nightmare if Marianna had not been there to listen to my frustrated complaints. Those days also introduced me to the super-cool Amanda and Sergio. Thank you kool-kats, for being there.

I want to thank Diana for her friendship and for being there to discuss everything under the sun with me. And how can I forget the aperitvo-s and the dinners with the S&C babes: Diana, Zeynep and Roma. Thanks for those pleasant memories, babes. And I also "hereby" acknowledge my appreciation of the "quick aperitivo-s" with the S&C babes and Silvia and the gentleman who is the victim of all our merciless jokes: CCD… people, those were, undoubtedly, some of the most amazing times!!!

The super-enthusiastic Alberto, Fred- my partner in crime, Vale- the one who brought the taste of southern Italy to me, Jelena, Elisabetta, Giulietta, Paolo, Giacomo, Jacobo, Monica, Arin, Silvia, Walter, and the new arrivals- Ladan, Linh and Erica, and of course Manuela, all made the Torre Lab a big happy family. Keep it goin' people!!

In Trieste, I made some very good friends: Rajesh with the infinite patience, the electronic/techno-music guy Shripad, the super-cook Fauzia, the Nairs… I want to thank the macho-guy Shyju for his valuable advices and friendship which has come to mean lot to me.

In all the years of my Ph.D., my friends in the far far away land of India proved "out of sight, out of mind" to be wrong. Nanda, Luna, Ajay, Seema, Abhay, (Arzin too!!) and Aparna made the distance seem nothing. Thank you for all those emails.

I cannot express enough my gratitude for the support of my family during all these years. Without your support and encouragement, I would have been a very different person. Thank you for everything.

And Carlo, you are the best thing that ever happened to me. Thank you for bearing with me during this period of overwhelming stress and frustration with your wisdom and advices, kindness and love.